Synthesis of Cu Doped Titania Nanoparticles and Thin Films and Studies on its Structural and Thermal Performance for Dye Sensitized Solar Cells

By

Sehar Shakir

NUST-2012-60746-MCES-64112-F

Session 2012-14

Supervised by

Assoc. Prof. Dr. Zuhair S. Khan

A Thesis Submitted to the Centre for Energy Systems in partial fulfillment of the requirements for the degree of

MASTERS of SCIENCE in

ENERGY SYSTEMS ENGINEERING

Center for Energy Systems (CES)

National University of Sciences and Technology (NUST)

H-12, Islamabad 44000, Pakistan

Certificate

This is to certify that work in this thesis has been carried out by **Ms. Sehar Shakir** and completed under my supervision in Advanced Energy Materials and Fuel Cells Lab, Centre for Energy Systems, National University of Sciences and Technology, H-12, Islamabad, Pakistan.

Supervisor:

_____

Dr. Zuhair S. Khan
Centre for Energy Systems
NUST, Islamabad

GEC member # 1:

_____

Dr. Muhammad Mujahid
School of Chemical and Material
Engineering, NUST
Islamabad

GEC member # 2:

_____

Dr. Amir Habib
School of Chemical and Material
Engineering, NUST
Islamabad

GEC member # 3:

_____

Dr. Parvez Akhter
Centre for Energy Systems
NUST, Islamabad

HoD-CES

_____

Dr. Zuhair S. Khan
Centre for Energy Systems
NUST, Islamabad

Principal/ Dean

_____

Dr. M. Bilal Khan
Centre for Energy Systems
NUST, Islamabad

Abstract

Fossil energy sources are continuously depleting and causing damage to the environment. Harnessing energy from the alternative sources is answer to challenges posed by the usage of fossil fuels. One of the potential options to mitigate the reliance on fossil fuels is to generate electricity by photovoltaic technologies. Dye Sensitized Solar Cells are among the top candidates with low-cost and with potential to replace the expensive crystalline Si solar technologies. Photoanode is one of the most important components in DSSCs for which oxide ceramics such as titania is one of the top choices. In this work, we have synthesized undoped and doped titania nanoparticles by simple and reliable sol-gel route. Metal doping can introduce structural defects in titania lattice that can result in increase in photocatalytic performance of solar cells. There was an indication in literature that Cu could initiate phase transformation in titania at lower temperature supportive to cell performance. Furthermore, Cu offers its candidature due to being relatively inexpensive and easily available. However, there is not enough data available in literature on performance of DSSCs based on Cu doped titania photoanode. Therefore, we are presenting herein systematic studies on Cu doped titania nanoparticles. Meanwhile, thin film coatings of titania and doped titania were made on FTO coated glass by assortment of methods like spin coating, doctor blade coating, etc. Various process routes such as effects of annealing temperature, Cu concentration, paste precursor and film thickness, film drying time, pore former dye effects, etc. were used in this study. Structural and thermal performance of materials and thin films were carried out using diversified techniques such as X-ray diffraction, Scanning electron Microscopy, TG-DT analysis, Fourier Transform Infrared Spectroscopy (FTIR), etc. Studies have revealed that dopant existed in the form of CuO in nanoparticles and thin films. Cu doping assisted in reduction in particle size and in band gap which was further verified by red absorption shift. Films with almost negligible crack were successfully made on FTO coated glass and it was found that crack density reduced with reducing drying time, increasing stirring time and adding HNO_3 along with water and ethanol as a precursor solvent. The inclusion of carbon microspheres formed cavities into the pellets of titania and Cu:TiO_2 and increased the porosity and surface area for greater dye adsorption. It was found that porosity increased from 31% to 42% by adding 2.5 wt%

carbon microspheres in 3wt% Cu doped titania thin films. IV measurements of the cells fabricated using Cu doped titania photoanode N3 dye, I^-/I_3^- electrolyte and gold coated FTO glass as counter electrode revealed a 11% increase in V_{oc} when compared to V_{oc} of cells made with similar components but using undoped titania photoanode

Keywords: Doped titania nanoparticles, doctor blade coating, DSSCs, carbon microsphere, TiO_2 thin films.

I would like to dedicate my thesis to my Loving Parents, Parents in law and Sisters.

Acknowledgement

All praises is to Allah Almighty who is the creator of this world. It's all due to His blessings that enabled me to work and successfully complete my research.

Research work is not done alone. There are several people involved making the project possible. I owe my overwhelmed and sincere gratitude towards the support and constant help of my mentor and my supervisor Dr Zuhair S.Khan, Head of Department, Centre for Energy Systems, NUST. I feel blessed to have a supervisor like him. He knows how to bring the best out of his researchers. He provided me with directions, technical support, motivation and his keen attention.

I am thankful to Prof. Dr. Muhammad Mujahid, Principal School of Chemical and Material Engineering (SCME) NUST for his guidance and technical support. I gladly express my regards to Dr. Amir Habib, Assistant professor SCME, NUST for his sincere support. I really feel blessed to be a student of Dr. Parvez Akhter who taught me the basics of photovoltaic technologies. I acknowledge his kind support. I doubt if I could ever convey my appreciation fully, but this work would have not been possible without the support of my GEC members.

I am really thankful for the support and help of my colleagues in Advanced Material Energy Materials and Fuel Cells lab. I would like to acknowledge the technical support provided by SCME and financial assistance provided by NUST. Last but not the least I would like to thank my department for enabling me to work in a very comfortable environment.

Table of Contents

List of Figures

List of Tables

List of Conference/Journal Papers

***Conference Paper:** Sehar Shakir, Hafiz M. Abd-ur-Rehman, Muhammad Akmal Rana, M N Akbar, Mustafa Anwer, Kamaal Mustafa, Zuhair S. Khan, "Sol-Gel Fabrication of TiO_2 Nanoparticles and Investigations on Cu Doping Effects for Application in Dye Sensitized Solar Cells", Conference on Frontiers of Nanoscience and Nanotechnology, Pakistan Institute OF Nuclear Science and Technology, Nilore, Pakistan.

***Conference Paper:** Sehar Shakir, Mustafa Anwer , Muhammad Akmal Rana, M N Akbar, Kamaal Mustafa, Zuhair S. Khan, "Improving Cell Performance of Dye sensitized Solar Cells by using Copper Doped TiO_2 Based Photoanode", The 3rd Asean-Pakistan Conference on Materials Sceince (APCoMS-3), NUST Islamabad, Pakistan.

Date of abstract submission: 14/07/2014, Conference date: November 25-27, 2014.

****Review paper:** Sehar Shakir, Zuhair S. Khan**,** "Review on the Effects of Metal Doping on TiO_2 Properties and Its Influence on Performance of Dye Sensitized Solar Cells"

To be submitted by start of October, 2014.

*****Original research article** Sehar Shakir, Abd-ur-Rehman, Zuhair S. Khan, "Synthesis of Cu Doped Titania Nanoparticles and Studies on its Structural and Thermal Performance for Dye Sensitized Solar Cells"

To be submitted by start of October, 2014.

*Attached as annexure I

**Attached as annexure II

***Attached as annexure III

Chapter 1

Introduction

1.1 The Need for Renewable Energy

Now-a-days, energy crisis, drinking fresh water and climate change are the most threatening matters for mankind. We are in need of adopting new policies that should utilize alternative energy sources rather than fossil fuels and provide sustainable solution to balance the requirement for affordable energy with the pressing issue of climate change. Intergovernmental panel on climate change (IPCC) put forward a report in February 2007 about the increase in global concentrations of methane, nitrous oxide and carbon dioxide because of the burning of fossil fuels and other pollution causing activities [1]. Carbon dioxide is the most influencing GHG (Green House Gas) which is mainly formed due to burning of coal. The increase in such gases cause an increase in temperatures, a phenomenon known as global warming. Global warming causes an increase of 0.13 °C per decade. It was predicted in report that average global temperature of the world will face an increase of 0.5 °C in coming ten decades. This estimate can be more depending on the amount of GHGs emitted in environment, and world population growth [2]. The gases formed due to burning of fossil fuels also have other effects than global warming like pollution causing uneasy living and affecting health badly. Global warming, besides increasing temperature, consequently caused melting of ice and glaciers imposing threats on marine life and have increased sea level at rate of 1.88 mm/year in years 1960-2005. It also increases the average temperature of oceans. Nitrous and sulphurous oxides are cause of acid rain and are linked to many respiratory and skin diseases [3]. These effects have been mild till now but if the emission of such pollution causing gases will continue along with rapid increase in population, the consequences will be severe. The affected climate will influence our daily lives as well ecological systems.

Another issue with the use of fossil fuel is its rapid depletion causing it to vanish. Fossil fuels tale millions of years to form and are finite. Annually 11 billion tonnes of oil is being consumed and if we kept on using it at this rate, all existing known deposits of oil will end by 2050. We do have gas too but its reserves can only add maximum ten more years taking us to 2060. Large deposits of coal are present in the world but to fill the oil and gas gap, if we start using coal its reserves will also end by 2090. One thing is to be kept in mind that the rate with which we are using fossil fuels today is slower than the rate with which we will be using in coming years due to population growth and industrialization. So fossil fuels will run out earlier than the estimated time [4].

In order to meet present and future energy requirements and to produce clean energy, use of alternative energy resources like solar photovoltaic technologies, solar thermal technologies, biofuels and clean coal technology should be employed. Among renewable resources, solar seems to be an attractive clean alternative energy source that can help to increase our energy independence and reduce the consequences of global warming. The sun is expected to shine for billions of years, well beyond the existence of Earth. Taking advantage of the abundant solar energy is one of the best ways of reducing the use of fossil fuels and therefore, driving down carbon emissions. Even though solar energy has a large potential to reduce emissions and provide substantial amounts of power to consumers, solar energy accounted for a very small percentage of the total energy produced by alternative energy sources due to high capital cost. "More energy from sun strikes earth in 1 hour ($4.3*10^{20}$ J) than all of the energy consumed by humans in an entire year'' [5].

1.2 Solar Cell Technology

A solar cell is a device that converts solar radiations, with specific wavelengths, into electricity. The concept of solar cell is related to the discovery of photoelectric effect. Einstein explained photoelectric effect in 1905 and received a Nobel Prize in 1921 but it was first discovered by A.E Becquerel in 1839. Photoelectric effect is the phenomenon of generation of photoelectrons or current when a piece of metal is irradiated to light. Light provides energy (photons hv) to electrons in atoms of the metal which excites them and make them move around and hence produce the current flowing through the

metal [6]. After the discovery of photoelectric effect, it took more than 30 years to develop first semiconductor p-n junction solar cell. This cell was developed by Russel Ohl in 1941 and lead to the development of first silicon solar cell by Chapin in 1957 [7]. The cost of these cells was very high with very low efficiency and they were only used in space applications. Very less attention was given to the discovery of solar cells until 1970 when the world globally faced oil crisis. Before 1970, solar cells were only used in space applications.

1.2.1 Physics of Solar Photovoltaic

Photovoltaic devices work on the phenomena of charge separation occurring at interface of two different materials. These materials have different conduction mechanism. Solar photovoltaic can be defined as the direct conversion of solar radiation into electric current. The materials that exhibit photoelectric effect absorb energy in form of photons of light and release free electrons. The separation or flow of these free electrons causes electric current to be generated.

The working of a solar cell can be divided into three simple steps:

1) Absorption of light

2) Charge separation

3) Charge collection

The chemical and physical processes behind these basic steps are different in different types of cells and depend on the materials used. Efficiency of each of these steps affects the efficiency of the solar cell. Efficiency can be maximized by selecting compatible materials to the cell design. Generally, semiconductor wafer creates an electric field when treated to form a positive side and a negative side (p and n junctions). When solar cell is irradiated to light, electrons are knocked out from semiconductor atoms. If the circuit is completed by contacting electrical conductors attached to both sides (positive and negative), electric current is generated.

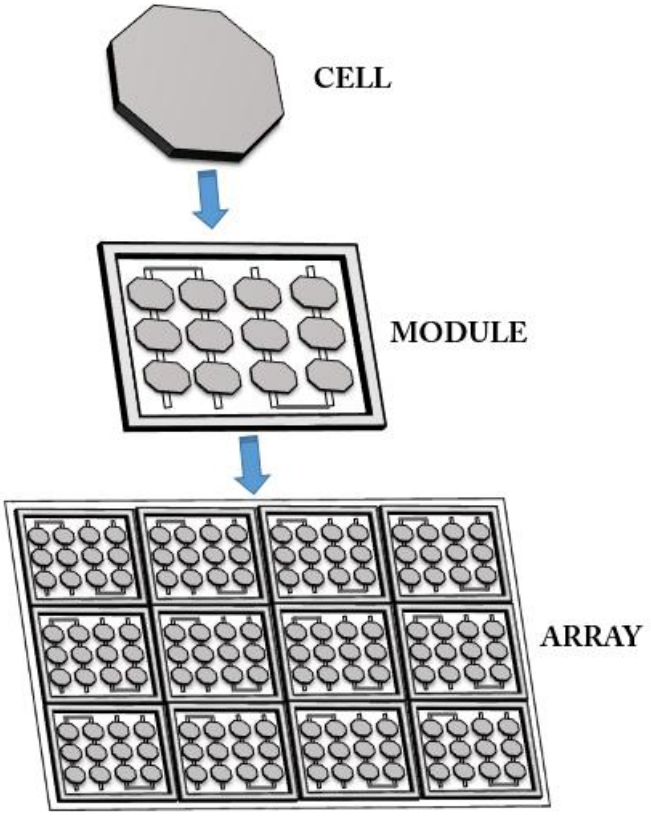

Fig. 1.1 Diagram showing a cell, module and an array.

Many solar cells when mounted in a frame or a support and joined electrically make up the solar module. The current produced by a module is dependent on the amount of light that strikes the module and on the area of module/array. Modules are mostly designed to supply electric current at certain voltage like 12 volts. Many modules when wired together to produce electric current forms an array. The current produced is direct current.

Photovoltaic has been dominated by p-n junction devices which are usually made up of silicon but emergence of third generation solar cells challenged this dominance of solid state junction devices [8].

1.2.1.1 Photovoltaic Performance

The generation of electricity by a solar cell or a panel is characterized by the current density-voltage (JV) curves or current-voltage (IV) curves. short circuit current (J_{sc}) is the maximum current generated when cell is short circuited and open circuit voltage

(V_{oc}) is the maximum voltage when cell is under open circuit state. The power produced by a cell or a panel is the product of voltage and current density. The maximum power point (MPP) is a point on the IV curve which represents the maximum power (P_{max}) in Watts produced by the cell i-e the point where product of voltage and current density is maximum.

$$P_{max} = J_{mpp} * V_{mpp}$$

Fill Factor is the ratio of maximum obtainable power to the product of V_{oc} and J_{sc}.

$$FF = \frac{J_{mpp} * V_{mpp}}{J_{sc} * V_{oc}}$$

From above equation P_{max} cab be written as

$$P_{max} = J_{sc} * V_{oc} * FF$$

Although different types of solar cells have different components and different working principles but these characteristics are common in all types of solar cells to determine their efficiency.

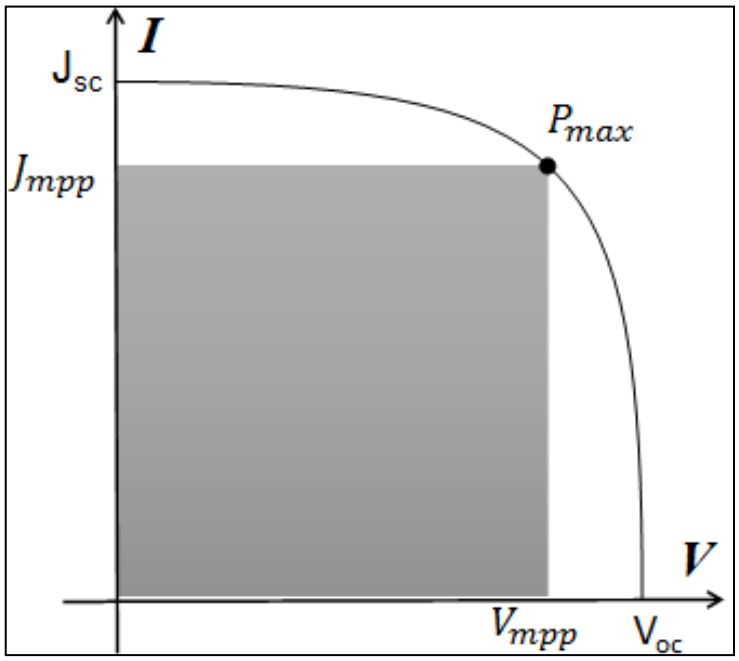

Fig. 1.2 IV characteristics curve for solar cells.

Maximum power generated by cell when divided by the incident light (W/m^2) determines the power conversion efficiency of a solar cell.

$$\eta = \frac{P_{max}}{P_{light}}$$

The efficiency of a solar cell is measured at standard test conditions i.e. at 1000W/m^2 irradiance, air mass 1.5 spectrum and 25 °C temperature.

1.2.2 Generations of Solar Cells

There are three generations of solar cells described below.

1.2.2.1 First Generation of Solar Cells

The first generation consists of high cost-high efficiency single crystalline or polycrystalline silicon solar cells. These cells have achieved efficiencies beyond 24.4 %.

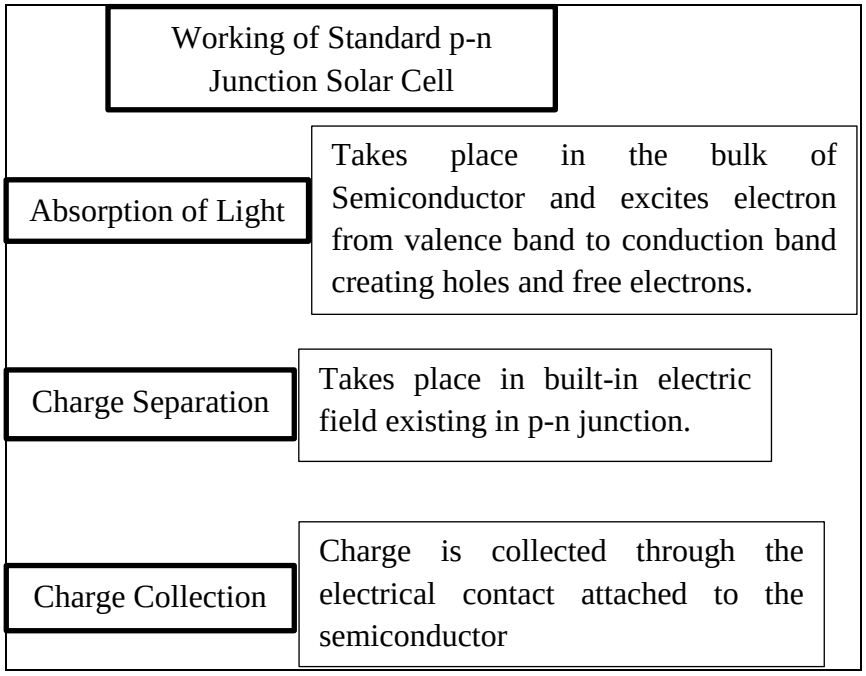

Fig. 1.3 Working of a standard p-n junction solar cell.

A standard silicon solar cell consists of a metal substrate, a p-n junction formed by p-doped and n-doped silicon layers, an anti-reflection coating (ARC), and a collector for current. When silicon is doped with impurity atoms from elements of group (V), an n-type semiconductor is formed. These impurities have an extra electron in their valence band. Doping silicon with such atoms forms localized energy states below the CB of silicon. When silicon is doped with impurity atom from elements of group (III), a p-type semiconductor is formed. These impurities have a vacancy for electron (hole) in its

valence band. These impurities create localized empty energy states above the VB of silicon. Thermal excitation causes the ionization of donor impurity atoms in n-type materials. The ionization occurs because CB edge of silicon and donor states are close to each other, hence generating free electrons in CB and leaving behind immobile empty donor states. The empty states (acceptor) in p-type material which are formed as a result of doping are partly filled by VB electrons creating mobile holes in VB.

When these two types of materials are brought in contact, the electrons and holes transport across the junction forming a thermal equilibrium between two materials. A charge-free depletion region is formed near the junction creating an electric field. When the p-n junction is illuminated, the electrons from VB excite to CB by absorbing energy from photons and generating holes in VB. The diffusion due to concentration gradient and drift due to potential gradient causes free motion of electrons and holes in high crystalline semiconductor. The built in electric field transports minority charge carriers, electrons in p-type layer and holes in n-type, to the opposite sides. Electrons reach n-type layer and holes reach p-type layer creating a potential difference between the opposite sides of the junction. These carriers are collected by electrical contacts at both ends. When external load is applied, electric current flows.

Although cost of production has decreased over the passage of time but first generation solar cells are still very costly. These solar cells require highly pure materials which are manufactured by expensive wafer processes involving many energy extensive steps [9].

1.2.2.2 Second Generation Solar Cells

Second generation consist of thin film solar cell technology including amorphous silicon solar cells, Cadmium Telluride (CdTe), micromorph tandem solar cells, and Copper Indium Gallium Diselenide (CIS or CIGS). Second generation solar cells are considered as low efficiency-low cost solar cells but recently their efficiency has been enhanced up to 20 % [10-12]. Issue with CdTe solar cells is the presence of toxic cadmium material. CIGS also contains toxic materials like selenium and cadmium in small amounts. This cause environmental risks reducing the importance of these cells as solar technology is meant to be environmentally benign. Amorphous Si solar cells have

very low efficiency (4-5%). However, amorphous Si tandem with three layers comprise amorphous silicon-germanium alloy are efficient up to 10% [13].

1.2.2.3 Third Generation of Solar Cells

Hence to compete with fossil fuels and fulfill the increasing demand of energy there is a need to develop low cost-high efficiency solar cells. Third generation solar cells can fulfill this need. Third generation of solar cells consists of Quantum Dot Solar Cells and Dye Sensitized Solar Cells having efficiency up to 12 %. DSSCs are technical and economical alternatives for expensive p-n junction solar cells [8]. DSSCs allow using less purified starting materials as they are not much sensitive to the impurities and defects whereas solid junction solar cells require high purity materials. This makes production of DSSCs less costly and the energy payback period is shorter [14].

Table 1.1 Comparison table of p-n junction solar cells and DSSCs.

Property	P-n junction solar cells	Dye sensitized solar cells
Power generation cost	High	Comparatively low
Efficiency	High	Low
Transparency	Opaque	Transparent
Color	Limited	Various
Stability	Good	Poor
Energy payback period	Longer	Shorter
Charge separation mechanism	Occurs due to formation of electric field in space charge layer	Occurs due to kinetic competition (like in photosynthesis)
Light absorption and charge separation	Both functions performed by semiconductor	Light is absorbed by dye and semiconductor solely performs charge transport

1.3 Dye Sensitized Solar Cell Technologies

1.3.1 Background

Until 2001, crystalline solar cell technology remained dominant. Crystalline and amorphous solar cells constituted about more than 99% of the manufactured solar cells. However work was being done to increase efficiencies of the other cells like multi-junction and thin film solar cells to commercialize them [15]. In 1972, Fujishima, a PhD student, under supervision of Honda, found that exposing TiO_2 electrode to light could split water. This photocatalytic water decomposition was later called as Honda-Fujishima effect [16]. However, there were some limitations that limited the conversion efficiency of cells using such electrodes for example, large bandgap of TiO_2 makes it absorb in ultraviolet region of electromagnetic radiation only. This led researchers to explore alternative metal oxides having appropriate properties. Use of GaAs electrodes gave acceptable efficiencies but problems with photo-corrosion degradation prevailed and in 1980s, the interest in photo-electro-chemical solar cells was decreased [17].

The research in Dye Sensitized Solar Cells started in 1960s when Tributch and Gerisher reported the enhancement of absorption range of wide band gap semiconductor. They observed increased absorption in visible region when the surface of wide bandgap semiconductor like TiO_2 was impregnated with dye molecules [18]. They used flat electrodes which showed low adsorption of dye and hence low absorption yield. This problem was overcome in 1985 by using rough surfaced semiconductor electrodes which ensured increased adsorption and efficiency of the cells [19]. In 1991, Brian and Gratzel succeeded to develop Dye Sensitized Solar Cell using I^-/I_3^- electrolyte, a mesoporous electrode to increase further dye adsorption, yielding an efficiency of 7%. DSSCs have reached photo conversion efficiencies for small laboratory cells up to 12 % and for solar modules they have reached to about 9 % [20].

1.3.2 Commercialization of DSSCs

Scientists are constantly working towards the commercialization of DSSCs. Dye sensitized solar cells and their modules are being manufactured in many parts of the world by different companies like sharp, Peccell, IMRA Aisin Seiki.Toyota, Dai Nippon and Toshiba technologies in Japan. Others include Solaronix in Switzerland, Dyesol in Australia, Konarka in United States of America, Solarprint in Ireland and G24 power limited in United Kingdom. DSSC technology was first commercialized by G24 in 2009. They have the capability of producing more than 500,000 linear meters of DSSC modules annually and possess a DSSC module production of 200 MW [21]. Solarprint is focusing on material synthesis, fabrication processes, device structures and device designs. "The company has built a world class team of highly skilled industry professionals from around the world and has been in pilot production since 2010 at its facility in Sandyford, Dublin''[22]. Dyesol has collaborated with various leading multinational companies to pave routes to market like collaborated with Tata steel Europe in UK to develop DSSC enabled steel roofing material, bringing building integrated photovoltaic (BIPV) in Korean market by teaming with Timi technologies, co-working with Dieted solar in USA to develop DSSC enabled glass façade etc. [23].

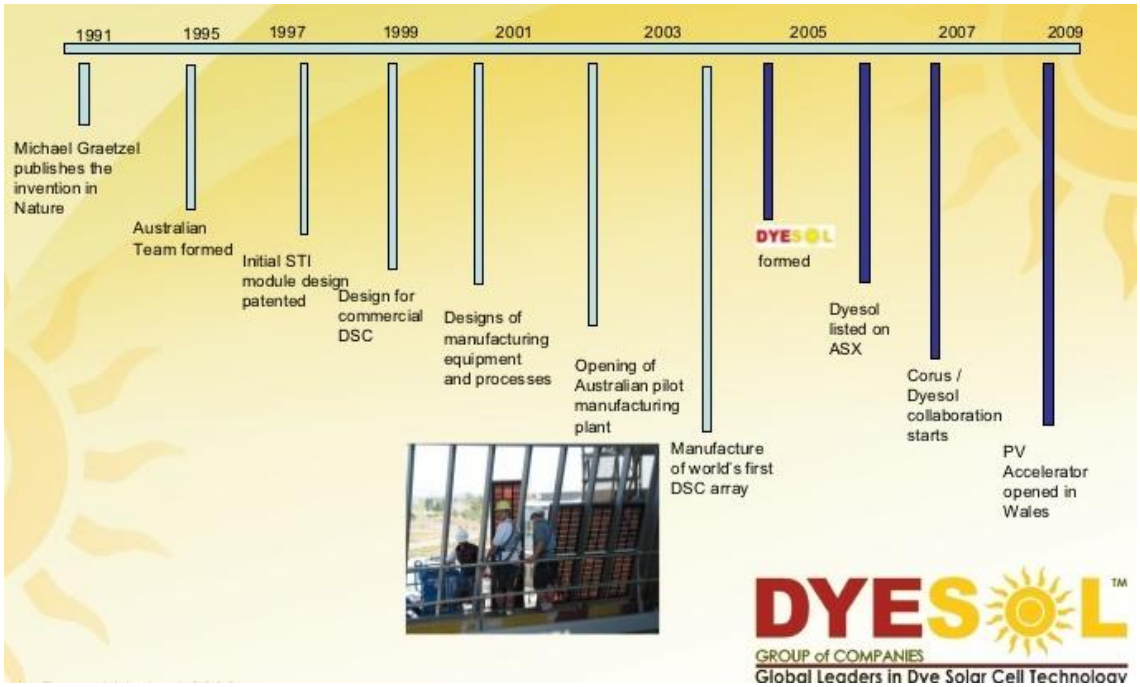

Fig. 1.4 Steps towards commercialization of DSSC technology by Dyesol [23].

Labs like Asian and Toyota central research and development lab have successfully demonstrated series connected DSSC modules in various international conferences and exhibitions and put their steps in commercializing DSSCs.

There are few factors that are holding the successful commercialization and use of Dye Sensitized Solar Cell technology some of which are discussed in this paragraph. Although glass substrates sustain high temperature and are robust but they are non-flexible, fragile and pricey. To overcome the negatives of using glass substrates, researchers investigated flexible DSSCs intensively but plastic based DSSCs offered lower efficiency because semiconductor film on them couldn't be annealed at required temperature which caused poor necking of semiconductor particles. Use of volatile electrolyte causes instability of the cells which encouraged researchers to look for solid-state DSSCs. Scientists studies solvent free-stable choices to substitute volatile electrolyte like hole transporters, solidified ionic liquids and polymer electrolyte but they had to compromise on efficiencies of the cells. The performance of outdoor DSSCs is degraded by UV light and heat therefore attention must be paid to develop heat sink and low cost UV coating.

Dye sensitized solar cell technology is relatively a new technology and long term performance of these cells has been questioned. However, with further improvements in its stability and efficiency, it can compete with silicon based solar cells.

1.3.3 Advantages and Applications of DSSCs

1.3.3.1 Advantages of DSSC Technology

Optimized performance in real world conditions

The advantage that these solar cells provide over other solar technologies is that they provide the facility to tune the dye according to the conditions of electromagnetic radiation hence can be used in outdoor as well as indoor applications. These cells, not like other solar cell technologies, can perform well in real world conditions like hazy and cloudy days, at dawn or dusk, at higher altitudes.

Low embodied energy and technology

Another advantage of DSSCs over other solar cell technologies is that these cells are based on nanotechnology. The nanostructured--semiconductor material TiO_2 is one of the most important materials of DSSC which forms the photo-electrode of the cell. The processing temperature for nanostructures materials is much lower e.g processing temperature for microparticles of TiO_2 is around 1000 °C and that for TiO_2 nanoparticles is 600 °C. This makes the processing of cells at lower temperatures hence saving energy and making them have less embodied energy.

Low Manufacturing cost

Production of DSSCs does not require highly pure materials, vacuum processing and strict cleanliness as required in conventional photovoltaic technologies. Their production also does not require expensive equipment. These cells can be prepared in a simple environment with least expensive equipment and facile methods like printing and baking processes. Therefore capital cost of these cells is low.

Variety of substrates

These cells can be produced on variety of substrates like metal, polymeric and glass substrates. These cells can be made on flexible or robust substrates. They absorb and convert light from both sides of panels.

Environment friendly materials

All the materials being used in DSSCs are non-toxic. There are no health concern related to their production and there are minimal protective measures to be observed during their production. Ru-based dyes are tested and found to be non-mutagenic. Some solar cells belonging to other technologies are based on very toxic materials like cadmium and selenium and they are to be handled very carefully observing many precautions.

Thin film technology saves resources

DSSCs involve thin films of the materials to be coated. Semiconductor layer is only up to 20 µm thickness and consists of a monolayer of dye being adsorbed which makes it about 80 thinner than a human hair. Whereas crystalline silicon cells require comparatively very thick materials and a lot of material is also wasted during processing. Hence employing these cells saves the resources.

Aesthetics

The flexibility offered by DSSCs in terms of transparency and coloration makes it attractive for architects. No other solar cell technology offers such flexibilities. Architects employ the use of these cells as doors, windows, internal dividing walls and skylights because of transparency and endless options of colors. DSSC based doors and windows can generate electricity, provide noise and thermal insulation and reduce intensity of harsh sunlight. The options of colors is provided by dyes which can be red, black, green, orange, grey, yellow and brown which can be really eye catching.

Readily available raw material

Titanium/Zinc, hydrogen, oxygen, silicon/iron and carbon are the mostly used chemical materials in DSSCs which are readily available and comparatively cheap. Platinum and ruthenium are also key ingredients in these solar cells but they are required in very small amounts.

High temperature performance:

The performance of these solar cells is less affected with increased temperature as compared to other solar cells. This allows them to efficiently work in direct sunlight.

1.3.3.2 Applications of DSSCs

- DSSCs have many applications few of which are stated below:
- DSSCs modules are used to generate electricity. They can be particularly used in remote areas where grid electricity is not available

- Individual cells may be used to power small devices like wrist watches, calculators etc.
- They can have their applications in Remote sensors, Building management (Motes), Mobile communications, Sonobuoys and remote transmitter.

Summary

In this chapter an introduction to the solar photovoltaic technology, its need and its importance has been discussed. There is a need for development of green energy generation systems which are alternative to conventional generation systems like using coal fired or oil fired power plants. The use of conventional energy resources are causing their depletion and may become extinct in coming years if we kept on using them. The pollutants caused by burning of such fossil fuels are responsible for global warming and other environment related bad impacts. Solar photovoltaic technology is a green option to replace the conventional energy generation technology. Scientists have been working to develop efficient and economical solar cells for their active commercialization. Crystalline silicon technology is quite a mature technology yielding high efficiency solar cells but main problem with this technology is its high cost. To develop low cost solar cells, scientists switched their attention towards thin film photovoltaic which offer low cost production of the cells. Dye Sensitized Solar Cells (DSSCs) belonging to third generation solar cells are suitable for the interests of scientist as they offer good efficiency and low cost. The efficiency of these cells can be improved with deep research as these cells have a tendency to reach up to 20-30% efficiency. Different companies in different continents of the world are working towards the production, research and commercialization of DSSCs. DSSCs offer many advantages over other solar cell technologies like they are low cost, environment friendly, the raw materials used are readily available and non-toxic, offers aesthetics etc. Therefore, this research has been made to study different factors to increase the cell performance of a DSSC.

References

[1] Meehl, G.A. and W. Collins, Global Climate Projections.

[2] Le Treut, H. and U. Cubasch, Historical Overview of Climate Change Science.

[3] Kampa, M. and E. Castanas, "Human health effects of air pollution", Environmental pollution, 2008. 151(2): p. 362-367.

[4] All data from https://www.cia.gov/library/publications/the-world-factbook/geos/xx.html.

[5] Tsao, J., N. Lewis, and G. Crabtree, "Solar FAQs".

[6] Willett, E., "The Basics of Quantum Physics: Understanding the Photoelectric Effect and Line Spectra", 2004: Rosen Publishing Group.

[7] McWhan, D., Sand and Silicon: "Science that Changed the World2012: OUP Oxford".

[8] Grätzel, M., "Dye-sensitized solar cells", Journal of Photochemistry and Photobiology C: Photochemistry Reviews, 2003. 4(2): p. 145-153.

[9] Zhao, J., et al., "19.8% efficient “honeycomb” textured multicrystalline and 24.4% monocrystalline silicon solar cells", Applied Physics Letters, 1998. 73(14): p. 1991-1993.

[10] Jackson, P., et al., "New world record efficiency for Cu (In, Ga) Se2 thin-film solar cells beyond 20%", Progress in Photovoltaics: Research and Applications, 2011. 19(7): p. 894-897.

[11] Xu, M., D. Xia, and Y. Sheng, "Thin-film solar cells", Mater Rev, 2006. 20(9): p. 109-111.

[12] Aberle, A.G., "Thin-film solar cells", Thin Solid Films, 2009. 517(17): p. 4706-4710.

[13] Li, B., et al., "Review of recent progress in solid-state dye-sensitized solar cells", Solar Energy Materials and Solar Cells, 2006. 90(5): p. 549-573.

[14] Bisquert, J., et al. "Comparative analysis of photovoltaic principles governing dye-sensitized solar cells and pn junctions in Optical Science and Technology", SPIE's 48th Annual Meeting. 2004. International Society for Optics and Photonics.

[15] Hagfeldt, A., "Brief overview of dye-sensitized solar cells", Ambio, 2012. 41(2): p. 151-155.

[16] Goetzberger, A., C. Hebling, and H.-W. Schock, "Photovoltaic materials, history, status and outlook", Materials Science and Engineering: R: Reports, 2003. 40(1): p. 1-46.

[17] Fujishima, A., "Electrochemical photolysis of water at a semiconductor electrode. nature", 1972. 238: p. 37-38.

[18] Grätzel, M., "Photoelectrochemical cells", nature, 2001. 414(6861): p. 338-344.

[19] Tributsch, H. and H. Gerischer, "The use of semiconductor electrodes in the study of photochemical reactions", Berichte der Bunsengesellschaft für physikalische Chemie, 1969. 73(8-9): p. 850-854.

[20] Desilvestro, J., et al., "Highly efficient sensitization of titanium dioxide", Journal of the American Chemical Society, 1985. 107(10): p. 2988-2990.

[21] Zalas, M. and M. Klein, "The Influence of Titania Electrode Modification with Lanthanide Ions Containing Thin Layer on the Performance of Dye-Sensitized Solar Cells", International Journal of Photoenergy, 2012. 2012.

[22] Data from "http://gcell.com/", taken on 02/07/2014.

[23] Data from "http://www.solarprint.ie/", taken on 02/07/2014.

[24] Data from "http://www.dyesol.com/" taken on 15/07/2014'.

Chapter 2

LITERATURE REVIEW

2.1 Working Principle and Photovoltaic Performance of Dye Sensitized Solar Cells

2.1.1 Working Principle

The current generation mechanism of DSSCs is similar to the phenomenon of photosynthesis in plants. Plants convert sunlight into energy using chlorophyll, a green pigment in cells, as light absorbers (sensitizers). In DSSCs function of chlorophyll is performed by an organic dye sensitizer. The water in plants is replaced by electrolyte in DSSCs and function of oxidized di-hydro nicotinamide adenine di nucleotide phosphate (NADPH) is substituted by wide band gap semiconductor [1, 2]. In both, photosynthesis and current generation by DSSCs, charge separation occurs by kinetic competition. Whereas, in p-n junction solar cells, charge separation takes place by formation of electric field in the junction [3]. Photon to energy conversion in DSSCs takes place into following steps [4-8]

Step 1: Excitation of Dye;

Absorption of photons excites the dye molecules from HOMO (Highest occupied molecular orbital) to LUMO (Lowest unoccupied molecular orbital) states. The excited dye state has a lifetime of nanosecond range.

Step 2: Electron Injection into Semiconductor;

Excited dye molecule injects the electron into conduction band of semiconductor and gets itself oxidized. This occurs in femtosecond timescale range. To ensure efficient electron injection, energy level of semiconductor conduction band must be about 0.2 V – 0.3 V lower than that of dye. The back reaction of electron from conduction band to oxidized dye molecule is much slower and lies in microsecond to millisecond range. This difference causes efficient charge separation in the cell.

Step 3: Electricity generation;

In the third step, electron diffuses through the photoanode, reaches TCO and travels to the outer circuit through to generate electric power (flow of electrons). In TiO_2 based nano-porous photoanode, layer contains anatase nanoparticles. Presence of oxygen vacancies in TiO_2 lattice makes it slightly n doped. The plane (101) is thermodynamically stable and is predominant in TiO_2 anatase nanoparticles. One photoanode contains around 10^{16} particles and have 1000 times larger projected area. The electron transport within TiO_2 layer occurs through diffusion since the nano-particles are very small to form an electric field. The electron transfer can be explained by trapping/detrapping model. Electron waits in the trap state for time t before hopping to next trap site. The trap state waiting time depends on the depth of the trap state. The electron transport can be defined by Fick's law of diffusion

$$\frac{\delta n}{\delta t \delta A} = -D \frac{\delta c}{\delta x}$$

Where, t is the waiting time, n is the number of electrons, A is the surface area, c is the electron concentration and D is the effective diffusion constant. Effective diffusion constant depends on the position of quasi Fermi level. Since the transport of electrons takes place by diffusion, diffusion length of electrons must be greater or at least equal to the thickness of photoanode. The optimized thickness of TiO_2 layer in photoanode varies from 9 μm to 15 μm.

After the flow of electron through outer circuit, it is collected at the counter electrode (C.E).

Step 4: Dye Regeneration and Electron Recapture;

Electron after reaching counter electrode is transferred to the electrolyte which consists of a redox couple. This electron regenerates the oxidized dye molecule in nanosecond timescale range. A loss of about 600 mV occurs which is the main reason which limits the V_{oc} of the cell. The loss occurs due to mismatch of energy between redox couple and the dye.

The complete steps of photon to current generation mechanism in DSSCs is shown by following equations where D is dye molecule, D^* excited dye molecule, D^+ oxidized dye molecule and e^- represents electron

1) $D + Photon \longrightarrow D^{*}_{(Lumo)}$ *(Excitation of Dye)*

2) $D^{*}_{(Lumo)} + TiO_2 \longrightarrow e^{-}_{(CB\ of\ TiO2)} + D^{+}$ *(Injection to semiconductor)*

3) $e^{-}_{(CB\ of\ TiO2)} + C.E \longrightarrow TiO_2 + e^{-}_{(C.E)} + electrical\ energy$ *(Electricity Generation)*

4) $D^{+} + \frac{3}{2}I^{-} \longrightarrow D + \frac{1}{2}I_3^{-}$ *(Dye Regeneration)*

5) $I_3^{-} + e^{-}_{(C.E)} \longrightarrow \frac{3}{2}I^{-} + C.E$ *(Electron Recapture)*

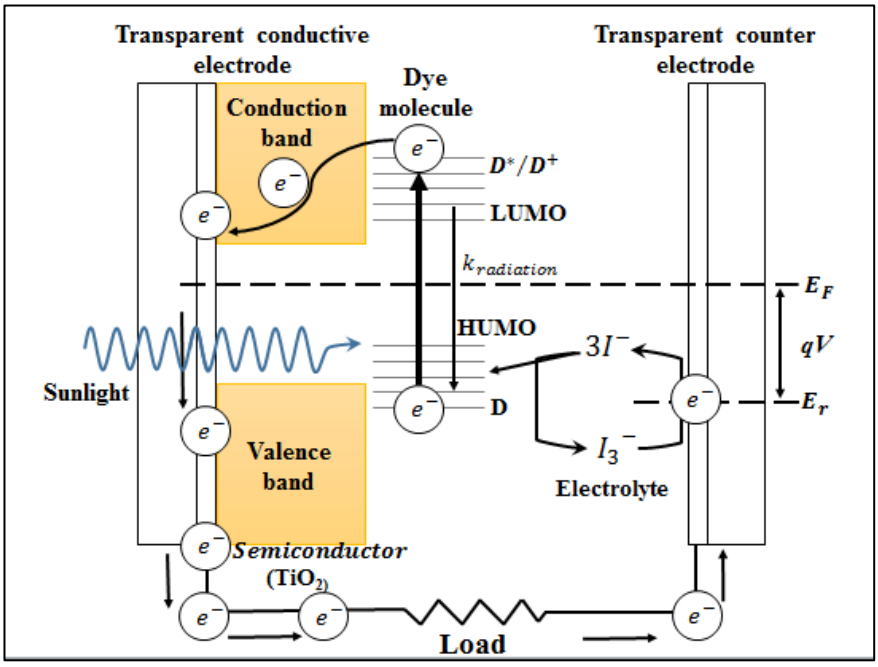

Fig. 2.1 Working of a Dye Sensitized Solar Cell.

2.1.3 Charge Transfer Kinetics in DSSCs

2.1.3.1 Electron injection process

The rate constant for the injection of electron from sensitizer to semiconductor conduction band is given by following expression of Fermi's golden rule

$$c = \frac{4\pi^2}{h} V^2 \rho(E)$$

Where c is rate constant for electron injection, h= Planck constant, V is electronic coupling of semiconductor and sensitizer and $\rho(E)$ is density of states of semiconductor conduction band. Hence from this expression it is clear that the electron injection rate

depends on the configuration of dye adsorbed on the wide band gap semiconductor and also on difference between E_{LUMO} of dye and $E_{C.B}$ of semiconductor.

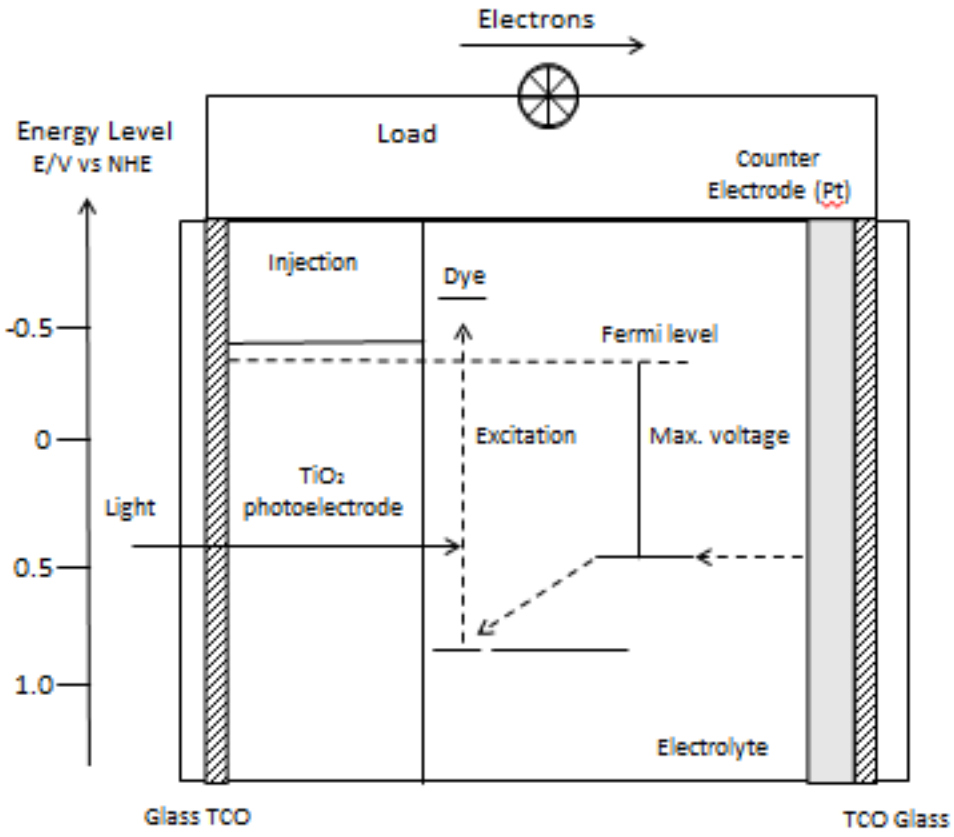

Fig. 2.2 Energy band diagram for DSSCs.

The rate constant for electron injection depends on the material of wide gap semiconductor used and on the electronic coupling between dye and semiconductor. Electron is injected from π^* orbital of excited dye molecule to CB of semiconductor. In TiO_2 based DSSCs, valence band consists of occupied 2d orbital of oxygen and conduction band consists of unoccupied 3d orbital of titanium with large and continuous density of states. N3 Dye adsorbs on TiO_2 surface with anchor group (carboxyl group) and results in large V between them. Hence efficient electron transfer takes place. Electron injection from dye to semiconductor has been studied using time resolved laser spectroscopy [28-47].

2.1.3.2 Recombination and dark current

Charge recombination reactions occurring at the interface between semiconductor and dye molecule are very slow as compared to the electron injection as explained earlier. Low recombinations lead to high cell performance due to efficient charge transfer. Charge recombinations between N3 molecule and TiO_2 semiconductor occurs due to the transfer of electrons from TiO_2 to Ru (III) (back electrons) whereas transfer of electrons from bipyridyl ligands to titania conduction band is responsible for electron injection. The transfer from TiO_2 to Ru (III) is a long distance process and hence is slower as compared to ultrafast electron injection. This is the reason for least recombination possibility at the dye / semiconductor interface.

Recombinations at the semiconductor/electrolyte interface causing dark current is a primary process in DSSCs [9]. Dark current or reverse bias leakage current is a small electric current flowing through the cell even when the cell is not exposed to irradiation or photons. An increase in dark current decreases V_{oc} of the cell as concluded from general equation of solar cell shown below [10]

$$V_{oc} = \frac{k_B T}{q} ln\left[\frac{I_{inj}}{I_{dark}} + 1\right]$$

Where I_{inj} is injection current, I_{dark} is dark current, T is absolute temperature of the cell, q is the magnitude of electron charge and k_B is boltzman constant. This equation relates V_{oc} to dark current and injection current.

The main reason for dark current in DSSCs is incomplete adsorption of dye on semiconductor surface. It occurs at points where the electrolyte is in direct contact with semiconductor. The following equation represents the dark current reaction in DSSCs

$$I_3^- + 2e^- (semiconductor) \longrightarrow 3I^-$$

These recombinations are associated with construction of DSSCs. Cells carefully made may lead to avoid such recombinations e.g. in cells based on ITO/FTO coated substrates, the above reaction may also occur at the surface of tin oxide when the TCO is not properly covered with semiconductor layer. But this reaction mostly occurs at semiconductor due to its high surface area as compared to SnO_2. Also the use of co-adsorbates like tert butylpyridine (TBP), a pyridine derivative, has been reported to

suppress dark current [11]. Co-adsorbates get adsorbed on the uncovered semiconductor surface and hence aid in improvement of V_{oc} by reducing dark current but may lead to decrease in J_{sc} due to negative shift in CB level of semiconductor. In p-n junction solar cells, the process of forward bias injection of electrons and holes is analogous to this reaction.

2.1.3.3 Electron transport

Electron transport in semiconductor films is an important process in these solar cells. Different mechanisms has been studied and suggested for the conduction of electrons in TiO_2 films like a trapping/de-trapping mechanism, diffusion mechanism and a mechanism that involves insulator metal transition. In general, the electrons diffuse by hopping 105 times between semiconductor particles. Studies have shown use of nanotube and nanowire structured semiconductors lead to higher diffusion rates and lower recombination [4] [12].

2.1.2 Factors affecting Photovoltaic performance DSSCs

2.1.2.1 Photovoltaic performance of a cell is based on Energy levels

Primarily, the photovoltaic performance of DSSCs depends on four energy levels of different components of the cell namely;

1. The ground state of sensitizer (HOMO).
2. The excited state of sensitizer (LUMO).
3. The Fermi level of semiconductor electrode (situated near CB level).
4. The potential of the electrolyte redox couple or mediator (I^-/I_3^-).

The energy difference between oxidized and ground states of sensitizer ($E_g=E_{HOMO}-E_{LUMO}$) determines the photocurrent. Smaller energy gap (E_g) allows absorption of long wavelength electromagnetic radiation from solar spectrum and hence larger photocurrent is obtained.

The difference in the conduction band level of semiconductor and LUMO of dye ($\Delta E_1=E_{LUMO}-E_c$) determines the efficiency of charge injection of excited electrons from dye to C.B of semiconductor. For effective charge injection, LUMO energy level of dye should be adequately negative than C.B of semiconductor.

Electron acceptance by oxidized dye molecule depends on the difference in dye HOMO level and redox potential of electrolyte ($\Delta E_2=E_{HOMO}-E_r$). The redox potential of redox couple should be adequately negative than energy level of HOMO of sensitizer for effective acceptance of electron by dye or effective regeneration of dye.

The max potential (V_{max}) in DSSCs is determined by E_f and E_r as evident by Fig. 2.1. In DSSC based on TiO_2 electrode and I^-/I_3^- redox couple electrolyte, E_r and E_f were calculated to be 0.4 V Vs normal hydrogen electrode (NHE) and -0.5 Vs NHE respectively [13]. Therefore, in this case

$$qV = Er - Ef$$

$$qV = 0.9\,V$$

But this value can vary as it also depends on other components like solvent of electrolyte as E_f also depends on components and concentrations of electrolyte components.

2.2 Components and Materials of Dye Sensitized Solar Cells

2.2.1 Substrates

The most employed substrates in DSSCs are clear glass substrates possessing high optical transparency in NIR and VIS regions [4]. These substrates are readily available and offer lower cost. These glass substrates contain thin film of transparent conducting oxide on one side which acts as a conductive film of low electrical resistance (10-29 Ω/sq). Mostly fluorine doped tin oxide (FTO) or indium doped tin oxide (ITO) is coated as transparent conductive oxide on glass substrates. The transparency level of this electrode is reduced after being coated with nanostructured material (e.g TiO_2).

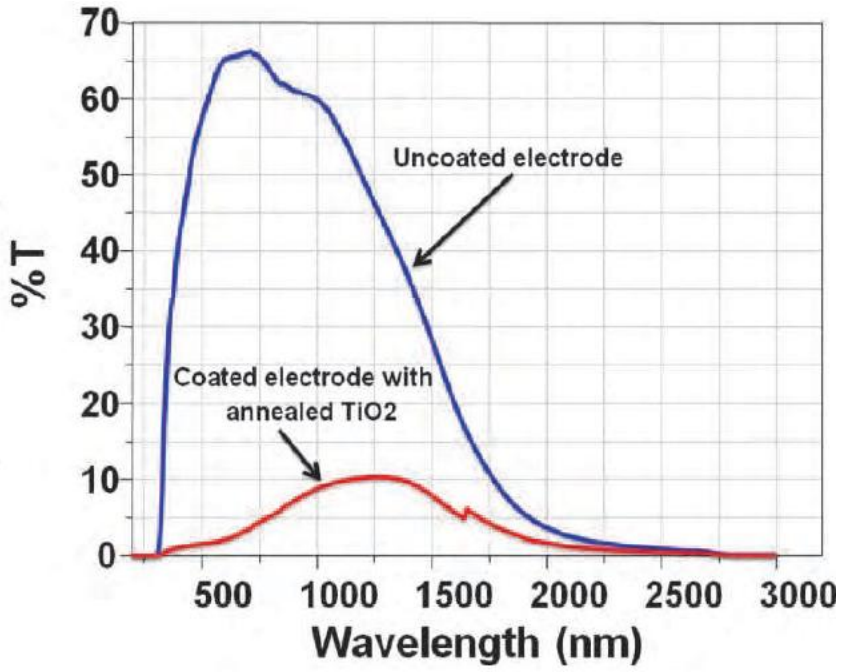

Fig. 2.3 Transmittance of TCO glass electrode before and after being coated with titania [10].

Other than conventional glass substrates, flexible metal substrates have also been used in DSSCs like titanium foil based substrate [12], Stainless steel based substrates [14] etc. Ti sheets are suitable as substrates because their Fermi level match with porous TiO_2 layer. Stainless steel is a low cost material but its oxidation forms an interlayer of Fe_2O_3. The energy level of this interlayer does not match with energy level of TiO_2, hence it is not suitable [15]. DSSCs are also made on light weight and flexible plastic substrates, but a big challenge for making such solid-state DSSCs is the formation of TiO_2 thin films at low temperature as plastic substrates offer temperature limitations [6]. Glass electrodes offer lower transparency but higher efficiency than plastic electrodes. This may be attributed to lower internal resistance of glass [16, 17].

2.2.2 Photo-anode

First and second generations of solar cells consisted of bulky semiconductor material based photoelectrodes e.g. silicon, cadmium sulphide, gallium arsenide etc. Cells made with these electrodes didn't show good stability as these photoelectrodes underwent photo-corrosion when exposed to light. Thus wide band gap semiconductors which were resistant to photo-corrosion were employed as photoanode materials in 3rd generation of solar cells. Sensitized wide band gap materials like TiO_2 and ZnO_2

showed good absorption of sensitizer. In DSSCs, there are three major roles played by photoanode:

(i) It provides a medium for the dye adsorption.
(ii) It accepts the excited electrons from the dye molecule into conduction band.
(iii) It transports the electron towards the TCO for its injection in external circuit.

Different semiconductors like TiO_2, Nb_2O_5 [18], ZnO [19, 20], SnO_2 [21], and $SrTiO_3$ [22] have been studied for their use in DSSCs as photoanode material. Nb_2O_5 and SnO_2 provided large roughness factor and increase in the diffusion length of generated electron [23]. Studies revealed TiO_2 to be the best material for photoanode due to its low cost, high availability, and chemical stability. To decrease recombinations and enhance photocatalytic efficiency use of coupled semiconductors like Bi_2S_3/TiO_2, ZnO/TiO_2 and CdS/TiO_2 has been reported [24-26]. ZnO has a band gap of 3.37 eV. The efficiency of ZnO photoanode based DSSC is less than that made with nanostructured TiO_2 photoanode due to insufficient sensitizer adsorption [27]. To enhance the separation of generated carriers, TiO_2 nanotubes have been reported to be beneficial [28].

As already explained, photoanode consists of mesoporous semiconductor thin films providing electrical connection with electrolyte and a medium for dye adsorption. Therefore the characteristics of this film like porosity, effective area, morphology, pore size etc. has direct influence on cell performance.

Porosity of electrode: Porosity of semiconductor electrode directly affects light absorption and electron transport. Optimizing the percentage of porosity in electrode can lead to better cell performance. Increase in porosity increases the light absorption by dye molecule and decreases the area of dye absorption. The reduction in adsorption area is due ti decrease in density of nanostructures. Patel et al. [29] varied the porosity of TiO_2 based electrode between 30-70% and reported that best performance was observed around 40% porous system. So the optimal porosity to achieve best device performance is optimized to be 40%. This porosity value is applicable to other semiconductor materials as well other than TiO_2 [30].

Thickness of Electrode: Thickness of the thin film is another factor that affects the cell performance. An increase in J_{sc} with increasing thickness of film from 1µm to 20µm has been reported in literature. 20 µm thickness is the optimized thickness of the film as increasing it beyond this value degrades the cell performance and decreases J_{sc}. The initial increase in J_{sc} may be attributed to the increase in internal surface area for dye absorption and hence light absorption. Hence thicker films adsorb more photons. The decrease in J_{sc} on further increasing thickness is because of the decrease in current density as more thickness causes hindrance for photons to reach lower part of photoanode. Increasing thickness decrease V_{oc} of the cell which can be explained by electron dilution effect [31]. The intensity of light decreases on penetrating into electrode and hence it decreases the excessive electron density. Another factor for the decrease in V_{oc} is that thicker electrodes possess higher series resistance [32].

2.2.3 Counter Electrode

Reduction of dye ions forms I_3^- ions (tri iodide) which are supposed to be reduced to iodide ions (I^-) at counter electrode. High electro-catalytic activity is key feature of the counter electrode. Platinum coated TCO substrate are widely employed as counter electrodes in DSSCs [33]. Because of the high price of platinum scientist are looking for low cost alternative options. Recently carbon nanotubes and graphene have been used as promising materials for counter electrode [34, 35]. Graphene is a sheet of hexagonally arranged sheets of sp^2 carbon atoms and possess high electro-catalytic activity and good conduction.

2.2.4 Electrolyte

The role of electrolyte in DSSCs is to de-oxidize the oxidized dye molecule by donating electron. It regenerates the dye molecule and arbitrates electrons between photoanode and counter electrode. Liquid electrolytes, solid state electrolytes, or quasi-solid state electrolytes are being used in DSSCs, most common being the liquid electrolytes. The following aspects should be kept in mind while selecting an electrolyte for use in DSSCs [36];

1) Electrolyte must be able to regenerate the oxidized dye molecule to its ground state rapidly and should be able to transport electrons between the two electrodes efficiently.

2) It should have good interfacial contact with semiconductor layer and counter electrode and should possess higher conductivity to allow fast diffusion of electrons.

3) It must not desorb or degrade dye from semiconductor layer and should possess long term stability (including electrochemical, thermal, optical, chemical and interfacial stability).

4) Electrolyte should not possess absorption in visible range.

2.2.4.1 Liquid Electrolytes

Electrolyte is a non-protonic organic solvent containing a redox system, such as I^-/ I_3^- couple. LiI, KI, R_4NI (tetra alkyl ammonium iodide) and NaI are mostly used in solvents like propionitrile, ethylene glycol, acetonitrile and propylene carbonate. The max efficiency has been achieved using liquid electrolyte in DSSC system[37]. I^-/ I_3^- and Br^-/Br_3^- are the two most common couples used in liquid based electrolyte systems. Suri et al. [38] reported enhanced V_{oc} and J_{sc} when they replaced I^-/ I_3^- redox couple with Br^-/Br_3^-. The redox electrolyte must be capable of reducing I_3 ions efficiently and quickly by injection of electrons.

Photovoltaic performance is dependent on each component of liquid electrolyte like redox couple and solvent or additive (not a compulsory component but small amount could be added to enhance photovoltaic properties). Organic solvent provides an environment for dissolution and diffusion of redox ions. The most important characteristics of organic solvent are dielectric constant of solvent, its viscosity and its donor number. A solvent with low viscosity is recommended since the ion conductivity depends on viscosity of solvent. Viscous the solvent, lesser is the ion conductivity, lower is the cell performance.

Liquid electrolytes limits cell stability and hence limits the commercialization of DSSCs because

- Solvents used are volatile that easily evaporates affecting cell stability and arising problems related to sealing of cell. These electrolytes cause corrosion of platinum electrode and photo-degradation and desorption of dye molecules [39].
- Liquid electrolytes may get leaked hence reducing the lifespan of the cell [40].

- Using liquid electrolytes in DSSCs makes it difficult to fabricate multi cell modules. Efficient modules must be separated chemically and linked electrically [41].

To overcome these limitations, scientists have been working on alternate materials to replace organic solvents in electrolytes

2.2.4.2 Solid State Electrolytes

Solid state DSSCs can be fabricated using two types of electrolyte medium;

1) Hole transport materials (HTMs)

2) Solid state electrolyte containing redox couple

DSSCs employing solid state electrolyte contains I^-/ I_3^- redox couple and has similar operation to liquid electrolyte based DSSCs. Operation of HTM based DSSCs differ only that the oxidized dye molecule is deoxidized by electron which is donated by the hole conductor [37]. The use of copper based inorganic HTM like CuBr, CuSCN and CuI as electrolyte materials in DSSCs has been investigated [5, 42]. A complete hole conducting/transporting layer of such materials can be deposited using vacuum or solution based deposition methods. They show good hole transporting ability but couldn't show good efficiency and stability. Therefore these shift the research interests towards organic HTMs. Organic light emitting diodes and organic thin film transistors are low cost HTMs being used as organic HTMs in DSSCs [43]. Zhang et al. used poly (3-hexylhtiophene (P3HT) as a polymeric hole transporter and reported an efficiency of 3.85% [44]. The efficiencies of HTM based DSSCs are quite lower than liquid electrolyte DSSCs due to higher recombinations and lower intrinsic conductivities of HTMs. Other good candidate options opening doors for investigations are PEDOT or PEDOT:TMA.

2.2.4.3 Quasi Solid State Electrolytes

Quasi solid state, also known as gel state, is a state of matter that is neither liquid nor solid. Quasi solid state electrolytes consist of a polymer host filled with liquid electrolyte. These electrolytes possess diffusive property of a liquid and cohesive property of a solid therefore assigning good interfacial contact and high ionic conductivity despite having high viscosity. They also show good stability [45, 46].

Good photovoltaic properties have been observed by adding polyvinylidene fluoride co hexafluropropylene) to KI/I_2 electrolyte [40].

2.2.5 Dye Sensitizers

The role of dye in DSSCs is to sensitize wide band gap semiconductor. Upon irradiation, dye molecule absorbs photon and gets oxidized. The excited electron is transported into conduction band of semiconductor which transports it further to outer circuit through the TCO layer.

Dyes are required to possess special characteristics as it is an important component of DSSC. The most important of them are [47, 48]

High molar extinction co-efficient of dye: The fraction of light absorbed by the cell is determined by the absorption coefficient of dye and concentration of the dye. Dye must have a high absorption coefficient in visible region and should be adsorbed properly on semiconductor layer to provide dense coverage of surface. Increased absorption of photoanode lets us decrease its layer thickness and hence reduction in recombination probability. If novel dyes could be synthesized that would show absorption NIR region, an increase in J_{sc} is expected. None of the dyes absorbs in region 900-1100 nm which is one of the reasons for DSSCs to exhibit less efficiency than crystalline silicon solar cell.

Energy level: The conduction band of semiconductor should be 0.2-0.3 eV less than the energy level of oxidized dye molecule so that efficient charge injection can take place. If charge injection is slow or inefficient, there is a possibility of back reaction i-e the reduction of oxidized dye molecule by conduction band electron.

Overlapping orbitals: Charge injection in semiconductor conduction band (3d-orbital of titanium) takes place from π^* orbital of anchoring group of dye molecule. So, There should be a good overlapping between the π^* orbitals of dye molecule and conduction band of semiconductor for efficient charge injection. This injection should take place in femto to pico second and time scale for recombination must be micro to mili second to ensure good injection yield.

Keeping above points in mind, researchers have been trying to synthesize new dyes like porphyrins and phthalocyanines. Porphyrins lack the absorption of red light and near infrared radiations. Phthalocyanines have LUMO level too low to efficiently transfer excited electron to conduction band of semiconductor. Enhanced efficiencies has been

reported using coumarine or polyene type sensitizer [49, 50]. Many natural sensitizers from fruit of calafate, berries and black rice etc. and natural anthocyanins have been used but none could help in commercialization of DSSCs [51-53]. Polypyridyl complexes of ruthenium with thiocyanate ligands have shown the best photovoltaic performance and stability as they exhibit sharp metal to ligand charge transfer bands in visible region of electromagnetic spectrum which is very necessary for injection of charge into conduction band of semiconductor efficiently.

2.2.5.1 N3 Dye

In 1970's, tris(2,2'-bipyridyl)Ru(II) sensitizer was extensively employed in DSSCs because they possessed long lived excited state. Sooner the attention of researchers shifted towards closely related bis(2,2-bbipyridyl)LL'Ru(II) complexes because they possessed comparatively broader absorption spectrum in visible region. So in 1990's N3 dye was introduced and is the best and most used sensitizer since then [54, 55]

Structure and excitation mechanism

It consists of two thiocyanate ligands (LL'), the choromophore of the dye, as shown in Fig. 2-3. These ligands are attached to carboxylate group, the anchoring group. The thiocyanate ligands are the most delicate and weak part of N3 dyes. Researchers have been trying to replace thiocyanate donor ligands but no remarkable results have been achieved [56]. The choromophore of dye [SCN] has its role in absorption of visible light and anchoring group forms ester linkages and bidentate coordination to immobilize the sensitizer to film surface. N3 dye show maximum absorption at 400 nm (extinction co-efficient $1.41*10^4\ M^{-1}cm^{-1}$) and 535 nm (extinction coefficient $=1.45*10^4\ M^{-1}cm^{-1}$) due to metal to ligand charge transition. The transition of electron from metal to π^* of anchoring group is responsible for excitation of the dye molecule [47].

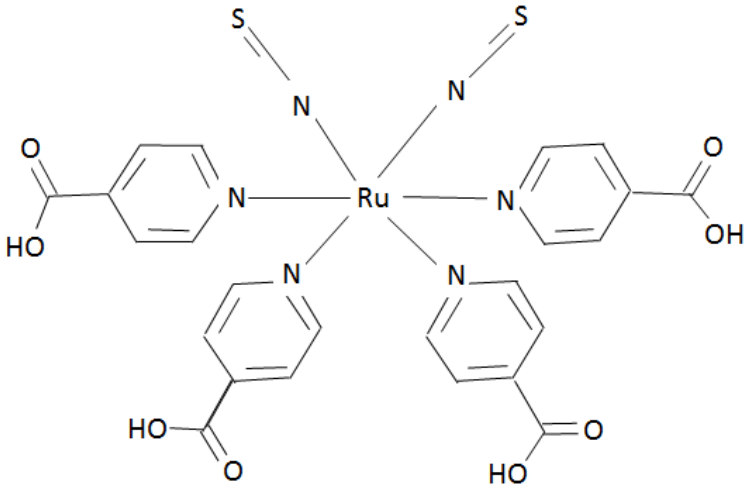

Fig. 2.4 Structure of N3 dye.

Protonation level of N3

The protonation level (number of protons) of dye has a direct effect on energy level of semiconductor conduction band and hence on efficiency of device [57]. The dye molecules are chemically linked to semiconductor in esterification and the protons in carboxylic group are partly shifted to the surface of semiconductor. The dye N712 contains zero protons and N3 contains 4 protons, and between the two N3 proved to be a better option [58]. Fermi level of TiO_2 is shifted down when number of protons is increased as they charge TiO_2 surface positively. This creates an electric field at the surface which increases the dye adsorption (anionic ruthenium complex) and also aids electron injection from dye to TiO_2.

Stability of N3 dye

The best feature about N3 dye is that the molecules show best compatibility with TiO_2 surface. It can endure 10^7-10^8 excitation cycles on TiO_2 surface but only 200 in solution because of the ester linkage with TiO_2. The dye, on adsorption, forms charge transfer complex with Ti^{3+} states. These states are created when charge is injected or they exist partly. The charge transfer complex allows local export of entropy by inducing a π back bonding and hence stabilizes the ruthenium complex [59].

Hence, N3 sensitizer shows good photovoltaic properties like matching excited and ground states or energy levels, good electro-chemical stability, broad absorption spectrum and long excited state lifetime.

Summary

In this chapter details on the working principles, factors affecting performance of DSSC, components and available materials for Dye sensitized Solar Cells have been summarized. The excitation of electron in dye adsorbed on wide band gap semiconductor photoanode when exposed to electromagnetic radiation causes the generation of electricity. The energy levels of the dye, wide band gap semiconductor and electrolyte strongly affects the performance of DSSCs. there are a large variety of available substrates, semiconductor material for photoanode, sensitizer and electrolytes for DSSCs. Solid state electrolytes can be used to replace liquid electrolytes (like I^-/I_3^-) electrolyte to enhance the stability of the cells but they yield low efficiency. Liquid electrolytes are volatile and degrade with increasing temperature but yield high efficiencies. TiO_2 and N3 dye are among the most suitable materials for photoanode of DSSCs. The problem with using TiO_2 as a semiconductor material for photoanode is that it absorbs only UV radiation of electromagnetic spectrum. Dyes are adsorbed on their surface to enhance their absorption in visible range and the main function of the dye is to donate electron on absorption of light.

References

[1] J. Lagref, M. K. Nazeeruddin, and M. Grätzel, "Artificial photosynthesis based on dye-sensitized nanocrystalline TiO_2 solar cells," Inorganica Chimica Acta, vol. 361, pp. 735-745, 2008.

[2] G. P. Smestad, "Education and solar conversion:: demonstrating electron transfer," Solar Energy Materials and Solar Cells, vol. 55, pp. 157-178, 1998.

[3] M. Späth, P. Sommeling, J. Van Roosmalen, H. Smit, N. Van der Burg, D. Mahieu, N. Bakker, and J. Kroon, "Reproducible manufacturing of dye-sensitized solar cells on a semi-automated baseline," Progress in Photovoltaics: Research and Applications, vol. 11, pp. 207-220, 2003.

[4] K. E. Jasim, "Dye sensitised solar cells-working principles, challenges and opportunities," A chapter in Solar Cells/Book, vol. 2, 2011.

[5] K. Tennakone, G. Kumara, I. Kottegoda, K. Wijayantha, and V. Perera, "A solid-state photovoltaic cell sensitized with a ruthenium bipyridyl complex," Journal of Physics D: Applied Physics, vol. 31, p. 1492, 1998.

[6] H. C. Weerasinghe, F. Huang, and Y.-B. Cheng, "Fabrication of flexible dye sensitized solar cells on plastic substrates," Nano Energy, vol. 2, pp. 174-189, 2013.

[7] S. William A. Vallejo L., Prof. Leonid A. Kosyachenko (Ed.), The Chemistry and Physics of Dye-Sensitized Solar Cells, a chapter in Solar Cells - Dye-Sensitized Devices vol. ISBN: 978-953-307-735-2, InTech, DOI: 10.5772/20609. : intech, 2011.

[8] K. Hara and H. Arakawa, "Dye-Sensitized Solar Cells," Handbook of Photovoltaic Science and Engineering, pp. 663-700.

[9] J. Van de Lagemaat, N.-G. Park, and A. Frank, "Influence of electrical potential distribution, charge transport, and recombination on the photopotential and photocurrent conversion efficiency of dye-sensitized nanocrystalline TiO2 solar cells: a study by electrical impedance and optical modulation techniques," The Journal of Physical Chemistry B, vol. 104, pp. 2044-2052, 2000.

[10] T. L. Floyd, Electronic devices: conventional current version: Pearson Prentice Hall, 2008.

[11] S. Huang, G. Schlichthörl, A. Nozik, M. Grätzel, and A. Frank, "Charge recombination in dye-sensitized nanocrystalline TiO2 solar cells," The Journal of Physical Chemistry B, vol. 101, pp. 2576-2582, 1997.

[12] T. B. Meyer, A. F. Meyer, and D. Ginestoux, "Flexible solid-state dye solar cells," in International Symposium on Optical Science and Technology, 2002, pp. 13-20.

[13] A. Hagfeldt and M. Grätzel, "Molecular photovoltaics," Accounts of Chemical Research, vol. 33, pp. 269-277, 2000.

[14] C. Lee, W. Lee, W.-T. Li, C. Yang, and P. Kao, "StSt triple-layered conducting substrates for large active area dye-sensitized solar cells," Materials research bulletin, vol. 48, pp. 2625-2629, 2013.

[15] S. K. Balasingam, M. G. Kang, and Y. Jun, "Metal substrate based electrodes for flexible dye-sensitized solar cells: fabrication methods, progress and challenges," Chemical Communications, vol. 49, pp. 11457-11475, 2013.

[16] S. Ito, G. Rothenberger, P. Liska, P. Comte, S. M. Zakeeruddin, P. Péchy, M. K. Nazeeruddin, and M. Grätzel, "High-efficiency (7.2%) flexible dye-sensitized solar cells with Ti-metal substrate for nanocrystalline-TiO 2 photoanode," Chemical Communications, pp. 4004-4006, 2006.

[17] Y. Jun, J. Kim, and M. G. Kang, "A study of stainless steel-based dye-sensitized solar cells and modules," Solar Energy Materials and Solar Cells, vol. 91, pp. 779-784, 2007.

[18] A. Le Viet, R. Jose, M. Reddy, B. Chowdari, and S. Ramakrishna, "Nb2O5 photoelectrodes for dye-sensitized solar cells: choice of the polymorph," The Journal of Physical Chemistry C, vol. 114, pp. 21795-21800, 2010.

[19] A. B. Martinson, J. W. Elam, J. T. Hupp, and M. J. Pellin, "ZnO nanotube based dye-sensitized solar cells," Nano letters, vol. 7, pp. 2183-2187, 2007.

[20] M. Quintana, T. Edvinsson, A. Hagfeldt, and G. Boschloo, "Comparison of dye-sensitized ZnO and TiO2 solar cells: studies of charge transport and carrier lifetime," The Journal of Physical Chemistry C, vol. 111, pp. 1035-1041, 2007.

[21] A. Birkel, Y.-G. Lee, D. Koll, X. Van Meerbeek, S. Frank, M. J. Choi, Y. S. Kang, K. Char, and W. Tremel, "Highly efficient and stable dye-sensitized solar

cells based on SnO2 nanocrystals prepared by microwave-assisted synthesis," Energy & Environmental Science, vol. 5, pp. 5392-5400, 2012.

[22] S. Yang, H. Kou, J. Wang, H. Xue, and H. Han, "Tunability of the band energetics of nanostructured SrTiO3 electrodes for dye-sensitized solar cells," The Journal of Physical Chemistry C, vol. 114, pp. 4245-4249, 2010.

[23] B. V. Bergeron, A. Marton, G. Oskam, and G. J. Meyer, "Dye-sensitized SnO2 electrodes with iodide and pseudohalide redox mediators," The Journal of Physical Chemistry B, vol. 109, pp. 937-943, 2005.

[24] H. Yu, J. Huang, H. Zhang, Q. Zhao, and X. Zhong, "Nanostructure and charge transfer in Bi2S3-TiO2 heterostructures," Nanotechnology, vol. 25, p. 215702, 2014.

[25] N. Ghows and M. Entezari, "A novel method for the synthesis of CdS nanoparticles without surfactant," Ultrasonics sonochemistry, vol. 18, pp. 269-275, 2011.

[26] G. Marci, V. Augugliaro, M. J. Lopez-Munoz, C. Martin, L. Palmisano, V. Rives, M. Schiavello, R. J. Tilley, and A. M. Venezia, "Preparation characterization and photocatalytic activity of polycrystalline ZnO/TiO2 systems. 1. Surface and bulk characterization," The Journal of Physical Chemistry B, vol. 105, pp. 1026-1032, 2001.

[27] J. B. Baxter, A. Walker, K. Van Ommering, and E. Aydil, "Synthesis and characterization of ZnO nanowires and their integration into dye-sensitized solar cells," Nanotechnology, vol. 17, p. S304, 2006.

[28] Y. Duan, N. Fu, Q. Liu, Y. Fang, X. Zhou, J. Zhang, and Y. Lin, "Sn-doped TiO2 photoanode for dye-sensitized solar cells," The Journal of Physical Chemistry C, vol. 116, pp. 8888-8893, 2012.

[29] K. R. c. a. I. m. Dipal B. patel, "Effect of Electrode's Geometric shape, Thickness and Porosity on the Performance of Dye Sensitized Solar Cell," IJTEMAS, vol. III, january 2014 2014.

[30] M. Ni, M. K. Leung, D. Y. Leung, and K. Sumathy, "An analytical study of the porosity effect on dye-sensitized solar cell performance," Solar Energy Materials and Solar Cells, vol. 90, pp. 1331-1344, 2006.

[31] R. Gómez and P. Salvador, "Photovoltage dependence on film thickness and type of illumination in nanoporous thin film electrodes according to a simple diffusion model," Solar Energy Materials and Solar Cells, vol. 88, pp. 377-388, 2005.

[32] M. Ni, M. K. Leung, and D. Y. Leung, "Theoretical modelling of the electrode thickness effect on maximum power point of dye-sensitized solar cell," The Canadian Journal of Chemical Engineering, vol. 86, pp. 35-42, 2008.

[33] Z. Tang, J. Wu, M. Zheng, J. Huo, and Z. Lan, "A microporous platinum counter electrode used in dye-sensitized solar cells," Nano Energy, vol. 2, pp. 622-627, 2013.

[34] S. Huang, H. Sun, X. Huang, Q. Zhang, D. Li, Y. Luo, and Q. Meng, "Carbon nanotube counter electrode for high-efficient fibrous dye-sensitized solar cells," Nanoscale research letters, vol. 7, pp. 1-7, 2012.

[35] H. Wang and Y. H. Hu, "Graphene as a counter electrode material for dye-sensitized solar cells," Energy & Environmental Science, vol. 5, pp. 8182-8188, 2012.

[36] B. Li, L. Wang, B. Kang, P. Wang, and Y. Qiu, "Review of recent progress in solid-state dye-sensitized solar cells," Solar Energy Materials and Solar Cells, vol. 90, pp. 549-573, 2006.

[37] M. Grätzel, "Photovoltaic performance and long-term stability of dye-sensitized meosocopic solar cells," Comptes Rendus Chimie, vol. 9, pp. 578-583, 2006.

[38] P. Suri, M. Panwar, and R. Mehra, "Photovoltaic performance of dye-sensitized ZnO solar cell based on Eosin-Y photosensitizer," Materials Science-Poland, vol. 25, pp. 137-144, 2007.

[39] J. Wu, Z. Lan, S. Hao, P. Li, J. Lin, M. Huang, L. Fang, and Y. Huang, "Progress on the electrolytes for dye-sensitized solar cells," Pure and Applied Chemistry, vol. 80, pp. 2241-2258, 2008.

[40] M. G. Kang, N.-G. Park, K. S. Ryu, S. H. Chang, and K.-J. Kim, "A 4.2% efficient flexible dye-sensitized TiO< sub> 2</sub> solar cells using stainless steel substrate," Solar Energy Materials and Solar Cells, vol. 90, pp. 574-581, 2006.

[41] M. Matsumoto, Y. Wada, T. Kitamura, K. Shigaki, T. Inoue, M. Ikeda, and S. Yanagida, "Fabrication of Solid-State Dye-Sensitized TiO2 Solar Cell Using Polymer Electrolyte," Bulletin of the Chemical Society of Japan, vol. 74, pp. 387-393, 2001.

[42] K. Tennakone, G. Kumara, A. Kumarasinghe, K. Wijayantha, and P. Sirimanne, "A dye-sensitized nano-porous solid-state photovoltaic cell," Semiconductor Science and Technology, vol. 10, p. 1689, 1995.

[43] S. Luzzati, M. Basso, M. Catellani, C. Brabec, D. Gebeyehu, and N. Sariciftci, "Photo-induced electron transfer from a dithieno thiophene-based polymer to TiO< sub> 2</sub>," Thin Solid Films, vol. 403, pp. 52-56, 2002.

[44] W. Zhang, R. Zhu, F. Li, Q. Wang, and B. Liu, "High-performance solid-state organic dye sensitized solar cells with P3HT as hole transporter," The Journal of Physical Chemistry C, vol. 115, pp. 7038-7043, 2011.

[45] Z. Lan, J. Wu, S. Hao, J. Lin, M. Huang, and Y. Huang, "Template-free synthesis of closed-microporous hybrid and its application in quasi-solid-state dye-sensitized solar cells," Energy Environ. Sci., vol. 2, pp. 524-528, 2009.

[46] W. Kubo, K. Murakoshi, T. Kitamura, S. Yoshida, M. Haruki, K. Hanabusa, H. Shirai, Y. Wada, and S. Yanagida, "Quasi-solid-state dye-sensitized TiO2 solar cells: effective charge transport in mesoporous space filled with gel electrolytes containing iodide and iodine," The Journal of Physical Chemistry B, vol. 105, pp. 12809-12815, 2001.

[47] M. K. Nazeeruddin, E. Baranoff, and M. Grätzel, "Dye-sensitized solar cells: a brief overview," Solar Energy, vol. 85, pp. 1172-1178, 2011.

[48] M. Grätzel, "Dye-sensitized solar cells," Journal of Photochemistry and Photobiology C: Photochemistry Reviews, vol. 4, pp. 145-153, 2003.

[49] K. Hara, M. Kurashige, S. Ito, A. Shinpo, S. Suga, K. Sayama, and H. Arakawa, "Novel polyene dyes for highly efficient dye-sensitized solar cells," Chemical Communications, pp. 252-253, 2003.

[50] R. Sánchez-de-Armas, M. Á. San Miguel, J. Oviedo, and J. F. Sanz, "Coumarin derivatives for dye sensitized solar cells: a TD-DFT study," Physical Chemistry Chemical Physics, vol. 14, pp. 225-233, 2012.

[51] A. S. Polo and N. Y. Murakami Iha, "Blue sensitizers for solar cells: natural dyes from Calafate and Jaboticaba," Solar Energy Materials and Solar Cells, vol. 90, pp. 1936-1944, 2006.

[52] S. Hao, J. Wu, Y. Huang, and J. Lin, "Natural dyes as photosensitizers for dye-sensitized solar cell," Solar Energy, vol. 80, pp. 209-214, 2006.

[53] J. Fernando and G. Senadeera, "Natural anthocyanins as photosensitizers for dye-sensitized solar devices," Current Science, vol. 95, pp. 663-666, 2008.

[54] M. K. Nazeeruddin, A. Kay, I. Rodicio, R. Humphry-Baker, E. Müller, P. Liska, N. Vlachopoulos, and M. Grätzel, "Conversion of light to electricity by cis-X2bis (2, 2'-bipyridyl-4, 4'-dicarboxylate) ruthenium (II) charge-transfer sensitizers (X= Cl-, Br-, I-, CN-, and SCN-) on nanocrystalline titanium dioxide electrodes," Journal of the American Chemical Society, vol. 115, pp. 6382-6390, 1993.

[55] A. Adeloye, P. Ajibade, F. Cummings, L. Le Roux, S. Mamphweli, "Synthesis, photophysical and preliminary investigation of the dye-sensitized solar cells properties of functionalized anthracenyl-based bipyridyl and phenanthrolyl Ru (II) complexes," Journal of Chemical Sciences, vol. 125, pp. 17-27, 2013.

[56] Y. Qin and Q. Peng, "Ruthenium sensitizers and their applications in dye-sensitized solar cells," International Journal of Photoenergy, vol. 2012, 2012.

[57] S. G. Yan and J. T. Hupp, "Semiconductor-based interfacial electron-transfer reactivity: decoupling kinetics from pH-dependent band energetics in a dye-sensitized titanium dioxide/aqueous solution system," The Journal of Physical Chemistry, vol. 100, pp. 6867-6870, 1996.

[58] F. Schiffmann, J. VandeVondele, J. r. Hutter, R. Wirz, A. Urakawa, and A. Baiker, "Protonation-dependent binding of ruthenium bipyridyl complexes to the anatase (101) surface," The Journal of Physical Chemistry C, vol. 114, pp. 8398-8404, 2010.

[59] L. Andrade, S. M. Zakeeruddin, M. K. Nazeeruddin, H. A. Ribeiro, A. Mendes, and M. Graetzel, "Influence of Different Cations of N3 Dyes on Their Photovoltaic Performance and Stability," International Journal of Chemical Engineering, vol. 2009, 2009.

Chapter 3

Why Metal Doping in Titania

3.1 Why Titania Based Electrode for DSSCs

Titania is an inexpensive, chemically stable, nontoxic, and biocompatible material with interesting photocatalytic activities and high dielectric constant [1]. Nanoscale titania is a multifunctional material that has its applications as anode material in DSSCs and many other fields [2]. Titania is an n-type semiconductor because of presence of oxygen deficiency [1]. It has three polymorphs: brookite (orthorhombic), rutile (tetragonal), and anatase (tetragonal). The band gap of brookite is approximately 3.2eV, rutile has a band gap of 3.0eV, and band gap of anatase is 3.2eV. Anatase and rutile are the main polymorphs [3].

3.1.1 Photocotalytic Mechanism in Titania

The photocatalytic mechanism in titania starts with the absorption of photon. The excitation occurs when the photons with energy equal to or greater than the band gap of titania is absorbed. This allows the formation of an electron-hole pair on the surface of titania molecule. A hole (positive) is created in Valence band (VB) and an excited electron is promoted to the Conduction Band (CB). The electrons in Excited-state can get trapped in metastable states on surface, dissipate the input energy as heat due to recombination or react with electron acceptors/donors on semiconductor surface [4]. Anatase possesses the energy band 3.2 eV, which corresponds to 400 nm in electromagnetic spectra. The electron in pristine titania gets excited when irradiated to photons in UV region which constitutes only 4 % of total solar spectrum and about 40 % solar photons belongs to visible region. Also material efficiency is reduced due to recombination [5]. Scientists have been trying to induce visible light activity and enhance generated carrier separation efficiency by introducing different changes in titania like incorporating nonmetals, transition metals, rare earth metals, creating oxygen vacancies and introducing structural defects [6, 7]. The incorporation of dopants

and defects create sub band states in titania band gap and enhance their visible light absorption by shifting the absorption edge towards visible region.

3.2 Methods to Enhance Visible Light Absorption in Titania

Several methods have been reported in literature to enhance the visible light photoactivity of titania.

1) To enhance spectral response of titania it has been doped by metals (Cu, Fe, Mg, Cr etc.) and nonmetal impurities (B, N etc.).

2) To enhance the separation of generated carriers, titania nanotubes have been reported to be beneficial [2].

3) It has been found that noble metal and titania heterogeneous materials have excelled titania nanotubes and doped titania in properties as these heterogeneous materials inhibits the recombination's and enhances visible light absorption [9, 10].

4) To decrease recombination and enhance photocatalytic efficiency use of coupled semiconductors like $Bi_2S_3TiO_2$, ZnO/TiO_2 and CdS/TiO_2 has been reported [11-13].

There are many ways to dope titania like ion assisted Sputtering, ion implantation, CVD etc. But these processes are very expensive. Solution based processes for doping like sol-gel and other hydrothermal processes contribute cost effective and large scale production [8, 14]. The most important and highly employed method for synthesizing solution based cost effective method is sol-gel synthesis.

3.3 How Metal Doping in Titania Increases its Visible Light Absorption

When metals are doped in titania, three different modification mechanisms have been suggested, formation of impurity energy levels, narrowing of band gap and formation of oxygen vacancies [8].

Doping generates an intermediate energy level between valence band and conduction band of titnai. Therefore metal doped titania shows enhanced visible photoactivity due to formation of this new energy level in band gap of titania. It is formed by the scattering of metal nanoparticles in its lattice [8]. Doping titania with a transition metal leads to the reduction in the band gap energy which is attributed to the inclusion of metal ions into titania crystal lattice. It has been studied that doping titania with aliovalent ions changes the material properties and absorption properties because of the modification in local lattice symmetry and defects. When titania is doped with metal, metal ions either locate themselves on the surface sites or inside bulk titania. This causes lattice deformation due to rearrangement of adjoining atoms to neutralize charge deficiency. This lattice deformation and rearrangement modifies electronic structure and hence the band gap shift occurs.

Also, oxygen vacancies are created due to presence of small amounts of metal ions in the lattice sites of titania [4, 9]. These are created due to charge compensation effect.

3.4 Discussion on Metal doped Titania Based DSSCs

When titania is doped with metals, the dispersion of metal nanoparticles in titania matrix produces a new energy level. The electrons need less energy to excite from defect state to CB of titania as compared to the photon energy required in exciting electrons in undoped titania. Metal doping offers reduction in electron-hole recombinations by improved trapping of electrons and enhanced photocatalytic activity [8]. Considering crystal structure of titania, it is difficult to substitute O^- with any other anion than to replace Ti^{4+} with another cation because of the difference in ionic radii and charge states.

Cationic doping of TiO_2 with rare earth metals and transition metals (such as Sm, Cu, Nd, Zr, Gb, Zn, Pr , Co, Er, Ni, Ce, Cr, La, Mn, Pt, Mo, Ag, Nb, Au, V, Sn, Fe, Ru or W) has been extensively studied. Researchers have found that doping titania with transition metal increase thermal stability, decrease photothreshold energy of titania. A decrease in lifetime of carriers has also been indicated [1]. This limits the overall conversion efficiencies. Sometimes transition metals in TiO_2 behave as trapping sites for generated electron-hole pairs and hence the inclusion of these metals in titania leads

to lowering of quantum efficiency. In anatase phase, they can also cause thermal instability. Despite doping metals in TiO_2, a reduction in band gap energy has been attained by researchers, but an exceptional enhancement in photocatalytic activity has not been observed [2, 3].

Doping TiO_2 semiconductor of photoanode render three main advantages in DSSCs: reduction in the photocatalytic activity of DSSCs, reduction in band gap thus enhancement in efficiency and reduction in recombination rate. Some researcher have studied and reported better device performances when utilizing doped semiconductor as compared to performance of cells based on undoped semiconductor. Several dopants have been doped in titania semiconductor of DSSCs but none of them could enhance the open circuit voltage (V_{oc}) and short-circuit current density (J_{sc}) together at the same device.

Feng et al. [18] prepared Ta-doped titania nanowire arrays for DSSCs and found a considerable increase in open circuit voltage (V_{oc}) due to negative shifting of CB of titania. A decrease in photoconductivity of chromium doped TiO_2 has been indicated. The decrease is due to presence of Cr^{3+} ions in lattice displacing Ti^{4+} ions [19] . Whereas, M. Geetha et al. [20] reported doping chromium showed improvement in photoelectric performance of dye sensitized solar cells. They found an enhancement of light to electric conversion efficiency by a factor of 2.33 with 0.05 mol % Cr doping in titania photoanode. Tran van nam et al. [21] found doping magnesium caused a negative shift of the CB edge 1.142 and -1.16 eV for surface and bulk respectively. They also observed shift of Fermi level to negative energy. These effects improved J_{sc} but decreased the V_{oc} of DSSCs. Yandong Duan et al. [2] studied the effect of Sn doping in titania photoanode of DSSCs and found 12.1 % increase in efficiency compared with efficiency of cell containing pure titania based photoanode. Maciej Zalas and Maciej Klein [22] studied the influence of rare earth metal doping on performance of DSSCs. They found doping had no effect on crystal structure of electrode but strongly affect properties of DSSCs and a change in electronic properties was reported. These modified electrodes prevented back transfer of electrons and enhanced dye absorption ability. The best device performance was obtained in devices

which used Ce and Yb as dopants. But many of rare earth metals modifications in DSSCs (like Tm, Gd, Eu, Y, etc.) decreased photoconversion of DSSCs. An enhancement in efficiency has been indicated by using vanadium doped TiO_2 as photoanode in DSSCs [23]. Xi Xang et al. indicated improvement in J_{sc} due to reduction in charge recombination, amelioration in electron lifetime and increase in power conversion efficiency in DSSCs fabricated using W-doped TiO_2 as photoanode [24]

Effect of co-doping has also been studied. Ko et al. [25]. They found enhancement in device efficiency when the semiconductor was co-doped with tungsten and aluminum. Qiuping Liu et al. [26] investigated cell made by using Zn and Mg co-doped titania electrode and found 26.7 % increase in conversion efficiency as compared to undoped titania based DSSCs.

Wang et al. [31] and M Hirano et al. [32] synthesized Photoactive and adsorptive Niobium-Doped Anatase (TiO_2). They report that the crystalline structure of titania is not altered even when large amounts of dopant (20 wt %) has been doped . XRD peaks show a slight shifting towards left that indicates the inclusion if niobium in titania lattice because Ti^{+4} has smaller radius (0.61 Å) as compared to Nb^{+5} (0.64 Å). Larger shift of peaks has been observed when higher amount of dopant has been incorporated [29, 32]. While increasing niobium loading, the onset of absorption shifts towards longer wavelengths. A red shift has been observed in UV-Vis spectra for 10 wt % doping as compared to undoped titania and allows doped titania to absorb 40 % more light than pristine titania [27, 32]. Decrease in bandgap by Nb doping in titania has also been reported by Salvador et al. [33]. They performed electrochemical measurements and found photocurrent quantum efficiency to calculate the bandgap (Eg). They varied quantum efficiency with photon energy to determine value of Eg experimentally. They report highest band gap reduction (Eg=2.9eV) and highest quantum efficiency by 0.2 wt % doping of niobium. Increasing Nb content further increased band gap which was an indication of segregation of Nb_2O_5. Reported by X Lu et al. [30] cell consisting photoanode made from Nb doped titania nanoparticles (5 mol %) showed 18.2 % more energy conversion efficiency and enhanced conductivity than cell consisting photoanode made from undoped titania nanoparticles. An enhancement in opto-

electronic properties and device efficiency of cell containing niobium doped titania photoanode has been reported [34]. A decrease in V_{oc} when dopant concentration was increased from optimized amount has been seen. This is due to the positive shifting of V_{fb}. Lowering of V_{oc} can be avoided and photocurrent density can be improved by optimizing and carefully selection of electrolyte, dye and photo-anode material.

The ionic radius of Ti^{4+} (0.0605 nm) and that of Fe^{3+} makes the substitution of dopant in titania lattice possible. Due to doping iron in titania lattice and iron ion radius being smaller than Ti^{4+} ion, compaction of titania lattice is observed and denser phase is formed [39]. Iron exists as its oxide form in titania matrices and the crystallinity of titania is hardly affected by iron doping [37]. It was reported that the presence of iron as dopant in titania lattice initiates the formation of rutile phase. The formation of rutile phase increases with increase in iron loading. An increase in wt% of rutile phase has been indicated from 14% (undoped) to 23% (doped). Changing different concentrations of iron dopant in titania, a reduction in band gap has been seen up to 2.9 eV and this make photo-response of doped titania possible in visible region. The impurity levels formed by doped metal oxides not only act as absorption centers of VIS-light but also act as recombination centers of electron/hole pairs. It is found that the recombination of the photo-generated electron/hole pairs take place quickly in the Fe-doped titania films [35] whereas Wang X et al. [39] observed a decrease in recombination's of generated carriers. A decrease in photocatalytic activity has been observed by presence of Fe ions [37]. Iron doped titania showed higher specific surface area when compared to undoped titania.

It has been reported that doping copper in titania enhances the photo-activity [36-38] and reduces the band gap of titania. The enhancement of the photo-catalytic activity was discussed as an effect due to the Cu content as well as to the formation of stable Cu (I) in the Cu-doped titania semiconductors. Doped samples show shifting of absorption peak in UV spectra to visible region or longer wavelengths [38, 39]. Copper can be a good candidate material for doping titania for application in DSSCs. it is in-expensive and readily available. However, not enough data is present for the application of Cu doped titania as a photoanode material in DSSCs.

Summary

In this chapter importance of titania, its properties and its use in DSSCs has been discussed. Titania is a candidate material for the photoanode because of its stability and good performance. However, the problem with titania is that it only absorbs UV part of the light. Enhancing its absorption can lead to better performance of the cell. For this reason, metal doping in titania has been studies. Doping titania with metal allows formation of impurity energy levels, narrowing of band gap and formation of oxygen vacancies in titania lattice. Work has been done by researchers to study the effects of including metal dopant in titania photoanode of DSSCs. metals like iron, niobium, neodymium, tantalum etc. An increase in V_{oc} of the cell has been reported using metal doped electrodes with optimized doping concentration but none of the dopants could increase both V_{oc} and J_{sc} of the cell. Cu seems to be a good candidate for metal doping in titania for application in DSSCs. However, not enough data is present for the application of Cu doped titania as a photoanode material in DSSCs.

References

[1] Banerjee, A.N., The design, "fabrication, and photocatalytic utility of nanostructured semiconductors: focus on TiO2-based nanostructures", Nanotechnol Sci Appl, 2011. 4: p. 35.

[2] Duan, Y., et al., "Sn-doped TiO2 photoanode for dye-sensitized solar cells", The Journal of Physical Chemistry C, 2012. 116(16): p. 8888-8893.

[3] Pelaez, M., et al., "A review on the visible light active titanium dioxide photocatalysts for environmental applications", Applied Catalysis B: Environmental, 2012. 125: p. 331-349.

[4] Hoffmann, M.R., et al., "Environmental applications of semiconductor photocatalysis", Chemical reviews, 1995. 95(1): p. 69-96.

[5] Chandiran, A.K., et al., "Doping a TiO_2 Photoanode with Nb^{5+} to Enhance Transparency and Charge Collection Efficiency in Dye-Sensitized Solar Cells", The Journal of Physical Chemistry C, 2010. 114(37): p. 15849-15856.

[6] Meng, F., et al., "Visible light photocatalytic activity of nitrogen-doped $La_2Ti_2O_7$ nanosheets originating from band gap narrowing", Nano Research, 2012. 5(3): p. 213-221.

[7] Liu, G., et al., "Enhanced photoactivity of oxygen-deficient anatase TiO_2 sheets with dominant {001} facets", The Journal of Physical Chemistry C, 2009. 113(52): p. 21784-21788.

[8] Zaleska, A., "Doped-TiO_2: a review", Recent Patents on Engineering, 2008. 2(3): p. 157-164.

[9] Chen, X. and S.S. Mao, "Titanium dioxide nanomaterials: synthesis, properties, modifications, and applications", Chemical reviews, 2007. 107(7): p. 2891-2959.

[10] Tanabe, I., et al., Photoelectrochemical and optical behavior of single upright Ag nanoplates on a TiO2 film. The Journal of Physical Chemistry C, 2010. 115(5): p. 1695-1701.

[11] Yu, H., et al., "Nanostructure and charge transfer in Bi2S3-TiO_2 heterostructures" Nanotechnology, 2014. 25(21): p. 215702.

[12] Ghows, N. and M. Entezari, "A novel method for the synthesis of CdS nanoparticles without surfactant", Ultrasonics sonochemistry, 2011. 18(1): p. 269-275.

[13] Marci, G., et al., "Preparation characterization and photocatalytic activity of polycrystalline ZnO/TiO2 systems", 1. Surface and bulk characterization. The Journal of Physical Chemistry B, 2001. 105(5): p. 1026-1032.

[14] Asahi, R., et al., "Visible-light photocatalysis in nitrogen-doped titanium oxides", science, 2001. 293(5528): p. 269-271.

[15] Tang, Z., et al., "A microporous platinum counter electrode used in dye-sensitized solar cells", Nano Energy, 2013. 2(5): p. 622-627.

[16] Huang, S., et al., "Carbon nanotube counter electrode for high-efficient fibrous dye-sensitized solar cells", Nanoscale research letters, 2012. 7(1): p. 1-7.

[17] Wang, H. and Y.H. Hu, "Graphene as a counter electrode material for dye-sensitized solar cells", Energy & Environmental Science, 2012. 5(8): p. 8182-8188.

[18] Feng, X., et al., "Tantalum-Doped Titanium Dioxide Nanowire Arrays for Dye-Sensitized Solar Cells with High Open-Circuit Voltage", Angewandte Chemie, 2009. 121(43): p. 8239-8242.

[19] Maruska, H.P. and A.K. Ghosh, "Transition-metal dopants for extending the response of titanate photoelectrolysis anodes", Solar Energy Materials, 1979. 1(3): p. 237-247.

[20] Geetha, M., K. Suguna, and P. Anbarasan, "Photoanode Modification in DSSC Using Chromium Doped TiO_2 nanoparticles by sol-gel method", Archives of Physics Research, 2012. 3(4): p. 303-308.

[21] Van nam, T., N.T. Trang, and B.T. Cong. "Mg-doped TiO_2 for dye-sensitive solar cell: an electronic structure study", in Proc. Natl. Conf. Theor. Phys. 2012.

[22] Zalas, M. and M. Klein, "The Influence of Titania Electrode Modification with Lanthanide Ions Containing Thin Layer on the Performance of Dye-Sensitized Solar Cells", International Journal of Photoenergy, 2012. 2012.

[23] Liu, J., et al., "Influence of VB group doped TiO_2 on photovoltaic performance of dye-sensitized solar cells", Applied Surface Science, 2013. 277: p. 231-236.

[24] Zhang, X., et al., "Dye-sensitized W-doped TiO_2 solar cells with a tunable conduction band and suppressed charge recombination", The Journal of Physical Chemistry C, 2011. 115(25): p. 12665-12671.

[25] Ko, K.H., Y.C. Lee, and Y.J. Jung, "Enhanced efficiency of dye-sensitized TiO_2 solar cells (DSSC) by doping of metal ions", Journal of colloid and interface science, 2005. 283(2): p. 482-487.

[26] Liu, Q., et al., "Improved photovoltaic performance of dye-sensitized solar cells (DSSCs) by Zn+Mg co-doped TiO_2 electrode", Electrochimica Acta, 2013. 95: p. 48-53.

[27] Mattsson, A., et al., "Adsorption and solar light decomposition of acetone on anatase TiO_2 and niobium doped TiO_2 thin films", The Journal of Physical Chemistry B, 2006. 110(3): p. 1210-1220.

[28] Teleki, A., N. Bjelobrk, and S. Pratsinis, "Flame-made Nb- and Cu-doped TiO_2 sensors for CO and ethanol", Sensors and Actuators B: Chemical, 2008. 130(1): p. 449-457.

[29] Siddiki, M., et al. "Synthesis and characterization of Nb doped titania for dye sensitized solar cells", Photovoltaic Specialists Conference (PVSC), 2009 34th IEEE. 2009. IEEE.

[30] Lü, X., et al., "Improved-Performance Dye-Sensitized Solar Cells Using Nb-Doped TiO2 Electrodes: Efficient Electron Injection and Transfer", Advanced Functional Materials, 2010. 20(3): p. 509-515.

[31] Wang, Y., B.M. Smarsly, and I. Djerdj, "Niobium Doped TiO_2 with Mesoporosity and Its Application for Lithium Insertion", Chemistry of materials, 2010. 22(24): p. 6624-6631.

[32] Hirano, M. and K. Matsushima, "Photoactive and Adsorptive Niobium-Doped Anatase (TiO_2) Nanoparticles: Influence of Hydrothermal Conditions on their Morphology, Structure, and Properties", Journal of the American Ceramic Society, 2006. 89(1): p. 110-117.

[33] Salvador, P., "The influence of niobium doping on the efficiency of n-TiO_2 electrode in water photoelectrolysis", Solar Energy Materials, 1980. 2(4): p. 413-421.

[34] Emeline, A.V., et al., "Photoelectrochemical behavior of Nb-doped TiO_2 electrodes", The Journal of Physical Chemistry B, 2005. 109(51): p. 24441-24444.

[35] Maeda, M. and T. Yamada, "Photocatalytic activity of metal-doped titanium oxide films prepared by sol-gel process", Journal of Physics: Conference Series. 2007. IOP Publishing.

[36] Li, M., "The research and development of Fe doped TiO_2", Research of Materials Science, 2013. 2(2).

[37] Navío, J.A., et al., "Iron-doped titania semiconductor powders prepared by a sol–gel method. Part I: synthesis and characterization", Applied Catalysis A: General, 1999. 177(1): p. 111-120.

[38] Di Paola, A., et al., "Preparation of polycrystalline TiO_2 photocatalysts impregnated with various transition metal ions: characterization and photocatalytic activity for the degradation of 4-nitrophenol", The Journal of Physical Chemistry B, 2002. 106(3): p. 637-645.

[39] Wang, X., et al., "Pyrogenic iron (III)-doped TiO2 nanopowders synthesized in RF thermal plasma: phase formation, defect structure, band gap, and magnetic properties", Journal of the American C.

Chapter 4

Review on Experimental and Characterization Techniques

4.1 Solution Based Synthesis Techniques

4.1.1 Sol-gel Synthesis of Nanoparticles

Sol-gel synthesis is one of the most common methods for synthesis of nanoparticles. Sol can be defined as a colloid suspension of solid particles in liquid [1]. Sol-gel synthesis may involve a metal-organic approach in which metal alkoxides are dissolved in organic solvents or it may involve a metal-inorganic approach in which metal salts like nitrates, chlorides, oxychlorides etc. are used as precursors in water. Metal-inorganic approach for synthesis of particles is much cheaper than the former but the reactions are rapid and difficult to control.

Metal alkoxides $M(OR)_z$ belong to the family of metal-organic compounds, where M is a metal (Ti, Si, Al, Ce, Zr etc.), OR is an alkoxy group or organic ligand attached to metal atom and z represents the oxidation state of metal. In metal organic route the main reactions are hydrolysis and condensation of metal alkoxides which lead to polymerization. The first step is the hydrolysis of alkoxy group

$$M(OR)+H_2O \longrightarrow M(OH)+ROH$$

The next step is polycondensation reaction. The result of this reaction is the formation of polymers and oligomers based on metal oxo skeleton. The residual in this process is reactive alkoxy and hydroxo groups. Polycondensation reaction occurs in two steps. First the formation of oxygen bridges known as oxalation and second is the formation of hydroxo bridges known as olation.

$$M(OH)+(XO)M \longrightarrow MOM+XOH$$

Where X represents H or R, depending upon the hydrolysis ratio (H_2O/M). The kinetics of oxalation is slower than the kinetics of olation.

$$M(OH)+(HO)M \longrightarrow M(OH)_2M$$

After polycondensation, metal-oxo-macromolecular network is formed. A sol is formed in which macroscopic size has not been achieved by the polymerized structures. A gel is formed when the bushy structures are formed due to recombination of metal oxo polymers. The structure of these oxo polymers are dependent on temperature, hydrolysis ratio, nature of solvents and that of catalysts, use of nucleophilic reagents and complexing ligands etc.

4.1.2 Hydrothermal Synthesis of Nano/micro Particles

In hydrothermal synthesis, crystals are synthesized using water soluble precursors. The synthesis process and conditions depend on the precursor solubility in water at high slightly temperature and high pressure than normal room conditions [2]. To provide the appropriate conditions, crystal growth and synthesis is done in an autoclave. Autoclave is a pressure vessel made up of steel and usually lined with Teflon. The precursor is dissolved in hot water and the mixture is placed in autoclave at high temperature. Different temperature is maintained at two ends of autoclave. Cooler end is the site for the crystal growth and at hotter end solute gets dissolved. In hydrothermal method of preparing nano or micro sized particles, operating conditions are optimized to get the desired shape of the crystals. It is because the size and shape of synthesized particles depends on the operating conditions like reaction path, pressure and temperature. High vapor pressure materials can easily be synthesized using this method. This method enables us to have a good control over shape, size and composition but it is very difficult to observe the phenomenon during the growth of the crystal. Now-a-days hydrothermal reactors are available making it even easier to control the conditions. The reactor is turned on after setting desired conditions of temperature and pressure. When the desired conditions are achieved in the reactor, the raw material is pumped into it [3]. It is an environmental friendly and a low cost synthesis technique.

4.1.3 Dip Coating

Dip coating is another solution based wet chemistry method for deposition of films with thickness from 25 nm to 60 μm allowing high precision.in dip coating deposition process the coating material is in liquid form, usually a solution or a sol and substrate to be coated is immersed, remained in solution for some time and then withdrawn with well-optimized speed. The coating process takes place under controlled atmospheric and monitored temperature conditions [4]. The steps involved in deposition process are shown in Fig. 4.1.

The thickness of the coating can be easily controlled. It depends on the viscosity of the solution, withdrawal speed and the solid content in solution. Faster the substrate is withdrawn, thicker is the coating and viscous the solution, thicker is the film.

The advantage of using dip coating deposition method is that it is cheap and simple. It allows us to control the film thickness. Dip tanks come in variety of shapes and sizes which allows coating on large and small substrates. But the drawback of using such deposition process is the uncontrolled uniformity of the film. Film may be thicker at one edge of the substrate and thinner at other.

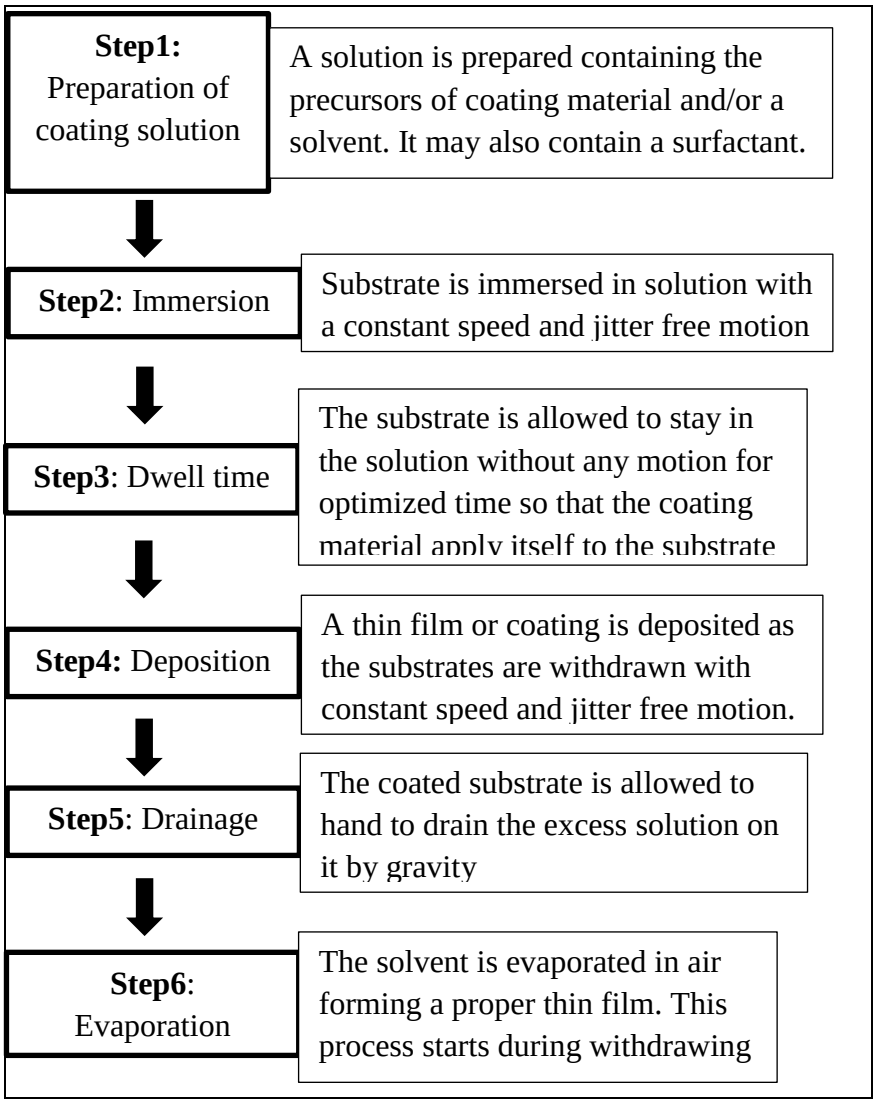

Fig. 4.1 Schematic diagram for Dip coating deposition process.

4.1.4 Spin Coating

Spin coating is a deposition technique which involves the use of centrifugal force to uniformly deposit thin films onto substrates. The deposition machine is called spin coater. Coating material is a colloid in liquid form or semi liquid form but thinner than paste. It usually contains volatile solvent. Small amount of this colloid is put in middle of the substrate to be coated and placed on the stub of the spin coater which holds the substrate using vacuum or double tape is applied at the non-coating side of the substrate to be fixed on the stub. After holding the substrate, coater spins the substrate by spinning at required rpm and centripetal acceleration spreads the colloid evenly onto the substrate. The substrate is dried and process may or may not be repeated depending

upon the desired thickness. Thickness of the film can be controlled easily. Thickness depends on the angular speed of spinning, viscosity of the colloid, amount of solid content in colloid and drying rate. Higher the speed, thinner is the deposited film.

Spin coating has its advantages over dip coating as it allows uniform deposition of material throughout the substrate and also allows the deposition of films as thin as 5nm. Spin coating requires expert hands as very slight variations in the depositing parameters can cause drastic variations in deposited films.

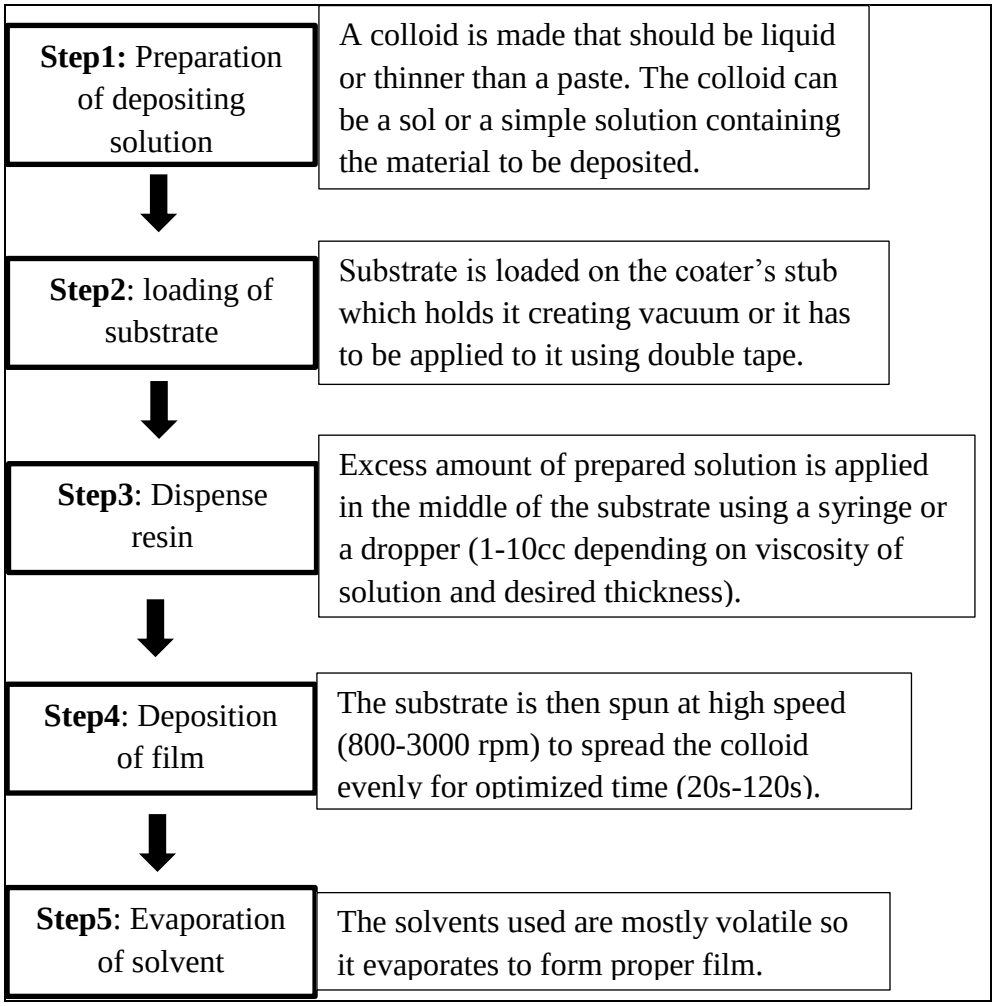

Fig. 4.2 Schematic diagram for spin coating deposition process.

4.1.5 Doctor Blade Coating

Doctor blade coating is the simplest and cheapest method of coating films on substrates. It is a simple spreading of a paste using a sharp edged metal applicator. Slurry or paste is made using precursors, a surfactant and a volatile solvent. Doctor blade comes with

screws to adjust thickness from few nanometers to micrometer range. Substrates are fixed to a flat table using tape and part of substrate to be coated is exposed only. The rest is covered by tape. Ample amount of the slurry is put on one end of the substrate and screws of doctor blade are adjusted according to the desired thickness. Doctor blade is glided over the substrate manually in one go. The coated films are then dried. The thickness of the film depends on viscosity of paste, surface tension and coating speed (moving speed of the hand.

The advantages of using doctor blade deposition techniques is that is simple, cheap and does not require expensive coaters or electric driven machines. But it allows less thickness control as compared to other solution based techniques.

4.1.6 Spray Pyrolysis

Spray pyrolysis, also known as chemical deposition spray pyrolysis, is another solution based wet chemistry route to deposit thin films onto substrates. Pyrolysis is a process in which thermo-chemical decomposition of organic materials occurs in absence of oxygen at high temperature. The deposition system consists of an atomizer, an heated substrates and a liquid source. In the deposition process a solution containing the coating precursors is sprayed onto heated surface where they react to form the coating of desired material. In other words chemical reaction occurs at the surface of substrates forming the desired and undesired products [5]. The precursors are chosen such that the byproducts of reaction are volatile and do not stay on the substrate along with coating. This method is specifically used for deposition of different oxides. Viguie and spitz classified different types of spray pyrolysis deposition processes on basis of reactions occurring after spraying which are stated below [6]

Process A: after spraying, droplets reach the surface of substrate and the solvent dries. A solid matter is left behind which reacts in its dry form.

Process B: In this process, the solvent starts evaporating as soon as it comes out of the spraying nozzle. Only dry solid matter reaches the substrate surface for decomposition.

Process C: as soon as the solvent is sprayed it starts vaporizing till it reaches the substrate. The solid matter starts vaporizing after impinging on substrate. The resultant vapors diffuse to the substrate and undergo heterogeneous reaction.

The properties of deposited coatings are dependent on precursors and processing conditions like the droplet size, temperature of substrate and type of reaction occurring at the substrate. Droplet size depends on the nozzle aperture and method of atomization. Ultrasonic spraying produce smaller droplet and aerosol spraying produce larger droplets. The advantage of using this technique is that it is simple and low cost. It has potential for mass production and is rapid. It offers ease of adding dopants, reproducibility of films and does not require vacuum.

4.1.7 Electrodeposition

Electrodeposition is another method for creating thin films on a work piece. Although this is a very old technology, it has recently been adopted for use in IC manufacturing, especially for depositing the copper films that are replacing aluminum films in most advanced integrated circuits. In electrodeposition, the source and work piece are both immersed in a liquid electrolyte and also are connected by an external electrical circuit. When a voltage is applied between the source and work piece, ions of the source material dissolve in the electrolyte, drift under the influence of the field towards the work piece, and chemically bond on its surface. Over time, a thin film is thus deposited. In some circumstances, an external electric field may not be required; this is called electroless deposition. Electrodeposition and electroless deposition are sometimes referred to as “plating,” and the deposited film is sometimes said to be “plated out” on the work piece.

4.2 Vacuum Based Deposition Techniques

4.2.1 Physical Vapor Deposition

Physical vapor deposition (PVD) is one of the very important methods of thin-film growth on substrates which involve ultra-high pressure environment for deposition.

4.2.1.1 Evaporation and electron beam evaporation

Evaporation takes places in a vacuum chamber, and by one mean or another, creates a low-pressure vapor of the material to be deposited. Some of this vapor will condense on the work piece and thereby start to deposit as a thin film. Simply melting a material in vacuum, depending on its vapor pressure, may sometimes produce a useful deposit of material. Sublimation furnaces are engaged to efficiently evaporate selenides, sulfides, and some other oxides. The evaporative materials are sintered and pressed to form pellets that are then subjected to radiant heat source. The most common example of these kind of evaporative materials include graphite, pyrolytic BN, and refractory metals, mostly formed by hot pressing of powder to form pallets. The heating is normally done by external tungsten wire resistance heating elements.

The heating of evaporant source by resistive heating element (in conventional evaporation process) include disadvantages like contamination caused by the supportive materials, crucibles, and heaters that hinders the deposition of pure films. It also includes the drawback of evaporating high melting point materials at high rates. Electron beam evaporation overcomes these limitations and therefore it is a better vacuum based evaporative film deposition technique. This technique has the advantage of evaporating a wide range of materials at practical rates. The technique works by placing the evaporative material in water cooled crucible or copper hearth. A small fraction of evaporant sublimes or melts that assured the purity of evaporative material as the crucible is water cooled that hinders its melting and contamination with the source evaporant.

The electron beam deposition technique usually have the configuration that works by emitting the electrons from heated filaments that are isolated from direct line of sight of both the substrate and the evaporative source. This strategy eliminates the film contamination caused by heated filament at cathode. The cathode is negatively biased

with respect to anode potential in a range of 4 to 20 kV, which causes the acceleration of electrons. Furthermore, the electrons are subjected to transverse magnetic field that deflects and focus the electron beam on the crucible containing the evaporative source at ground potential.

4.2.2.2 Sputtering

Sputtering is an example of physical vapor deposition process in which bombardment of energetic particles on the target material cause the ejection of source atoms from target material. The atoms can only be ejected if the kinetic energy of the bombarded particles is very high ($\gg$ 1 eV). The prolonged bombardment of highly energetic particle can be harmful as it leads to a substantial erosion of materials. However, it is frequently utilized for depositing thin films, analytical techniques and etching process. It is also the most important PVD method for integrated circuit manufacturing. The interconnections that carry electrical signals from one electronic device to another on an IC chip typically have been made from aluminum alloys that have been sputter deposited. Sputtering can be used to deposit both conducting and insulating materials.

Sputtering process is driven by collisions that cause the momentum exchange between the atoms and ions in the materials. In a sputtering chamber, argon or other atoms in a gas are first ionized and then accelerated by an electric field towards a source material to be deposited, called a "target." These ions dislodge and eject atoms from the surface of the source material, some of which drift across a gap towards the work piece; those that condense on its surface are said to be deposited. Depending on the how long the process continues, it is possible to sputter deposit films that are many microns thick.

4.2.2 Chemical Vapor Deposition

Chemical vapor deposition (CVD) represents another set of techniques that are widely employed for deposition. LPCVD, APCVD, PECVD are the different types of chemical vapor deposition method. In CVD, the source of the material to be deposited exists in gaseous form. The source gas and other gases are introduced into a heated vacuum chamber where they undergo a chemical reaction that creates the desired material as a product. This product condenses on the work piece creating, over time, a layer of the

material. In some CVD processes, the chemical reaction may take place preferentially on the work piece itself.

The CVD methods were very old and were used to deposit tungsten coatings as a protective layer on the filaments of incandescent bulbs to increase their life. Now high temperature, high quality CVD methods for producing epitaxial growth of thin films and coatings are dominantly used in wide variety of applications including the manufacturing of solid state electronic devices, cutting tools and ball bearings, the production of nuclear reactor components and rocket engine. Thin films of polycrystalline silicon, tungsten, and titanium nitride are commonly deposited by CVD as part of IC manufacturing. Nanowire growth, also often proceeds via CVD.

4.3 Characterization Techniques

Characterization techniques are external techniques used in material science to probe into the properties and internal structure of the materials under study. Characterization techniques can be employed for structural analysis, thermal analysis, composition analysis etc. Few of the techniques are explained below

4.3.1 XRD

XRD is an analytical technique for quantitative determination and identification of phases and orientations in crystalline compounds. XRD is a non-destructive and versatile technique that yields crystallographic information of the specimen. About 95% of solid materials on earth are crystalline like metals, salts, semiconductors, minerals etc. this technique is useful in determining structural properties like grain size, lattice parameters, Epitaxy, thermal expansion, type and lengths of chemical bonds in a specimen, size of atoms, arrangement of atoms, phases and crystallographic orientations.

Working principle

"When crystalline materials are irradiated by X-rays, they interact with atoms of the material and refract X-rays of characteristic energy. An individual pattern is generated by each material. In a mixture of materials, each substance gives its own pattern independently. XRD works on the principal of constructive interference of refracted X-rays",

When X-rays interact with matter, 3 phenomena may occur, Ionization, fluorescence and diffraction. In XRD, when X-rays hit atoms, the electrons in atom start vibrating with frequency same as the frequency of striking X-rays. In most of the directions destructive interference will occur i.e. both rays will be out of phase and no resultant X-rays will leave solid sample.

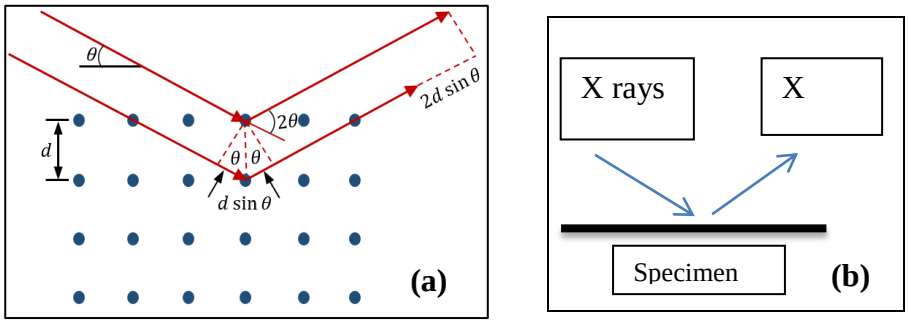

Fig. 4.3 (a) X-ray interaction with atoms according to bragg's law (b) Probe beam and measuring particle in XRD.

In few directions, constructive interference will occur i.e. waves will be in phase and well defined X-ray beams will diffract from the sample determined by Bragg's law

$$n\lambda = 2d\sin\theta$$

θ is the angle between incident ray and scattering planes known as incident angle (incident angle is equal to scattering angle), d is the spacing between the planes, λ is wavelength of the X-rays and n is an integer value. These diffracted X-rays can be detected by a detector to make a diffractogram. A diffractogram is a graph which is plotted between 2θ on x-axis and intensity on y-axis. This diffractogram is compared with internationally recognized data base (using or without using software). This data base contains reference patterns of almost all crystalline compounds. The detector records intensities of the diffracted beams and angles. This pattern is a fingerprint of the material. Miller indices (h,k,l values) defines the interplanar spacing and orientation. Number and position of peaks (2θ values) enables to determine lattice type, cell parameters and crystal class. Intensity of peaks gives information about position and types of atoms in the specimen.

4.3.2 Scanning Electron Microscopy (SEM)

SEM is an imaging technique that uses electrons instead of light to study morphology, particle shape and defects of films and powders. SEM provides magnification up to 300,000X and has an effective probing depth of 10 nm to 1 μm.

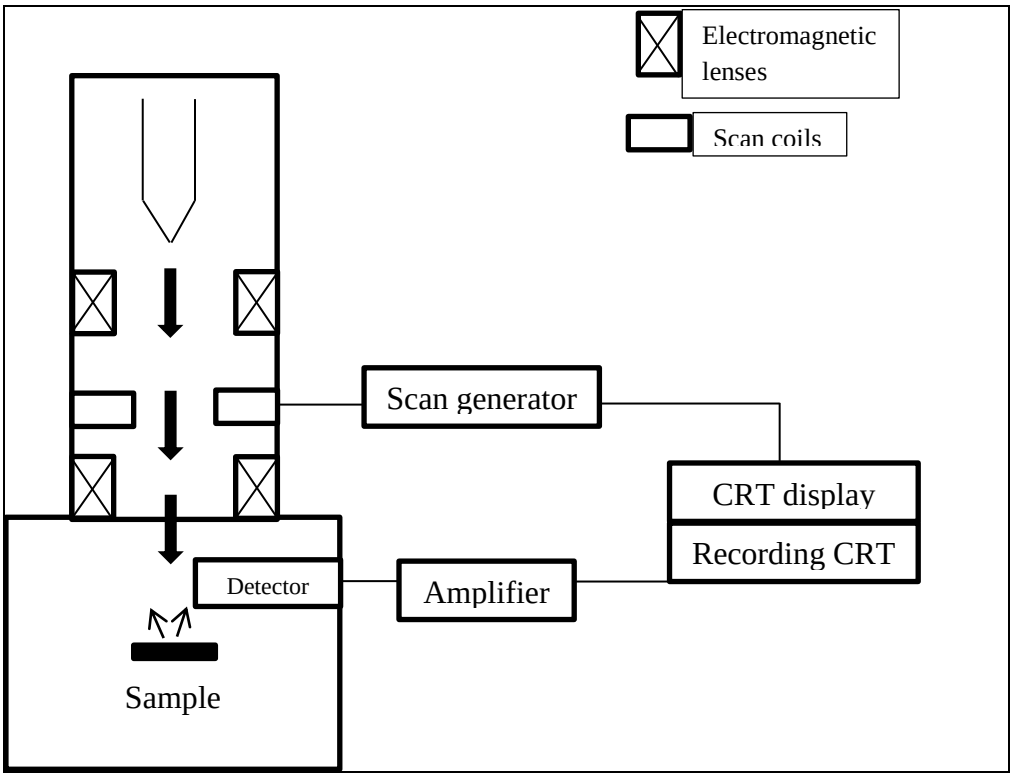

Fig. 4.4 Schematic diagram of Scanning Electron Microscope.

Working principle

‘’A focused electron beam is interacted with the surface of the sample and secondary electrons and backscattered electrons are knocked out of the sample creating an electric current which forms the image’’.

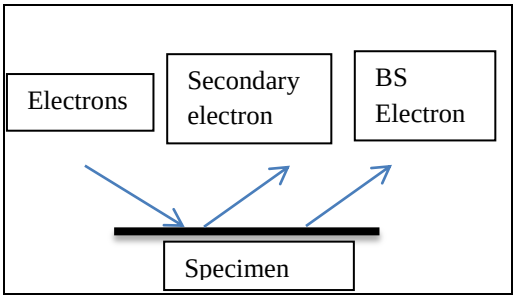

Fig. 4.5 Probe beam and measuring particle in SEM

Electrons, emitted from a heated filament, are accelerated towards the sample. A high vacuum is required because gas molecules may cause interference with electron beam and with backscattered or secondary electrons. The electrons interact with the atoms of the sample and may produce secondary electrons, characteristic X-rays and back

scattered electrons. First electromagnetic lens de-magnifies the primary beam second electromagnetic lens focuses. These signals are detected by a detector. Most scanning electron microscopes contain secondary electron detectors only while a few may have X-ray or other detectors as well. Back scattered electrons are generated due to elastic scattering. Detector along with cathode ray tube generates the micrograph image.

Sample preparation

Sample preparation is an important step for proper imaging of the samples and depends on the type of sample under observation. For example if sample to be examined is an insulator, a coating of a conducting film is deposited before imaging. When electrons interfere with the surface of electrically insulating materials a charge is built up which makes analysis difficult. If sample is a conductor, no coating is required. If sample is a powder it is simply placed on the stub, coated with conductor if an insulator and an image is obtained. But if films are under examination, substrates are properly prepared. The preparation steps are explained in Fig. 4.6.

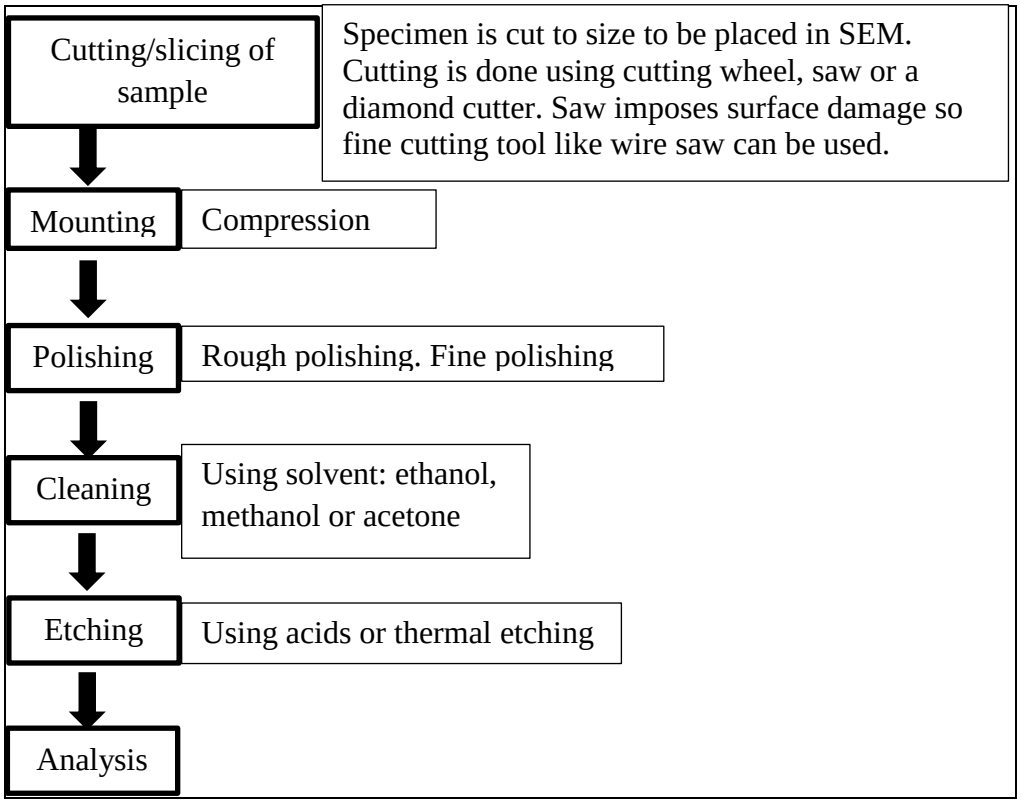

Fig. 4.6 Schematic flow for sample preparation for SEM of films.

4.3.3 Energy Dispersive Spectroscopy (EDS)

EDS or EDX is a compositional elemental analysis technique for chemical characterization of the specimen. The electrons have an effective probing depth of 1µm. EDS is always used in conjunction with TEM, EMPA or SEM.

Working principle

"When focused beam of high energy electrons is bombarded onto a solid sample, X-rays are emitted. The detector in make use of these x-rays to obtain localized chemical analysis".

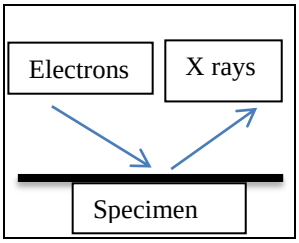

Fig. 4.7 Probe beam and measuring particle in EDX

When electrons strike the specimen, the electrons contained in specimen are excited creating vacant places in the atomic shells. Electrons in the higher shells fill these vacancies. The energy is released in this process in form of x rays. All elements emit X-rays with characteristic energy values. Each element in periodic table has its specific energy value which makes elemental analysis through EDS possible. Kα X-rays are emitted when an electron from L shell fills the vacancy in K shell of the atom. Letters K,L,M represents the shell from where electrons are emitted and α,β,γ represents the shell where they are substituted. Sample preparation is same as for SEM. In principle, all elements in periodic table from beryllium to uranium (atomic number 4 to 92) can be detected by EDS.

3.2.3 UV-VIS Spectroscopy

UV-Vis spectroscopy is an analysis technique in which uses visible (400 nm- 00nm) and ultraviolet (190 nm-40 nm) regions of electromagnetic spectrum to obtain information about organic molecules. It is performed to determine impurities in a

sample. Additional peaks other than the specimen substance's peak indicate the presence of impurities. It gives information about structural elucidation of specimen. Combination and location of peaks helps us to analyze whether saturation, unsaturation and hetero atoms exist in specimen or not. Quantitative analysis of compounds can be performed which absorb UV or Visible radiation using Beer-lambert law. Qualitative analysis can be performed to determine the type of compounds present in the specimen. The spectrum obtained by UV-VIS spectrophotometer is compared to spectra of known compounds. Qualitative analysis of functional group can also be determined as presence of a band at certain wavelength determines the presence of a particular group.

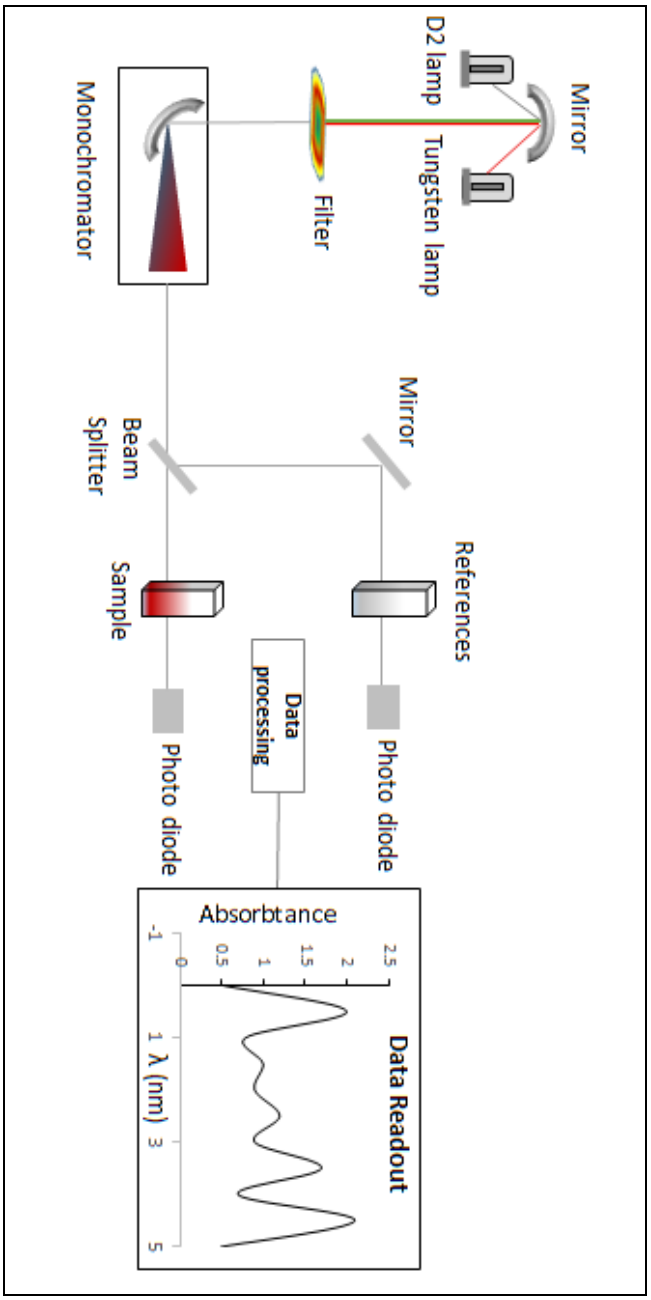

Fig. 4.8 Schematic diagram of UV-Vis spectrophotometer.

Working principle

When molecules that possess non-bonding or π electrons are irradiated to UV-Vis light, the electrons gets excited to higher anti-bonding orbitals. Lesser the energy gap between HOMO and LUMO of a material, easier is the excitation of electrons by longer wavelength radiations.

When a molecule with energy gap between HOMO-LUMO equal to ΔE is exposed to radiation with wavelength corresponding to ΔE, electron is bumped from HOMO to LUMO .This is referred to as σ - σ* transition. The plot between wavelength on x-axis and absorbance on y-axis is obtained and analyzed.

4.3.4 FTIR Spectroscopy

Infrared spectroscopy refers to the type of spectroscopy that works within the distinct region of electromagnetic spectrum known as infrared region. In this region of electromagnetic spectrum, the light has lower frequency and longer wavelength as compared to visible light. Infrared spectroscopy (IR spectroscopy) mostly includes the techniques based on absorption spectroscopy. This technique is widely used to study and identify chemicals. Infrared spectrometer is an instrument used in IR spectrometry to produce spectrum of a given liquid, solid, or gaseous sample. This technique is used to Identify functional group and structure elucidation of specimen, identification of substances, detection of impurities, quantitative analysis etc.

Working principle

"If a molecule confront electromagnetic radiations whose frequency matches to the frequency of any of its vibrational modes, it will absorb energy from radiation and the transition of particle to higher vibrational energy state take place. ΔE (change in energy) between two vibration states is equivalent to energy associated with absorbed wavelength".

The covalent bonds in a flexible, unlike rigid bonds, are flexible and always in a state of a vibration. Vibration could be bending or stretching. The vibrational motion possessed by these molecules is the characteristics of their respective atoms. All organic compounds absorbs are capable to absorb IR which matches to their vibration. The principle of IR spectrometers is similar to the UV-Visible spectrometer that allows chemists to obtain absorption spectra that are a distinctive reflection of their molecular structure.

IR spectrum obtained is a graph between percentage transmittance and wavenumber presenting the variation of percentage transmittance with the frequency of the infrared radiation.

4.3.5 Thermo Gravimetric Analysis

Thermo gravimetric analysis abbreviated as TGA is a thermal analysis technique in which weight loss or weigh gain of the sample powder is observed as a function of time or increasing temperature. The sample is subjected to a controlled atmosphere and controlled temperature conditions. In other words the changes in chemical like dehydration, solid-gas reactions, chemisorption, decomposition etc. and physical properties like desorption, absorption, adsorption, vaporization, sublimation etc. are determined.

Working

When materials are subjected to heat, physical and chemical changes occur. The weight of the material is either increased or decreased. Thermo gravimetric analyzer consists of a pan placed in a programmable furnace. This pan is supported by a sensitive precision balance. The specimen is placed onto the pan and a heat rate and a temperature range up to which changes is the material is to be observed is given to the furnace. The furnace is heated from lower limit of temperature range (usually from room temperature), reaches the maximum point and then it is cooled. The mass change is monitored during the heating and cooling process. The environment of furnace is controlled by an inert or a reactive gas [7].

The data obtained from TG analysis of the sample enables the interpretation of loss of volatile components in the sample, its thermal stability and decomposition. The data obtained is plotted in form of a graph between increasing temperature on x-axis and weight loss percentage on y-axis. In the given temperature range, if a graph shows a straight line meaning no weight change, this means that the specie is thermally stable. Sometimes an initial weight loss is shown in the graph and then the line becomes straight which means the specie is thermally unstable at low temperature and then becomes stable. The data from TG analysis also provides information about the

maximum use temperature of the material beyond which the material will degrade. It also provides information about reaction kinetics, degradation mechanism, presence of inorganic content in material and decomposition patterns [8].

4.3.6 Differential Thermal Analysis

Differential thermal analysis is another thermal analysis technique that notes the temperature difference between a reference material and a sample as a function of temperature or time. Both the sample as well reference material is subjected to same conditions of temperature and environment. DTA records the changes in energy of the sample during a transformation as a function of time or temperature. From the data we can determine the phase change or transition temperature of the sample like crystallization temperature, glass transition temperature, sublimation temperature, melting temperature etc. [9].

Working

This DTA apparatus is mostly hybrid with TGA apparatus. DTA apparatus consists of a device for measurement of heat of reaction (recording system), a programmable furnace (source of heat), and a sample holder. Sample holder contains a metallic or a ceramic block, sample containers and two thermocouples. One thermocouple is placed in sample and the other in an inert material (usually Al_2O_3) as a reference and both thermocouples are joined to a voltmeter. When the sample undergoes a phase change with increasing temperature, a deflection in voltmeter occurs. The deflection is because of the temperature differences between reference material and sample material because heat input raises the temperature of reference material and the heat is consumed as latent heat in changing the phase of sample material. This deflection is recorded and a graph between temperature or time on x-axis and heat flow on y-axis. The graph curve thus formed is called thermogram or DTA curve. Exothermic and endothermic reactions occurring in sample material are thus analyzed [10].

Summary

In this chapter a review on the experimental techniques including the methods of preparation of nano-particles and methods of deposition of thin films on substrates has been presented. Details on the working of different characterization techniques like XRD, SEM/EDX, TG-DTA etc. has also been summarized. The most common method of preparation of TiO_2 nanoparticles is through sol gel process which includes hydrolysis of alkoxides chain followed by the polycondensation reaction. Hydrothermal synthesis method is another low-cost technique for particle synthesis. Thin films can be coated on number of substrates using low-cost solution based techniques like dip coating, spin coating, spray pyrolysis etc. or the comparatively expensive vacuum based techniques like PVD, CVD etc. They require high and ultra-high vacuum for the deposition process. Among the techniques the expensive techniques like evaporation, electron beam evaporation, CVD etc. offer homogenous and fine coating allowing easy control over the film formation and thickness. Whereas solution based wet chemistry routes are cheap and can be done with simple apparatus. No high vacuum is required and can be done in low or no vacuum. After the synthesis of particles and deposition of thin films, it is required to characterize the particles and films. Different material characterization techniques like XRD, SEM/EDX, UV-Vis spectroscopy, FTIR spectroscopy etc. can be employed to study the samples. Structural and compositional analysis of films and particles can be done using XRD, SEM, AFM, EDX, UV-Vis spectroscopy etc., thermal analysis techniques like TG-DTA, dilatometry etc. can be employed to check thermal stability and reactions occurring with increasing temperature and electrical analysis can be done using four probe method for IV measurements or C-V measurements etc. structural analysis is performed to check the morphology, shape, size etc. of the films and particles and compositional analysis is done to analyze the presence of phases, amounts of phases, bonds, elements, amount of elements etc. The information obtained from these characterization data are utilized to optimize better conditions and to check the functioning of particles and films.

References

[1] C. J. Brinker and G. W. Scherer, Sol-gel Science: "The Physics and Chemistry of Sol-gel Processing", Academic Press, 1990.

[2] A. B. Djurisic, Y. Y. Xi, Y. F. Hsu, and W. K. Chan, "Hydrothermal synthesis of nanostructures," Recent patents on nanotechnology, vol. 1, pp. 121-128, 2007.

[3] K. Byrappa, "Handbook of Hydrothermal Technology", 2nd Edition: William Andrew, 2011.

[4] H. Mayer and R. Krechetnikov, "Landau-Levich flow visualization: Revealing the flow topology responsible for the film thickening phenomena," Physics of Fluids (1994-present), vol. 24, p. 052103, 2012.

[5] D. Perednis and L. Gauckler, "Thin Film Deposition Using Spray Pyrolysis," Journal of Electroceramics, vol. 14, pp. 103-111, 2005/03/01 2005.

[6] J. B. Mooney and S. B. Radding, "Spray pyrolysis processing," Annual review of materials science, vol. 12, pp. 81-101, 1982.

[7] P. Gabbott, "Principles and applications of thermal analysis", Blackwell Pub., 2008.

[8] J. R. Newton and E. Atkins, "Report on differential thermal and thermogravimetric analysis", U.S. Dept. of Interior; [for sale by the Supt. of Docs., U.S. Govt. Print. Off.], 1969.

[9] R. C. MacKenzie, "Differential Thermal Analysis: Fundamental aspects", Academic Press, 1970.

[10] W. J. Smothers and Y. Chiang, "Differential thermal analysis: theory and practice", Chemical Pub. Co., 1958.

Chapter 5

Experimentation

A number of experiments were performed to carry out the specific objectives mentioned in Chapter 1. Details of the following major experiments are given in this chapter

1) Sol gel synthesis of titania nanoparticles, annealing at different temperatures and their characterization.

2) Sol gel synthesis of 1wt% and 3wt% Cu doped titaina nanoparticles and their characterization.

3) Hydrothermal synthesis of carbon microspheres for pore formation and their characterization.

4) Formation of crack free Cu doped titania thin films and optimization of the doctor blade coating method.

5) Fabrication of Dye Sensitized Solar cells and their performance test.

5.1 Synthesis and Characterization of Nanoparticles

5.1.1 Sol-gel Synthesis of Titania Nanoparticles

Pristine (undoped) titania nanoparticles were prepared by sol–gel method titanium (IV) isopropoxide. 25 ml of titanium isopropoxide (Sigma-Aldrich) and 50 mL ethanol were mixed together and stirred. Isopropxide chain was hydrolyzed by addition of 30ml water. 6 ml HCl was added which acts as a catalyst in the process and was stirred continuously for 3 hours. The sol was kept for 24 hours and then dried in vacuum oven. Two sample powders were made by annealing at two different temperatures for same duration. One sample was annealed at 450 °C and other at 650 °C for 4 hours each.

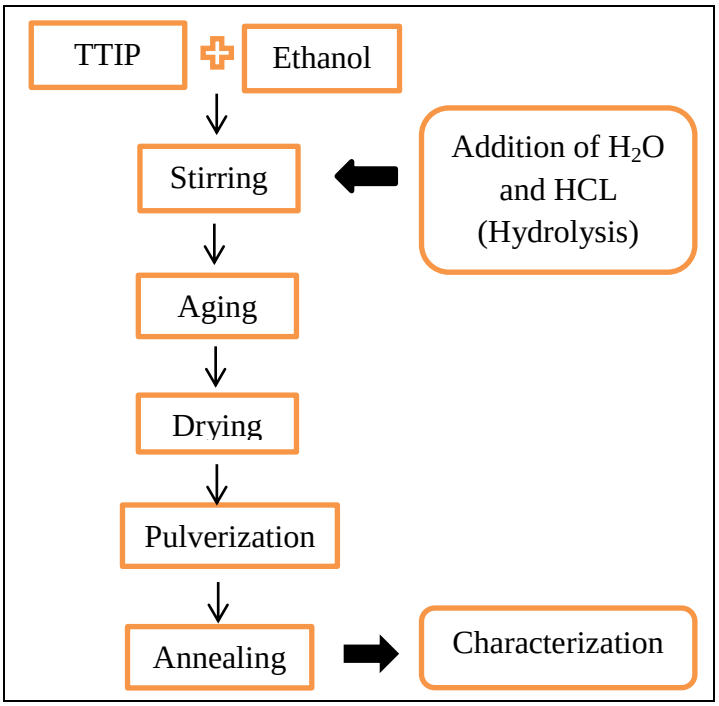

Fig. 5.1 Schematic diagram for sol-gel synthesis of undoped titania nanoparticles.

5.1.2 Sol-gel Synthesis of 1wt% and 3 wt% Cu Doped Titania Nanoparticles

Metal doping in titania renders several advantages like enabling band gap engineering, allowing visible light photoactivity of titania etc. Copper is a readily available metal and is a good candidate to be used as a dopant in titania for applications in DSSCs. However, the data available for its doping effects in DSSCs is scarce. Therefore, Cu doped titania nanoparticles were synthesized to study the effect of copper inclusion in titania lattice. In making doped titania nanoparticles, all the steps were similar as described above and only differ when the mixture was hydrolyzed. To prepare Cu-doped TiO_2 another solution was made containing $CuCl_2.5H_2O$, water and ethanol. This solution was added while hydrolyzing TTIP solution. The concentration of solution was adjusted to yield 1wt% and 3wt% copper content. This sol was also kept for 24 hours, dried and annealed at similar conditions as for undoped titania.

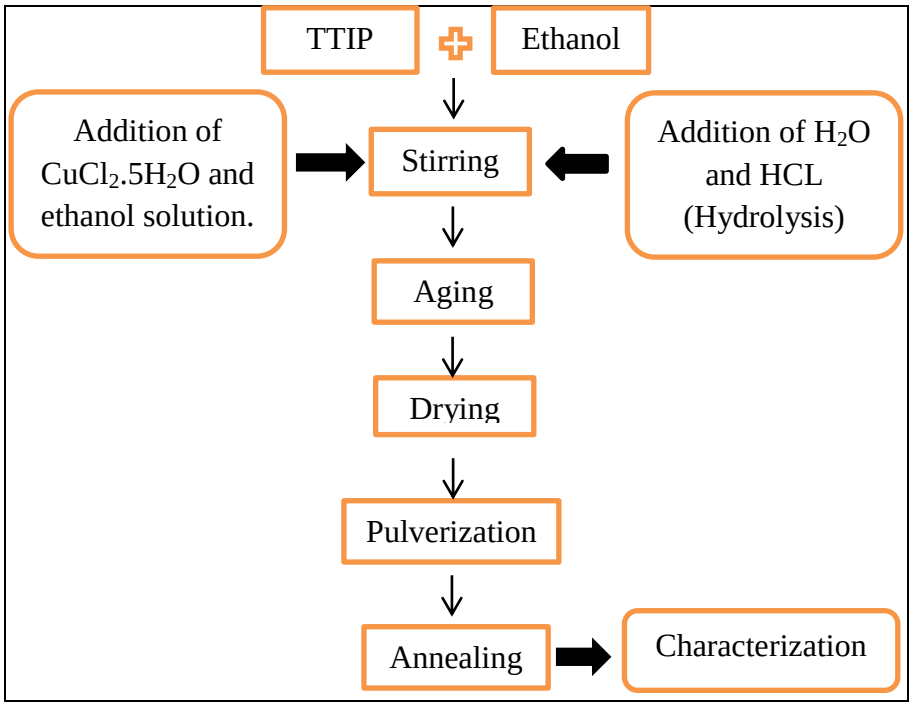

Fig. 5.2 Schematic diagram for sol-gel synthesis of Cu doped titania nanoparticles

5.1.3 Characterization of Nanoparticles

The obtained powders were characterized using following analytical techniques

The X-ray diffraction (XRD) pattern of the samples was characterized using a θ-θ STOE Germany X Ray diffractometer using X Rays from Cu-Kα for structure and phase analysis.

SEM and (EDX) of the samples were carried out using a JEOL 2300 scanning electron microscope at an operating voltage of 20kV with an EDX detector . Prior to analysis, particles were coated with gold using a JFC 1500 sputter ion coater.

UV-VIS spectra of the samples were obtained using a BMS 2800 UV–Vis spectrophotometer with $BaSO_4$ powder as the standard reference sample and data was taken from range 300nm to 900nm.

TG-DT analysis of the samples was performed using Perkin Elmer diamond TG/DTA version 2.0 with 2g sample weight each. Temperature range was set from room temperature to 500 °C.

FTIR spectra were obtained using Perkin Elmers spectrometer. The pallets were first made to be used in spectrometer. For making pallets, potassium bromide (KBr) was heated to 120 °C for 20 minutes to remove moisture. Cooled KBr was mixed with powder samples in 1% (w/w) mixture and pallets were made by pressing at 15 ton for about 3 min. These transparent pallets were inserted in spectrometer and spectra were obtained from 400 cm^{-1} to 4000 cm^{-1}.

5.2 Synthesis of Carbon Microspheres by Hydrothermal Method

Studies have shown that increasing porosity of the photoanode allows higher dye adsorption leading to enhanced light absorption. In order to increase the porosity of the photoanode carbon microspheres were synthesized using hydrothermal method. 10 g glucose was added in 50mL distilled water in a beaker and was stirred using magnetically for 2 hours at room temperature. The resulting mixture was filled in a Teflon lined stainless steel autoclave. Autoclave was placed in a vacuum oven and heated at 200 °C for 14 h. The oven was then turned off and cooled to room temperature. After being naturally cooled, autoclave was taken out of the oven and dark precipitates were collected. These precipitates were washed using distilled water for 5-6 times, collected on a filter paper and then dried in oven at 110 °C for 14 h. the obtained product was grinded using pestle and mortar and fine powder was obtained. The powder was subsequently annealed at 325 °C for 10h.

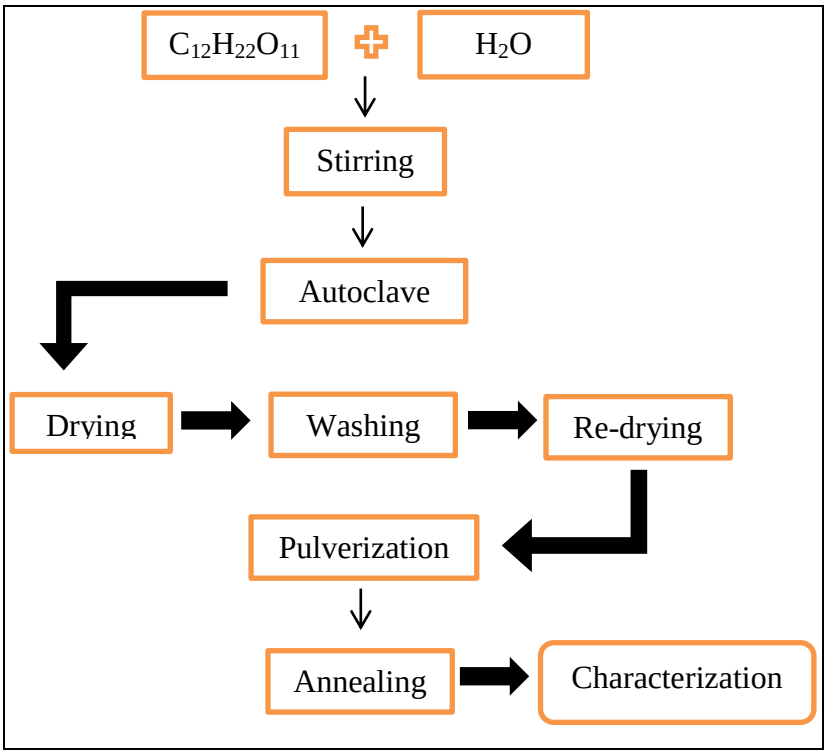

Fig. 5.3 Schematic diagram for synthesis of carbon microspheres.

5.2.1 Characterization of microsphere

These microspheres were characterized using XRD and EDX. Since the stubs used in EDX were already coated with carbon, so before placing carbon microspheres on the stub, the surface of stub was covered with aluminum tape. The stubs containing carbon microspheres were then placed in sputter ion coater for 3 minutes and gold was coated on them.

5.2.2 Inclusion of Carbon Microspheres in Titania

Carbon microspheres were included in 3wt% Cu doped titania to make it porous. Titania paste was prepared using 2g of 3wt% Cu doped titnia powder and 1mL distilled water. Carbon microspheres were dissolved in ethanol to make 2.5wt% solution and this solution was sonicated for 30 mins to ensure the proper dispersion of particles. This solution was added to the paste to make 2 different pastes with 0 wt% and 2.5 wt% microspheres. The pastes were stirred for 3 hours and then dried in vacuum oven at 100

°C for 5h. The resultant dried products were pulverized in pestle and mortar to make powders containing 0 wt% and 2.5 wt% carbon microspheres.

5.2.3 Formation of Pellets for Porosity Testing

Both the powders were subjected to hydraulic press for making pellets for porosity testing. 1 g of each powder was put separately in the dye of 13 mm diameter and a pressure of 5 kg/cm^2 was applied for 5 minutes. The pressure was released slowly and pellets were collected. Both the pellets were annealed at 500 °C in a muffle furnace.

5.2.4 Characterization of Pellets

BET surface area and porosity analysis of pellets were done by determining Nitrogen sorption at 80 K using Micrometrics Germini VII 2390 apparatus.

5.3 Fabrication of Dye Sensitized Solar Cells

5.3.1 Cleaning of Glass Substrates

FTO coated glass substrates were cleaned ultrasonically using ethanol, DI water and acetone. Substrates were first cleaned using ethanol for 30 minutes in sonicator, then using DI water for 30 minutes and lastly using acetone for 30 minutes. The substrates were dried in vacuum oven before coating them.

5.3.2 Deposition of Blocking Layer by Spin Coating

Sol using titania and Cu doped titania precursor was prepared as explained in section 5.1 and respectively. The sol was deposited using a Spin coater. Cleaned substrates were placed on the stub of the spin coater and vacuum was generated which allowed the coater hold the substrates properly. Few drops of sol was placed on the substrate and it was spun at 1000 rpm for 60s and then kept on spinning for another 120s to let it dry in air. The samples were then annealed. 2 samples were prepared, one sample with blocking layer of titania annealed at 450 °C and other sample with blocking layer of $Cu:TiO_2$ annealed at 450 °C.

5.3.3 Deposition of Thin Films of Titania and $Cu:TiO_2$

Paste was formed by a number of experiments the details of which has been explained in Table 6.6. The hit and trial method was used to optimize the paste coating method.

Best paste was formed by adding 15 mL ethanol, 1 mL distilled water, 1/3rd mL HNO_3 in 2g Cu-doped titania (3 wt% doped Cu) and 2g PEG ad stirred for 4 hours to make an homogenous paste. To deposit undoped TiO_2 layer on glass slide, undoped TiO_2 powder was used. The paste was coated on the conductive side of FTO/blocking layer coated glass substrates using a doctor blade coater. The coated films were dried at room temperature for several hours and then annealed at 450 °C. Undoped TiO_2 thin films were deposited on substrates which contained pristine TiO_2 blocking layer and Cu:TiO_2 thin films were deposited on substrates containing Cu:TiO_2 blocking layer.

5.3.4 Dye Adsorption

Above samples were immersed in a 0.0001M solution of the N3 dye in ethanol for 24 hours to let dye molecules adsorb on the surface of titania porous film. With completion of this step, photoanodes were ready to be used.

5.3.5 Counter Electrode

JFC 1500 ion sputtering device was used to deposit a layer of 80 nm thick gold on cleaned FTO glass substrates to make the counter electrodes. The layer of metal was deposited on conductive side of the glass substrate.

5.3.6 Clipping of Electrodes and Filling of Liquid Electrolyte

Electrolyte was prepared by stirring together 0.7g potassium iodide, 0.07g iodine crystals in 10mL ethylene glycol solvent. A dark yellowish brown solution of I^-/I_3^- electrolyte was obtained.

Then the two electrodes, photoanode and counter electrode, were clipped together and liquid electrolyte was filled in between them to form the Dye Sensitized solar cells.

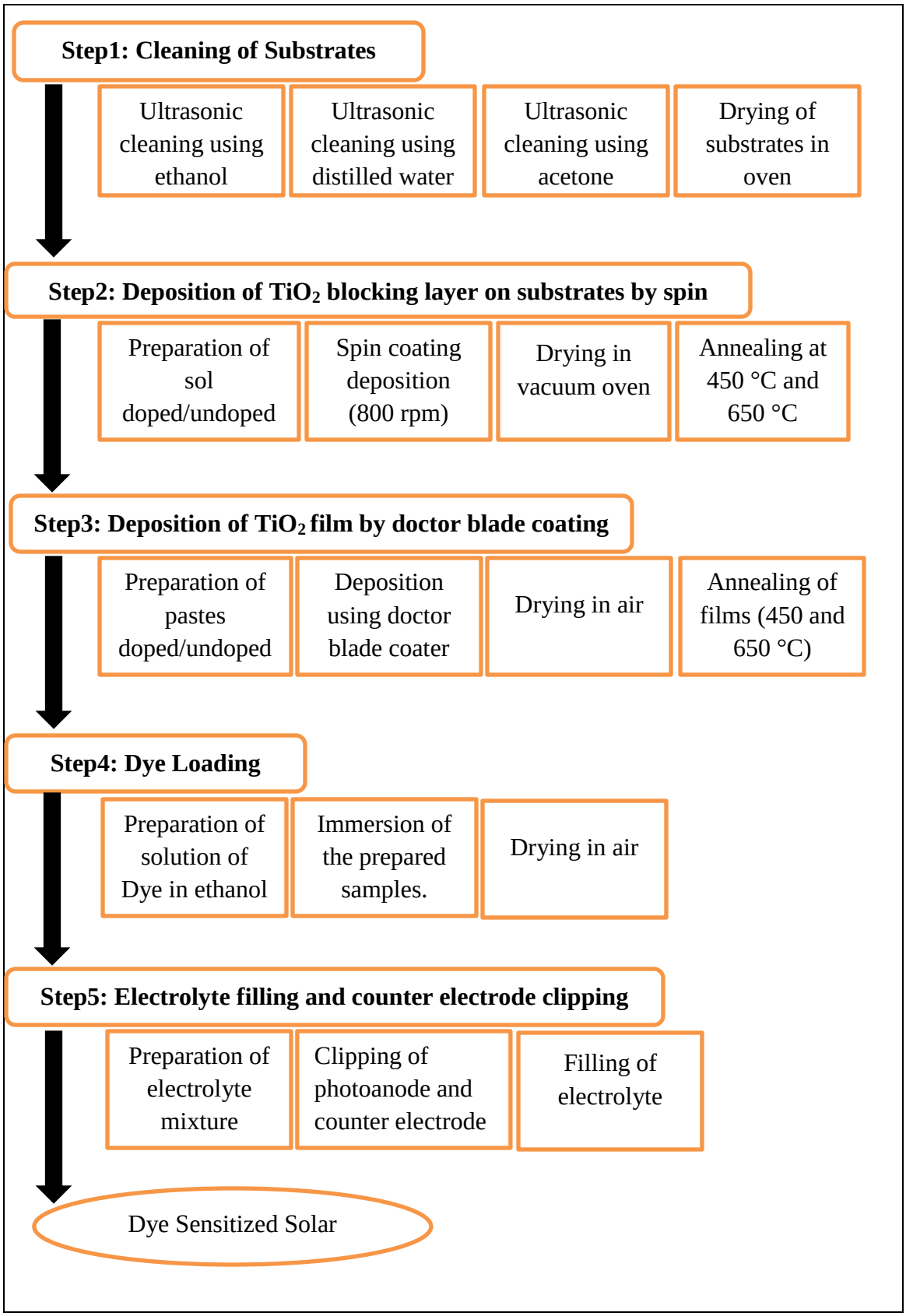

Fig. 5.4 Schematic diagram for the steps in fabrication of DSSCs

5.3.7 Characterization of Films and DSSCs

Thickness of film was determined using JEOL 2300 scanning electron microscope at an operating voltage of 20kV. Coated glass was cut using a diamond cutter and placed on the stub in cross-section direction. Aluminum tape was used to fix the glass slide and put in sputter ion coater to coat a layer on gold (conducting layer).

Optical Microscopic Images of coatings were obtained using Optika B-600 MET with camera Optika 40.

IV characteristics of DSSCs were obtained using Biological VSP (potentiostat system). A 300W metal halide bulb was used as a light source and distance between source and cell was kept 8cm. light intensity at this distance equals to the intensity on a bright sunny day.

Summary

In this chapter all the experimentation, experimentation techniques and characterization techniques that have been employed in the research has been explained. Undoped and doped titania nanoparticles were synthesized using sol-gel synthesis method and characterized using XRD, SEM/EDX FTIR, TG-DTA and UV-Vis analysis. Blocking layer on TCO coated substrate (FTO coated glass) was deposited using spin coater and mesoporous titania and doped titania coatings were deposited using doctor blade coater. Annealing at different temperatures were done using muffle furnace. The pasting conditions and paste made for depositing thin films were optimized to get crack free thin films. Thin films were characterized using SEM and XRD. The DSSC was assembled using N3 dye, I^-/I_3^- redox electrolyte and gold coated FTO glass as counter electrode and IV characteristics were measured. Carbon microspheres were synthesized using hydrothermal method and were characterized using EDX and XRD. Carbon microsphere were included in 3wt% Cu doped pellets and annealed to create cavities. The porosity and BET of the pellets were tested by nitrogen-sorption.

Chapter 6

Results and Discussion

6.1 Analysis of Sol-gel Prepared Undoped and Doped Titania Particles

Doping titania with other atoms influences its properties and causes change in its properties altering its light absorption mechanism, crystal structure, particle size and stability. The results and discussion in this section elaborate the structural and thermal studies on the doped and undoped titania nanoparticles. It also enlightens the change in absorption mechanism of the particles with doping.

6.1.1 Effect of Annealing Temperature and Cu Concentration on Crystal Structure of Nanoparticles (XRD Analysis)

Crystal phase of titania nanoparticles determine its functionality for various applications. The rutile phase of titania is recommended for its use in pigments [1] and anatase phase is recommended for photocatalytic applications [2]. Therefore, it is very important to investigate the changes in crystal structure by incorporation of different dopants in titania lattice. Undoped (pristine) and Cu-doped titania nanoparticles were prepared at the same conditions for comparisons.

The similarity in ionic radius of Cu^{2+} (0.73 Å) to that of Ti^{4+} (0.64 Å) enables copper to substitute titanium. Titania doped with Cu^{2+} initiates the formation of rutile phase along with anatase. The XRD pattern of undoped and 1wt% Cu-doped titania nanoparticles is shown in Fig. 6.1 (a,b) XRD patter of 3wt% Cu doped titania is shown in Fig. 6.2.

As shown in Fig. 6.1 (a), when annealed at 450 °C, titania changes from amorphous to crystalline phase. At 450 °C pure anatase phase is formed corresponding to JCPDS card# 78-2486. Anatase is metastable phase of Titania and is usually formed at low temperature during solution-phase synthesis [3]. As the annealing Temperature increases to 650 °C undoped titania shows a small rutile phase peak (110). It means at higher temperature rutile phase starts forming.

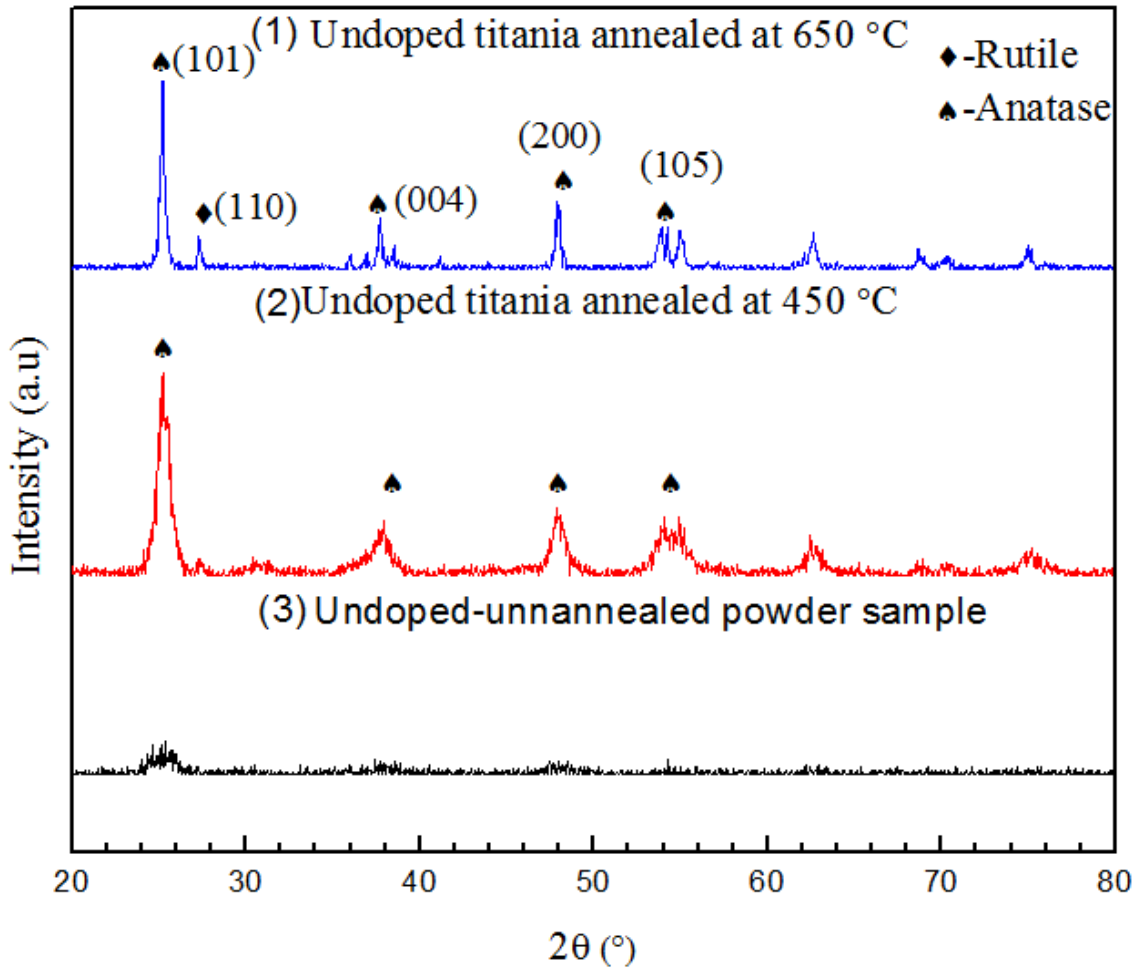

Fig. 6.1 XRD Spectra of undoped titania nanoparticles annealed at different temperatures.

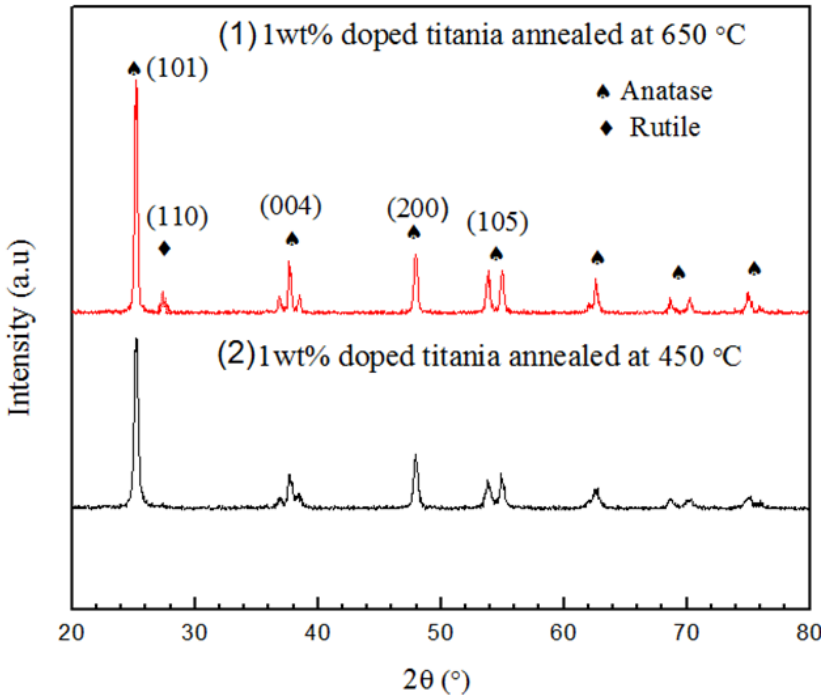

Fig. 6.2 XRD spectra of 1wt% Cu doped titania nanoparticles annealed at different temperatures

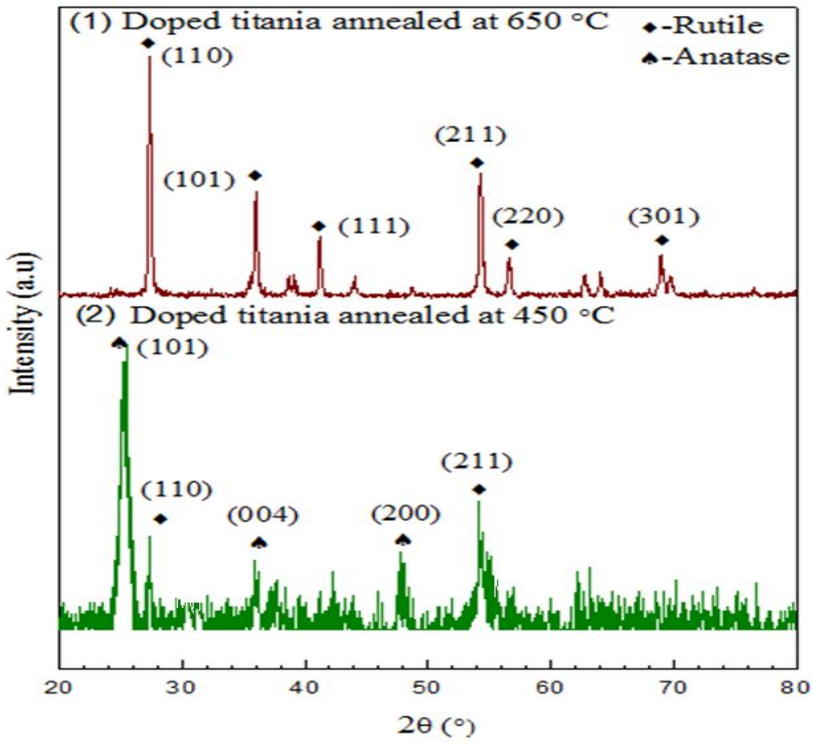

Fig. 6.3 XRD spectra of 3wt% Cu doped nanoparticles annealed at different temperatures.

Table 6.1 XRD table showing dominant and minor phases of samples.

Sample	Annealing Temperature (°C)	Dominant phase	Minor Phase
Undoped titania	450	Anatase	None
Undoped titania	650	Anatase	Rutile
1wt% Cu doped titania	450	Anatase	None
1wt% Cu doped titania	650	Anatase	Rutile
3wt% Cu doped titania	450	Anatase	Rutile
3wt% Cu doped titania	650	Rutile	None

Fig. 6.2 shows the XRD patterns of 1wt% Cu doped titania. Sample annealed at 450 °C completely show anatase phase and no other peak is being observed and sample annealed at 650 °C show a little peak of rutile phase. The reason for no prominent change when compared with XRD patterns of undoped titania samples might be low concentration of dopant. Therefore it can be concluded inclusion of impurities at this concentration didn't affect the crystal structure of titania.

Whereas, introducing 3 wt% copper in titania lattice initiates rutile phase as evident from Fig. 6.3 where peak of rutile phase can be observed when the sample for annealed at 450 °C and a complete transformation of phase is been shown at 650 °C where all peaks corresponds to rutile phase of titania (JCPDS card# 76-1934). Increase in rutile fraction with doping indicates inhibition of the formation of complete anatase phase due to incorporation of Cu on the titania lattice. The inclusion of copper in titania anatase creates a higher number of defects which results in quicker formation of rutile nuclei. During annealing, the replacement of Ti^{4+} by Cu^{2+} cause a decrease in free electron

concentration and an increase in oxygen vacancy concentration. Anatase to rutile phase transition occurs because of this increase in oxygen vacancies created in crystal lattice [4]. The phase transformation results are consistent with DT analysis explained latter. No peaks of copper are being observed in XRD of the doped Cu titania particle due to very low concentration of the dopant.

The crystallite size of the samples is calculated by using Scherer's equation,

$$d = \frac{K\lambda}{\beta cos\theta}$$

Where d is the crystallite size, k=shape factor, λ is the wavelength of X-ray radiation, β is full width at half maximum, and θ is the diffraction angle. The resultant sizes for undoped titania is 13.1nm and 43.1 nm annealed at temperatures 450 °C and 650 °C respectively and that for 3wt% Cu-doped titania is 11.6 nm and 36.6 nm annealed at temperatures 450 °C and 650 °C respectively. The trend in crystallite size due to annealing and doping has been shown in Table 6.2 and it shows increasing annealing temperature increases the crystallite size. The increase is due to increase in crystallinity of particles. Greater crystallite size indicates greater crystallinity of nanoparticles [5]. So we see, adding dopant decreased the crystallite size and crystallinity of the particles when compared with undoped samples at their respective temperatures. This means copper might exist in amorphous form (later confirmed by FTIR results). These results show that incorporation of dopants in host nanomaterials modified the crystal phase.

6.1.2 Effect of Crystal Phase of Titania on Performance of DSSCs

Anatase allows more absorption of dye and hence performs better when compared to other phases. But studies have shown that co-presence of anatase and rutile crystallites can enhance charge separation, photocatalytic activity and transfer of photo-generated electrons and holes [6]. DSSCs made with P25 (Degussa) showed higher efficiency and better photocatalytic performance. P25 is composed of anatase and rutile crystallites, anatase being the major phase and rutile being the minor (in rations 70:30 or 80:20).

Table 6.2 Crystallite sizes of undoped, 1wt% and 3wt% Cu-doped titania at 450 °C and 650 °C.

Sr no	Sample	Annealing Temperature (°C)	Crystallite Size (nm)
1)	Undoped Titania	450	13.1
2)	Undoped titania	650	43.1
3)	1wt% Cu doped titania	450	12.9
4)	1wt% Cu doped titania	650	13
5)	3wt% Cu doped titania	450	11.6
6)	3wt% Cu doped titania	650	36.6

These results showed that doping titania with 3wt% copper caused oxygen deficiency and created defects. While doping titania with 1wt% copper hardly had any effect on crystal structure. Therefore, other techniques were used to probe deeply into the effects of inclusion on 3wt% copper dopant in titania.

6.1.2 Effect of Annealing Temperature and Cu Addition on Morphology, Composition and Particle Size of Nanoparticles (SEM/EDX Analysis)

The high-resolution SEM micrographs of undoped and 3wt% Cu-doped titania nanoparticles annealed at 450 °C and 650 °C are shown in Fig.4

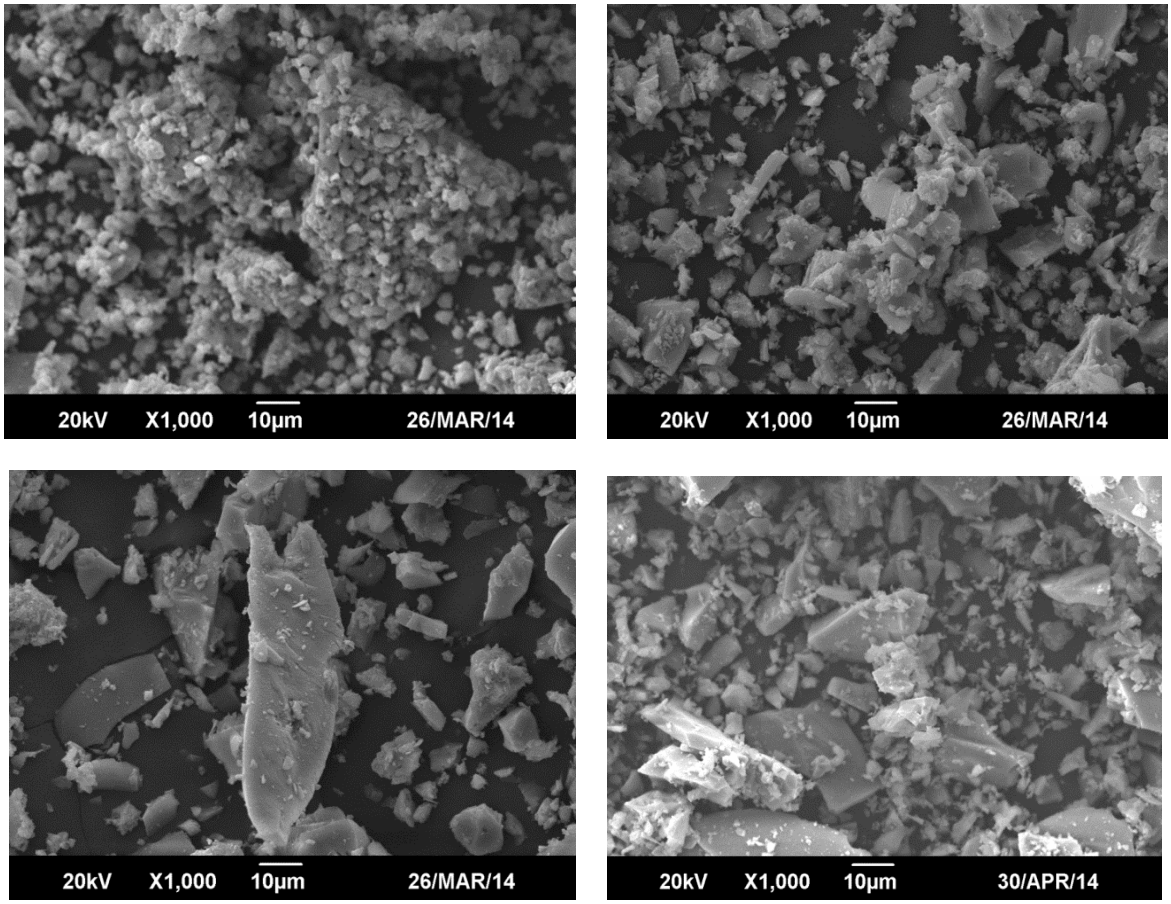

Fig. 6.4 SEM images (a) undoped titania particles annealed at 450 °C, (b) undoped titania particles annealed at 650 °C, (c) 3wt% Cu-doped titania particles annealed at 450 °C and (d) 3wt% Cu-doped titania particles annealed at 650 °C.

Fig. 6.4 shows that the particles are of arbitrary shape. With increasing annealing temperature of undoped titania nanoparticles from 450 °C to 650 °C, growth of particles can be seen in Fig. 6.4 (a) and (b). In Fig 6.4 (c) and (d) we can see an accumulation of some substance appearing lighter in images. The substance accumulation is increasing with increasing annealing temperature. This can be attributed to the formation of oxide with doping and increasing temperature.

The particle size distribution shows that the average particle size of undoped titania is 68.64 nm and 71 nm annealed at 450 °C and 650 °C respectively and that of 3wt% Cu doped nanoparticles is 61.84 nm and 60.50 nm annealed at 450 °C and 650 °C respectively. Increasing Annealing temperature decreased the average particle size of titania as shown in Table 6.3. Small particles offer large surface areas allowing better light absorption. Current density can be more than doubled by controlling particle size [7]. Large particles allows strong light scattering [8].

Table 6.3 Summary of SEM/EDX results.

Sample	Annealing Temperature (°C)	Atom%			Particle Size (nm)
		Ti	O	Cu	
Undoped titania	450	31.51	68.49	0	68.64
Undoped titania	650	31.10	68.90	0	71.27
3wt% Cu doped titania	450	28.08	70.67	1.24	61.84
3wt% Cu doped titania	650	24.74	71.51	0.74	60.50

The decrease in average particle size of 3wt% Cu doped samples can be observed. It is due addition of dopant cause inhibition of the growth and hence decrease in particle size. We observed a decrease in crystallinity in our XRD results as well. These results reported by Wang et al. [9] are consistent with our Cu-doped titania results. He observed a decrease in grain size and formation of amorphous crystal structure with doping iron and reported further decrease in particle size with increasing dopant concentration. Li et al. [10] studied Zn-doped SnO_2 nanomaterials and also reported a decrease in particle size. The change in grain size with addition of dopant is basically very important phenomenon for change in electronic structure. Hence addition of dopant and its concentration can be used to tailor the particle size of copper doped titania.

Fig. 6.5 shows the EDX pattern of the undoped and 3wt% Cu-doped titania nanoparticles, showing the presence of Cu, Ti, and O in the nanoparticles. No impurities can be observed. The results are summarized in table 6.3. In Fig 6.5 (c) and (d) presence of copper (~3 wt%) confirms the doping of the copper in titania and the result is consistent with results of XRD and FTIR spectroscopy.

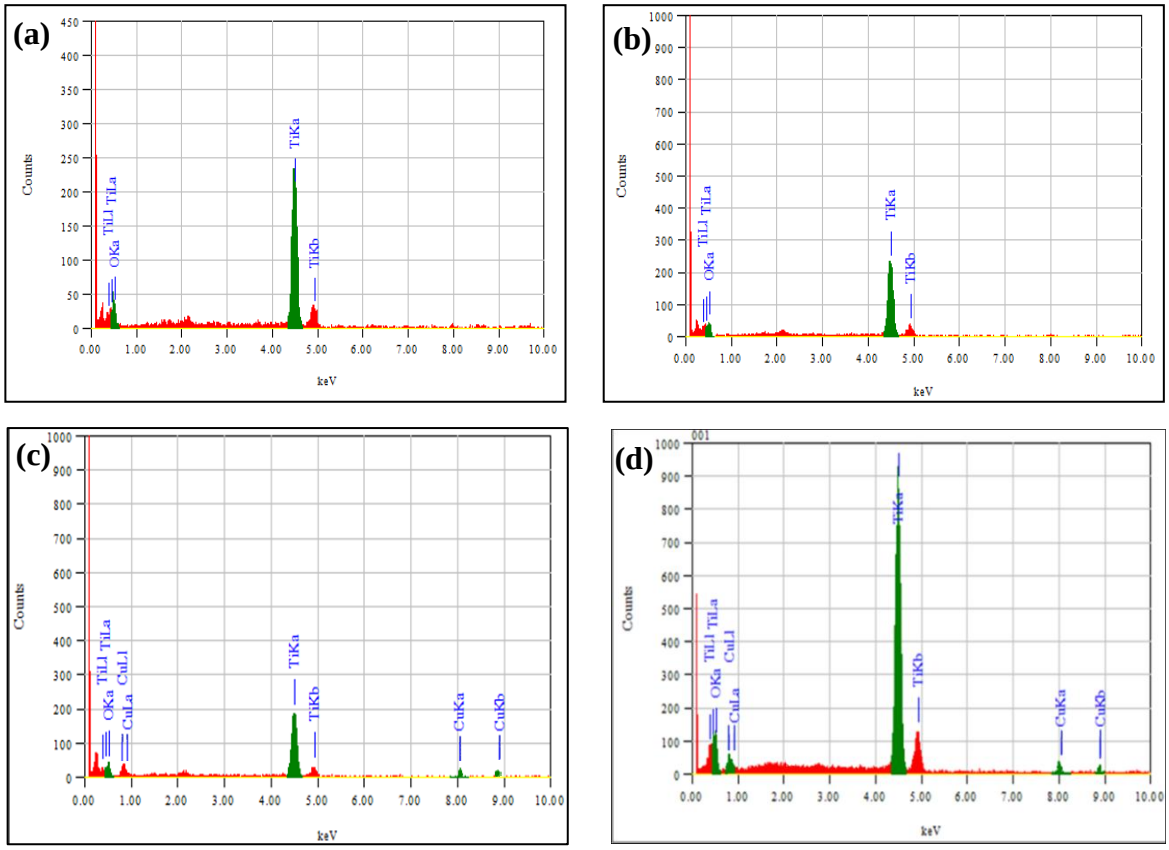

Fig. 6.5 EDX pattern of (a) undoped titania annealed at 450 °C (b) undoped titania annealed at 650 °C (c) 3wt% Cu doped titania annealed at 450℃ and (d) 3wt% Cu-doped titania annealed at 650 °C.

6.1.3 UV-Vis Analysis of 3wt% Cu Doped Titania Nanoparticles

Anatase titania has Eg value 3.31 eV and exhibits absorption peaks in UV region of electromagnetic radiations. The absorption spectrum of undoped and 3wt% Cu-doped titania is shown In Fig. 6.6. Doping copper in titania lattice shows an absorbance shift towards the visible spectrum. Undoped titania particles exhibits maximum absorption at 325 nm whereas, doped sample exhibits maximum absorption at 379 nm. The absorption peaks corresponds to the maximum absorption when electrons are excited

from the valence to the conduction band. Doped sample shows a shift in the absorption towards visible region. The CB in titania comprises of Ti 3d states and VB comprises of O 2p states. The 325 nm absorption peak is due to electronic transition from O 2p to Ti 3d. The absorption shift to 379 nm appears as a result of charge transfer at the interface from the O 2p VB to the Cu (II) state attached to titania. These Cu (II) states may be present either as Cu (II) nanoclusters or in the form of amorphous oxide phase of CuO. Li et al. [11] demonstrated that Cu (II) does not show this absorption peak if it is present as CuO, but displays this absorption when it is present only as Cu (II) ions attached to titania. However, Qiu et al. [12] suggested that the absorption peak shift appears due to charge transfer from titania to CuO clusters in CuO/Titania nanocomposite. Therefore, based on these observations, we can predict that the absorption appears due to charge transfer from O 2p to Cu (II) clusters or CuO amorphous phase. Hence it can be concluded that substitution of Ti^{4+} by Cu^{2+} atoms generates defect centers that cause the change in optical absorption. These results were later affirmed by FTIR analysis results which showed that in our case, copper existed as CuO form.

Doping titania with a transition metal leads to the reduction in the band gap energy which is attributed to the inclusion of copper ions into titania crystal lattice and/or formation of CuO on surface of the particles. It has been studied that doping titania with aliovalent ions changes the material properties and absorption properties because of the modification in local lattice symmetry and defects. When titania is doped with copper, Cu^{2+} ions either locate themselves on the surface sites or inside bulk titania. This causes lattice deformation due to rearrangement of adjoining atoms to neutralize charge deficiency. This lattice deformation and rearrangement modifies electronic structure and hence the band gap shift occurs [10].

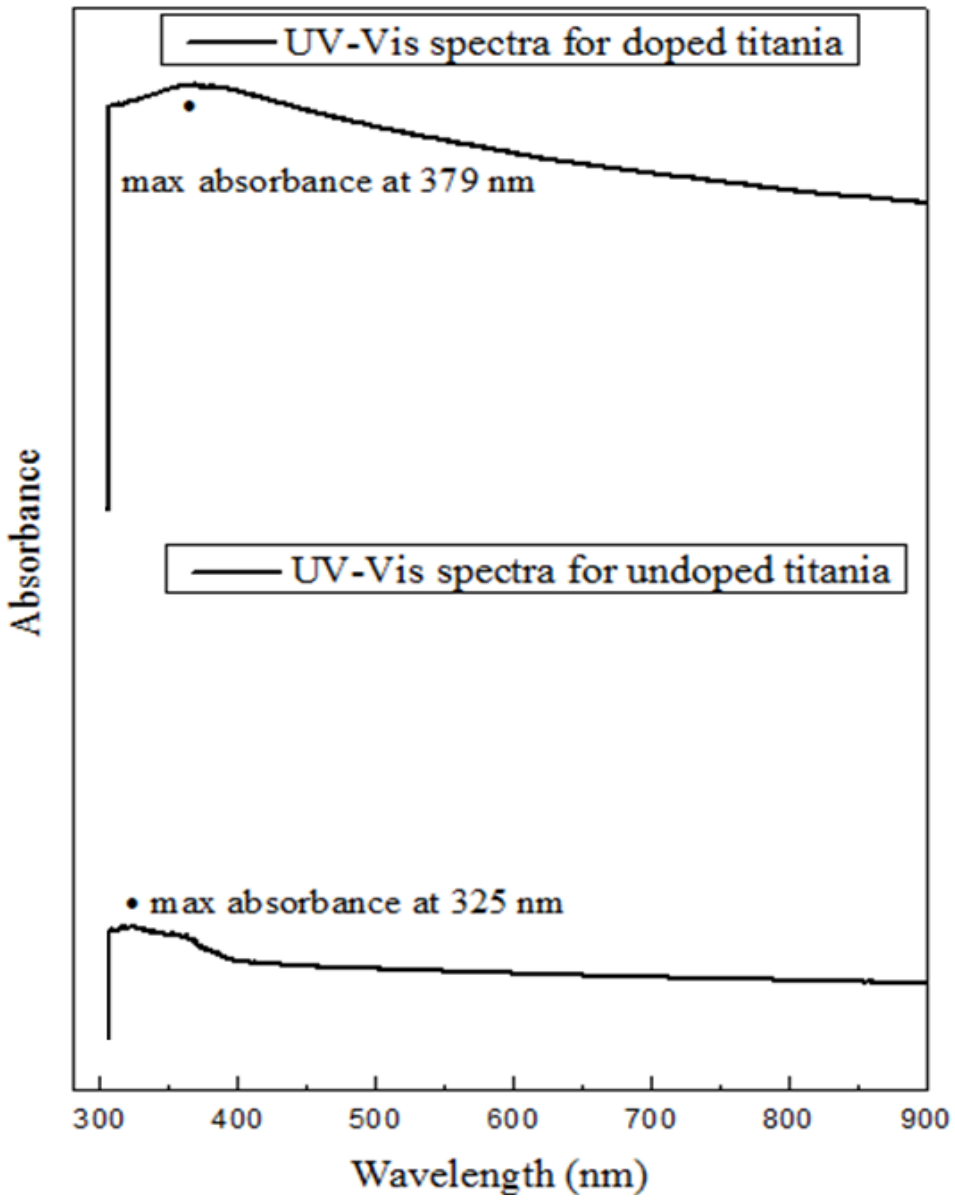

Fig. 6.6 UV-VIS spectra for undoped and 3wt% Cu-doped titania annealed at 450 °C.

Also, oxygen vacancies are created due to presence of small amounts of Cu^{2+} dopant in the lattice sites of titania [4, 13]. These are created due to charge compensation effect. It is, therefore, possible to control band gap shift and absorption of the doped nanoparticles controlled by lattice strain and doping-induced vacancies.

6.1.4 Thermal Analysis of Undoped and 3wt% Cu Doped Titania Nanoparticles Using TG/DT Setup

Fig. 6.7 shows the TG/DTA curves of doped and 3wt% Cu-doped titania nanoparticles. Looking at TG curves of both samples, initial weight loss is being observed at temperatures below 100 °C. This weight loss indicates the removal of water and ethanol from powders. At temperatures from 100 °C to 300 °C, a weight loss of 17% for undoped titania powder and 15% for doped titania powder is being observed. This loss can be attributed to the removal of un-hydrolyzed isopropoxide ligands in titania. A total of 18% weight loss for pristine powder and 17.5% weight loss for Cu-doped titania powders has been observed which is approximately same for both the powders. Weight loss tends to seize after 400 °C.

From DTA curves, we can observe one sharp exothermic reaction peaks in both the graphs. For undoped titania, the exothermic peak appears at 399 °C and for doped titania it appears at 310 °C. These exothermic peaks indicate a phase change of samples from amorphous to crystalline. These results are consistent with XRD results. Undoped titania powders need more heat to crystallize since they possess smaller crystallite size of particles. It is evident from DT curves that doped titania sample shows crystallization at lower temperature than undoped titania. Incorporation of Cu dopant in titania reduces its crystallization temperature. This corresponds to the XRD results which indicated formation of rutile phase in doped titania powder at lower temperature (650 °C Figure 6.2). In Fig 6.7 (b) formation of new peak can be observed at 480 °C which may be attributed towards the phase shift from anatase to rutile in 3wt% Cu doped sample.

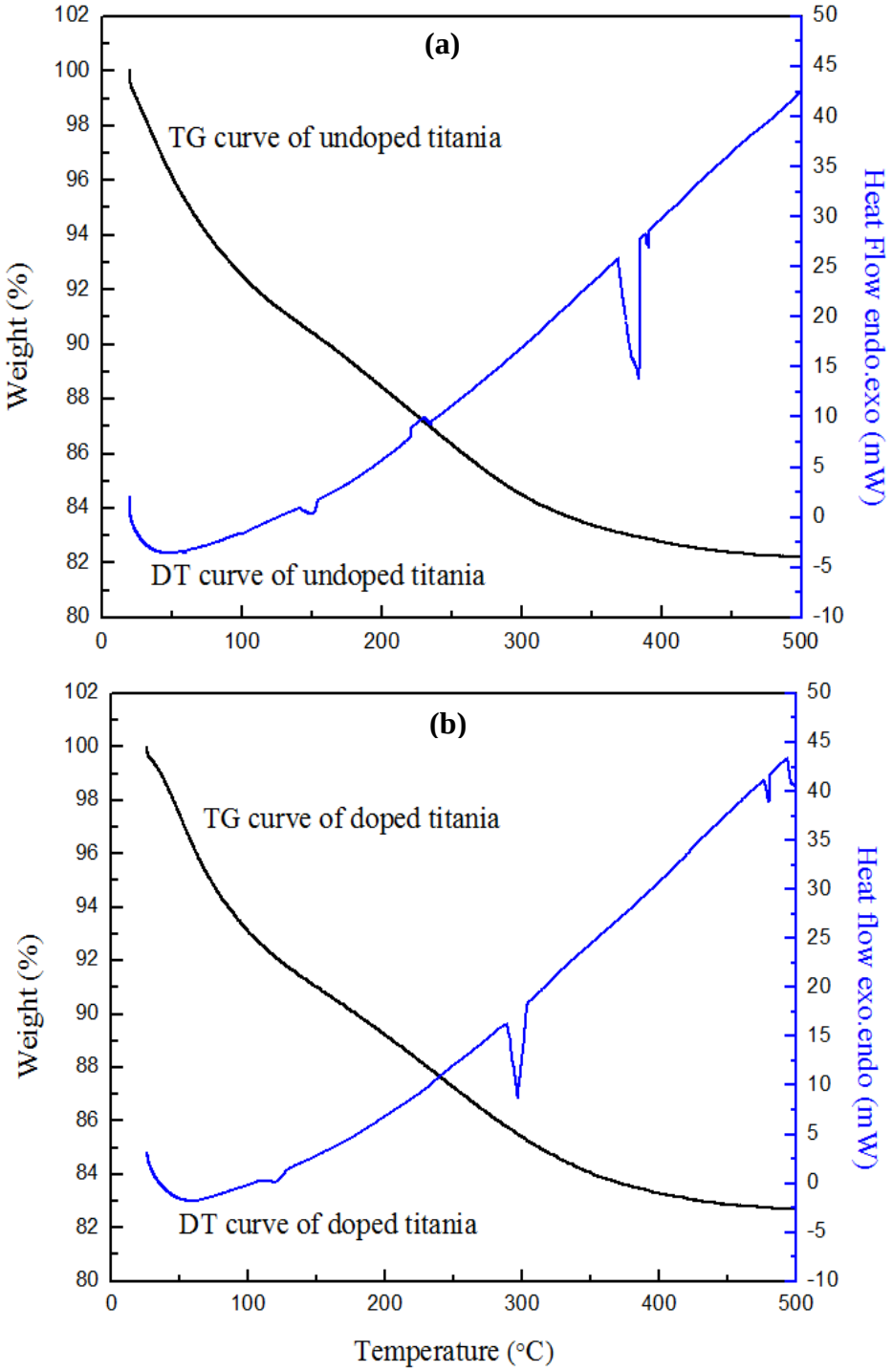

Fig. 6.7 TG-DT curves of (a) undoped and (b) 3wt% doped titania up to 500 °C.

6.1.5 FTIR Analysis

Infrared spectroscopy was done to investigate the surface properties of the prepared doped and undoped titania nano-powders. Chemical bonding of elements was explored

by correlating the obtained peaks in spectra with the stretching or vibration of different functional groups. The spectra were used to probe presence of carbon and OH groups in samples and also to examine the chemical state of copper in doped powder samples.

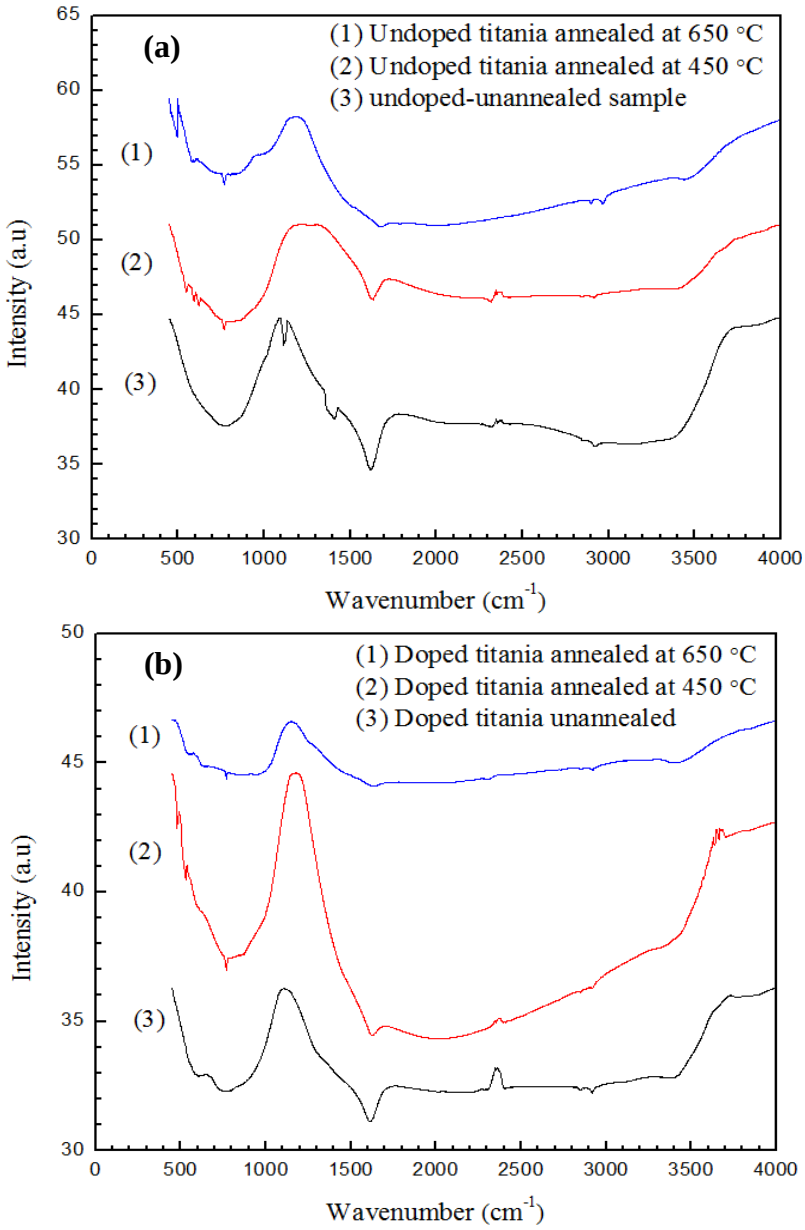

Fig. 6.8 FTIR spectra of (a) undoped titania and (b) doped titania at different annealing temperatures.

Fig 6.8 shows the FTIR spectra of undoped and doped titania powder samples at different annealing temperatures respectively. The common peaks at 3200-3600 cm^{-1} correspond to the stretching vibration of OH bond and peaks at 1630 cm^{-1} correspond to

the bending vibration of surface OH bond [14]. It is reported in literature hydrolysis reaction in sol-gel synthesis of nanoparticles is responsible for the presence of TiO_2-OH bonds, but chemically and physically adsorbed water on the surface of titania can also be the reason for the presence of this bond. From the figures a decrease in intensity of OH bonds can be clearly observed with increasing annealing temperature and lowest amount of surface OH groups are present in powders annealed at 650 °C due to dehydration during annealing. The surface hydroxyl content is directly proportional to photocatalytic activity. Increase in hydroxyl content enhances the photocatalytic activity. The reason is that the hydroxyl group can behave as a center for capturing the photo-excited electron [15].

For annealed samples appearance of bands at 621 cm^{-1}, 594-549 cm^{-1}, 412 cm^{-1} are attributed towards the Ti-O vibrations. The peak at 768 cm^{-1} is characteristic feature of crystalline titania (anatase/rutile) spectrum. This peak corresponds to the stretching vibration of Ti-O bonds in TiO_4 tetrahedral geometry [16].

The presence of peaks in un-annealed samples at 1045 cm^{-1} and 1114 cm^{-1} show the presence of carbon group (Ti-O-C). This can be attributed to the presence of alkoxy group formed in sol-gel process which is removed during annealing process. These results are in exact accordance with TG analysis.

In Fig. 6.8 (b) new peaks are observed at 480-529 cm^{-1} in powder samples annealed at certain temperatures which correspond to the stretching mode of Cu-O bond [17] [18]. This result along with EDX spectra confirms the incorporation and doping of copper in titania lattice and its existence as CuO. Peaks at 2300-2500 cm^{-1} can be attributes to CO_2 resulting from surrounding conditions.

6.3 Discussion on Inclusion of Carbon Microspheres in 3wt% Cu Doped Titania Pellets.

Fig. 6.9 shows the XRD pattern of synthesized carbon microspheres. The pattern corresponds to the XRD pattern of carbon referring to JCPDS card# 50-1086. No peak of any impurity is visible. This pattern was achieved after annealing the as received sample at 350 ° for 10h.

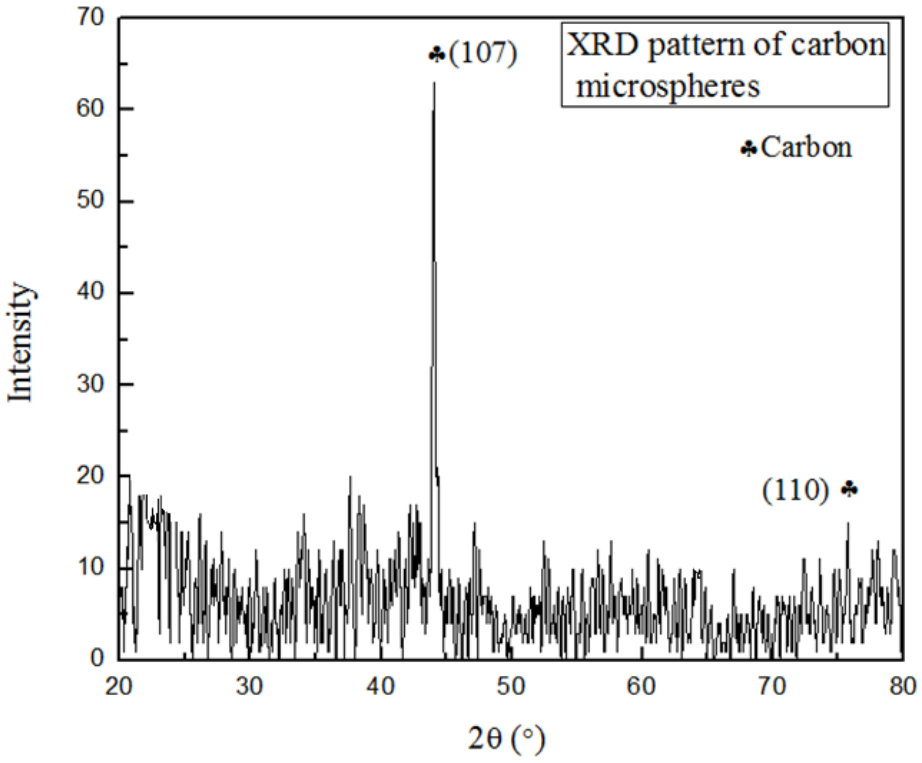

Fig. 6.9 XRD pattern of carbon microspheres annealed at 350 °C for 4h.

EDX was also performed on carbon microspheres which showed that the main component of is carbon (61 atomic%). The presence of oxygen component is because of the water molecules absorbed in the porous structure [19].

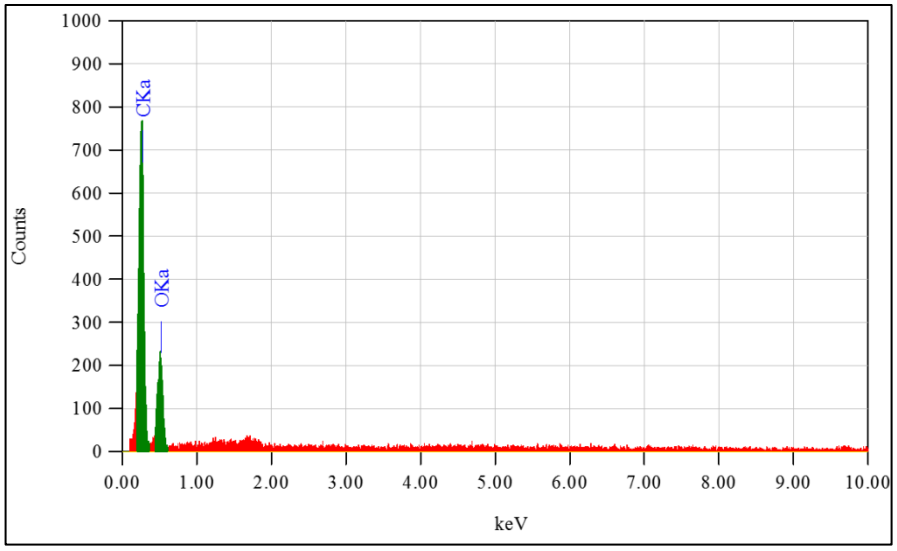

Fig. 6.10 EDX pattern of carbon microspheres annealed at 350°C for 10h.

The pellets that were made with carbon microspheres and without carbon microspheres were sintered at 500 °C. Carbon microspheres are removed at around 490 °C [20] and leads to the formation of pores. These pores or cavities are responsible for enhancing porosity, light scattering and surface area for dye adsorption and hence enhance performance of Dye sensitized solar Cells. Fig. 6.11 shows the isotherms of sample with and without the inclusion of carbon microsphere. The isotherms represents type IV which indicates the presence of the mesopores in the samples [21]. Other factors like pore size, BET surface area and porosity have been shown in table 6.4. It is clear from the values of BET surface area that inclusion of microspheres increased the surface area for enhanced adsorption of dye. This leads to higher photovoltaic performance of the cells due to enhancement of light absorption [22].

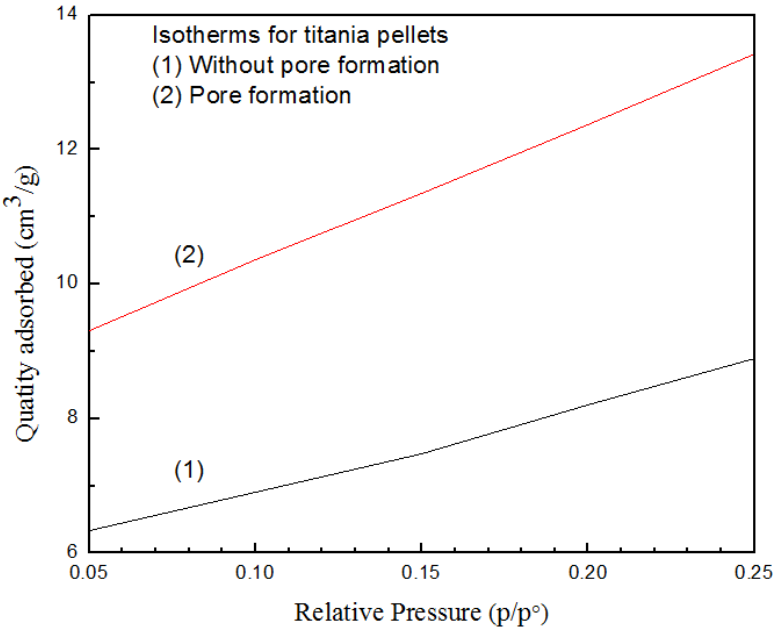

Fig. 6.11 N2-sorption isotherm for titania with and without inclusion of carbon microspheres.

The sample with carbon microspheres also showed enhanced porosity, pore volume and pore size. Porosity was calculated using formula

$$Porosity = \frac{Pore\ Volume}{Total\ Volume}$$

The optimized porosity for best performance of solar cells with thickness of photoanode around 20-25 µm is 40% as reported in the literature [23]. The sample showing porosity near to the optimized is the one that has pores due to carbon microsphere inclusion. Enhanced pore size aids the access of electrolyte and molecules of the dye to the surface of titania improving J_{sc} of the cells. Hence, to enhance the performance of photoanode and consequently, the performance of the cell, it is advisable to include carbon microspheres in the titania layer of photoanode.

Table 6.4 Summary of the results of N2-sorption.

Sr no	Sample	BET surface area (m2/g)	Pore size (Å)	Pore volume (cm3/g)	Porosity (%)
1)	Titania pellet without carbon microsphere	30.0134	16.5126	0.2498660	31
2)	Titania pellet with carbon microspheres	46.1338	20.5062	0.3014512	42

6.4 Analysis of Thin Film Coatings of 3wt% Cu Doped Titania

6.4.1 Control on Density of Cracks

In this section, we have studied and explained the effect of various process parameters such as drying time, film thickness, stirring time and solvents on film coating focusing the presence of cracks and its density. Cracking of inorganic films has been reported in previous studies [24] [25]. Several reasons have been proposed for formation of crack in films like the formation of cracks during annealing because of strain incompatibilities. During sintering cracks favorably develop from intrinsic defects. Cracking can also take place during cooling of annealed films. Cracks during cooling occur in system in which coated films and substrates have different thermal expansion coefficients. Cracks in thin film coatings of titania on substrates to be used in DSSCs can lead to short circuit the cell.

Initially when films were grown on FTO coated glass substrates, cracks were observed. It was observed that the density of cracks depended on the quality and thickness of the film as well as on drying time of the coating. Doping and annealing had no effect on cracks. Thicker films (~ 90-120 µm) showed higher crack density visible by naked eye. When the thinner films were grown (~30-60 µm) the size of cracks reduced to microscopic and weren't visible by eye. Camera images of thick and thin film coating are shown in Fig. 6.12.

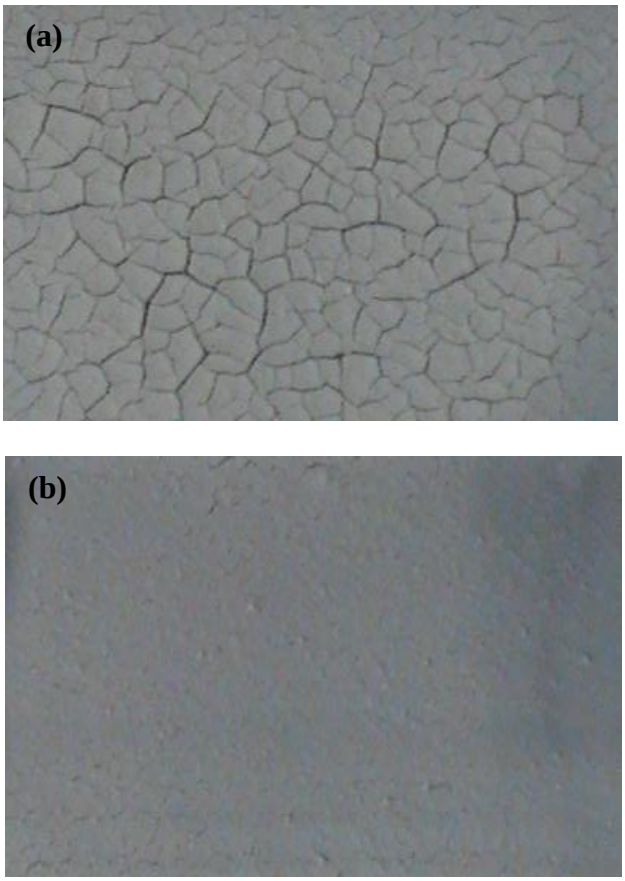

Fig. 6.12 Camera images of 3wt% Cu doped titania coatings on FTO glass with film thickness (a) 90 µm and (b) 40 µm.

It was observed that crack density also reduced with increasing drying time. When films were dried on hot plate, it took 5 minutes to get completely dried. The films got cracked, brittle and tore up from the substrates. The films that were dried at room temperature took 30 minutes to get dried. They didn't tear up from substrate and there were fewer cracks observed. The least number of cracks were seen in films whose drying time was increased to 2h by putting in a petri dish. The drying of porous materials in paste cause cracking of films because of the development of drying stresses These stresses are linked to tension forces that exist in liquid inside the pores of drying body. The reduction of crack density with increasing drying time can be observed in Fig. 6.13.

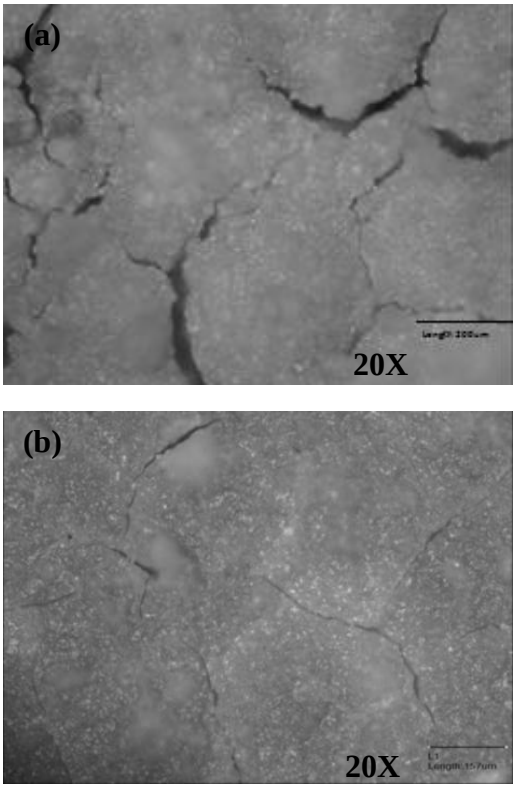

Fig. 6.13 Optical images of 3wt% Cu doped titania Thin film with drying time (a) 30 min. (b) 2 h

Table 6.5 Summary of dependence of crack density as a function of drying time.

Sr No	Drying time	Resultant film.
1)	5 min	Brittle and too many cracks
2)	30 min	Less density of cracks
3)	2h	Least crack density

Repeating experiments to obtain good paste and incorporating precautions while coating helped to minimize the cracks. A number of factors were studied including stirring time, solvents and addition of surfactant the details of which are summarized in Table 6.6.

Table 6.6 Summary of experiments and results of optimized slurry formation.

Exp	Solvents	Surfactant	Stirring time (min)	Result	Fig. 6.14
1	Acetic acid	None	30	Cracked film	a
2	Ethanol	None	60	Slight Reduction in cracks	b
3	Ethanol+water	None	120	Significant Reduction in cracks.	c
4	Ethanol+water $+HNO_3$	None	180	Negligible cracks	d
5	Ethanol+water $+HNO_3$	PEG (polyethylene glycol)	180	Negligible cracks	e

The optical microscopic images of experiments corresponding to table 6.6 are shown in figure 6.14. Films got improved with increasing stirring time. The maximum number of cracks was seen in paste formed using acetic acid Fig. 6.14 (a) and ethanol Fig. 6.14 (b). Addition of water increased the stirring time of paste which resulted in more homogenous and comparatively less cracked thin films Fig. 6.14 (c). The density of cracks exceptionally reduced by addition of HNO_3 Fig. 6.14 (d). The reason can be attributed to better dispersing of titania nanoparticles With addition of surfactant a better cohesion of film to substrate was observed but no effect on cracks was observed. It was observed annealing almost had no effect on cracks, neither did the doping.

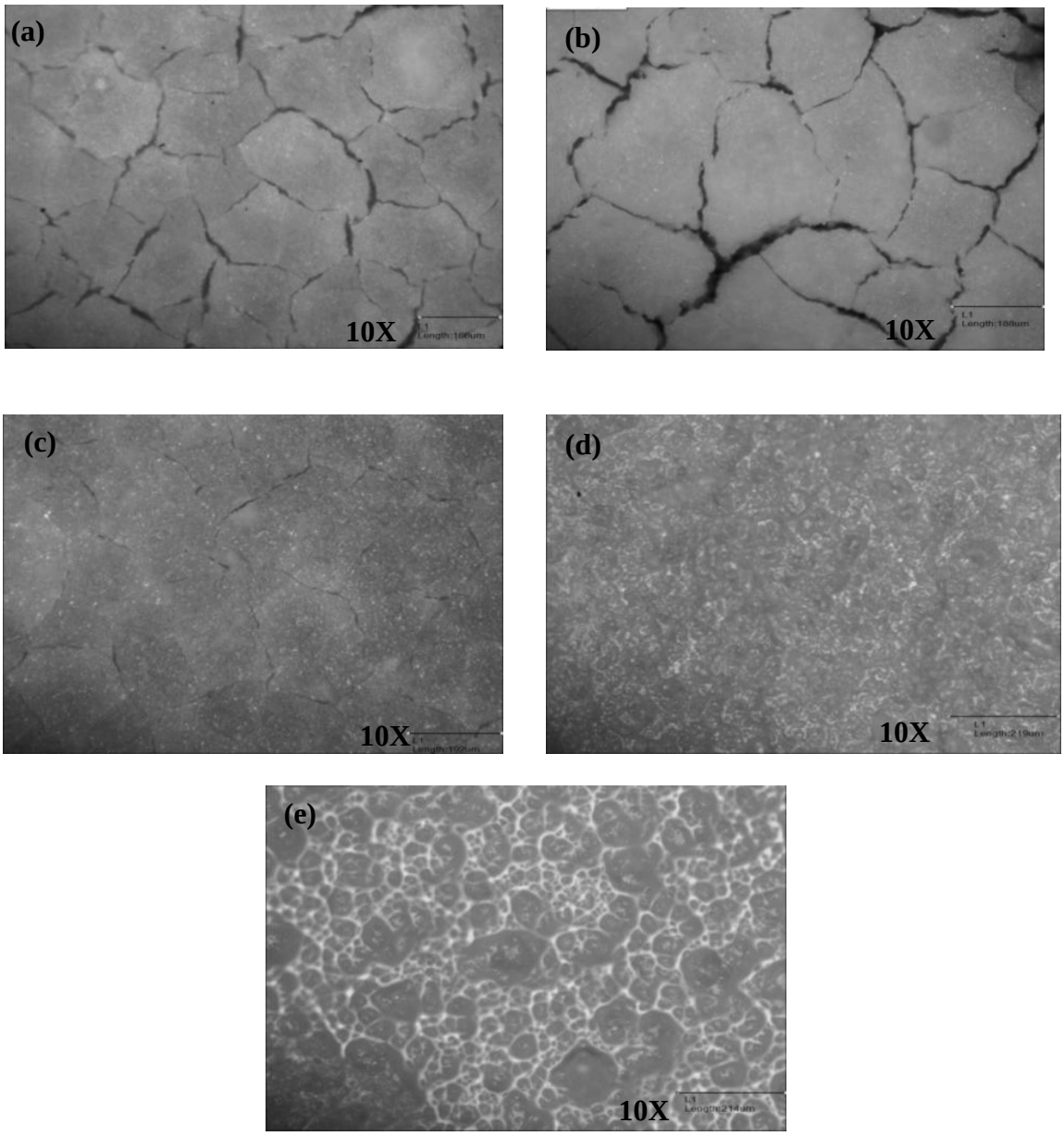

Fig. 6.14 Optical images of 3wt% Cu doped titania coatings FTO substrates.

6.4.2 Cross-section SEM Image of 3wt% Cu Doped Titania Film

Cross-sectional view of the film on FTO substrate is shown in Figure 6.15 showing a thickness of 30.29 µm.

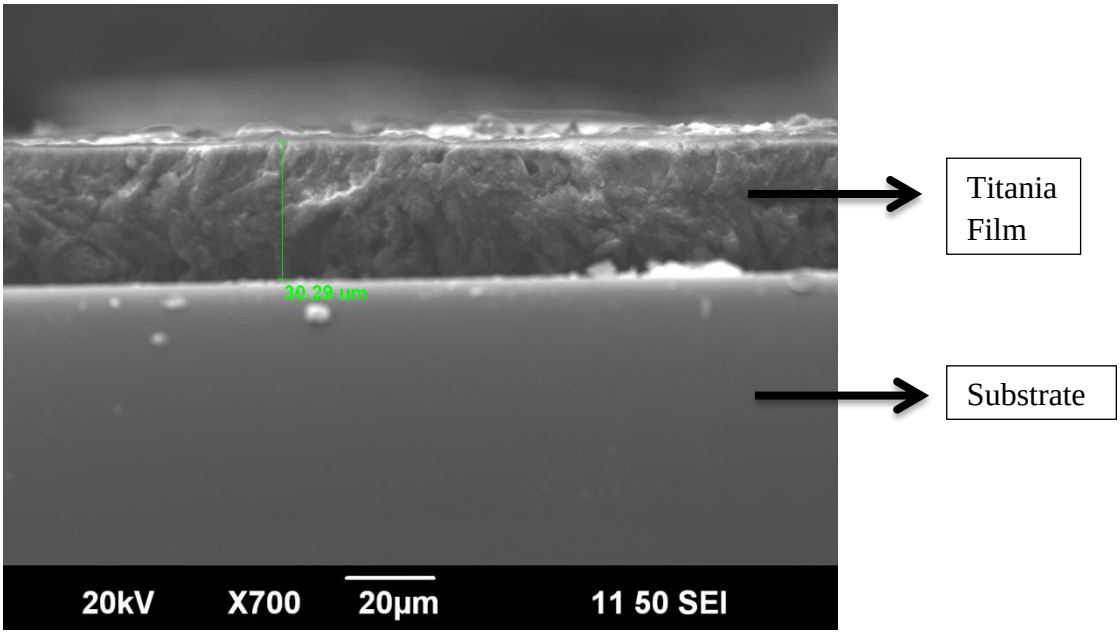

Fig. 6.15 Cross-sectional SEM of 3wt% Cu doped titania thin film.

6.5 Increase in V_{oc} of 3wt% Cu Doped Titania Based Dye Sensitized Solar Cells

IV characteristics of the cells are shown in Fig 6.16. It is evident from figures that using copper doped titania anode in DSSC affected V_{oc} and J_{sc} of the cell. An increase in V_{oc} and a decrease in J_{sc} is observed in IV characteristics of 3wt% Cu doped titania based DSSC when compared to undoped titania based DSSC.

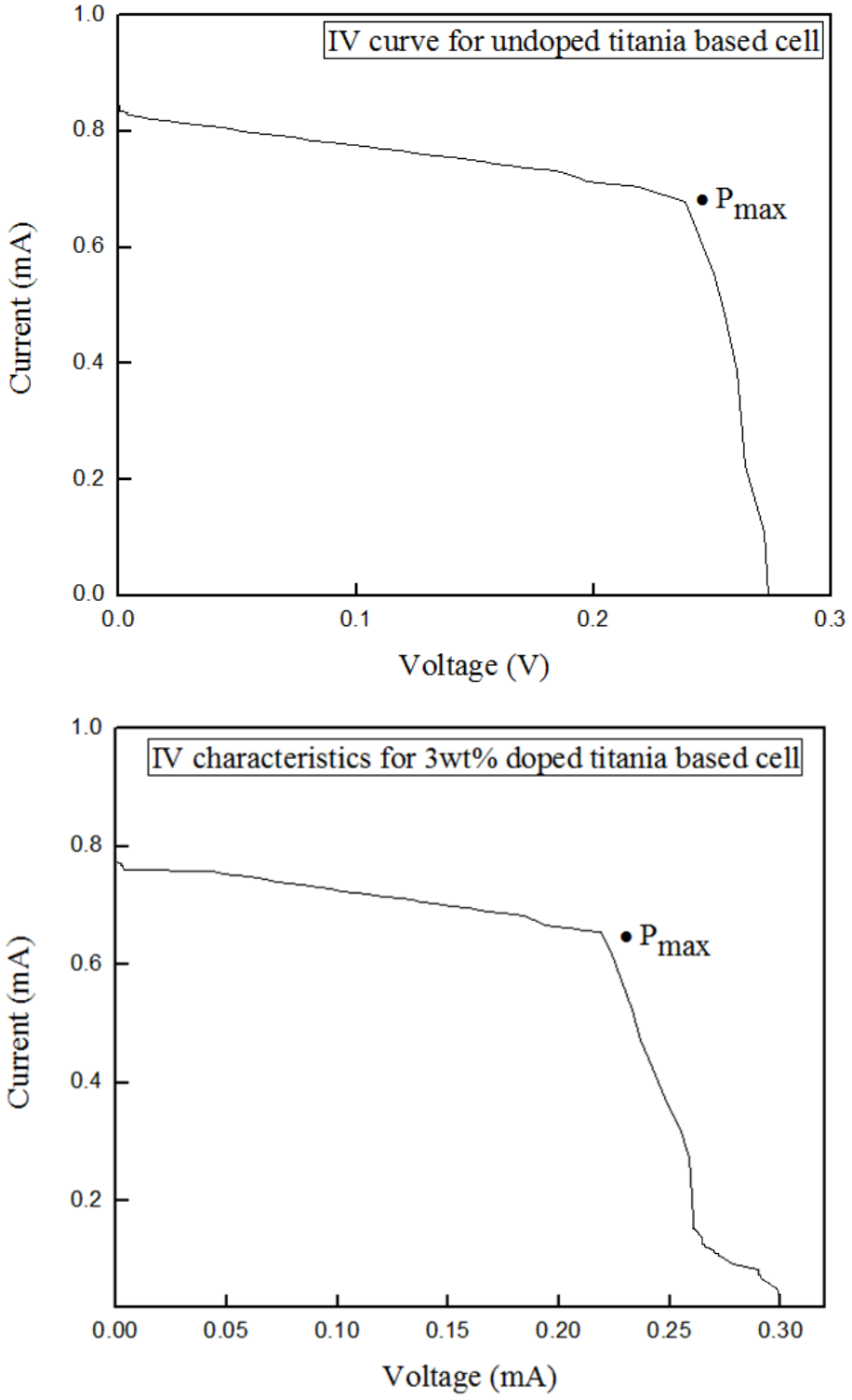

Fig. 6.16 IV characteristics of (a) undoped and (b) doped titania based dye sensitized solar cells.

Table 6.7 Summary of the IV characteristics of the doped and undoped titania based DSSCs.

Sr No	Cell	Annealing Temperature	V_{oc} (volts)	J_{sc} (mA)	η (%)
1	Undoped titania based DSSC	450 °C	0.27	0.83	0.14
2	3wt% Cu-doped titania based DSSC	450 °C	0.30	0.79	0.15

An 11% increase in V_{oc} and a 4.8% decrease in J_{sc} was calculated from IV curves. Increase in V_{oc} attributes to the reduction in band gap energy of titania as explained earlier in topic 6.1.3. Also co-presence of anatase and rutile phase in 3wt% Cu doped titania film leads to enhanced charge separation [6]. However, smaller particle size and visible light activity mechanisms should have increased J_{sc}. But decrease is J_{sc} occurred due to some other factor inhibiting the cell performance strongly. It was confirmed by XRD, FTIR and UV-Vis analysis of doped titania nanoparticles that copper existed as CuO form in titania lattice. The presence of this amorphous CuO layer causes hindrance in diffusion and injection of electrons leading to a decrease in J_{sc}. Also, due to presence of copper, redox reactions with electrolyte ions can occur causing a decrease in J_{sc}.

References

[1] J. dos Santos, T. Ogasawara, and R. Corrêa, "Synthesis of mesoporous titania in rutile phase with pore-stable structure," *Brazilian Journal of Chemical Engineering*, vol. 26, pp. 555-561, 2009.

[2] Y.-F. Li and Z.-P. Liu, "Particle size, shape and activity for photocatalysis on titania anatase nanoparticles in aqueous surroundings," *Journal of the American Chemical Society*, vol. 133, pp. 15743-15752, 2011.

[3] B. Choudhury, M. Dey, and A. Choudhury, "Defect generation, dd transition, and band gap reduction in Cu-doped TiO2 nanoparticles," *International Nano Letters*, vol. 3, pp. 1-8, 2013.

[4] J. Nair, P. Nair, F. Mizukami, Y. Oosawa, and T. Okubo, "Microstructure and phase transformation behavior of doped nanostructured titania," *Materials research bulletin*, vol. 34, pp. 1275-1290, 1999.

[5] C. Chia, S. Zakaria, M. Yusoff, S. Goh, C. Haw, S. Ahmadi, N. Huang, and H. Lim, "Size and crystallinity-dependent magnetic properties of CoFe nanocrystals," *Ceramics International*, vol. 36, pp. 605-609, 2010.

[6] D. C. Hurum, A. G. Agrios, K. A. Gray, T. Rajh, and M. C. Thurnauer, "Explaining the enhanced photocatalytic activity of Degussa P25 mixed-phase TiO_2 using EPR," *The Journal of Physical Chemistry B*, vol. 107, pp. 4545-4549, 2003.

[7] L. Du, A. Furube, K. Hara, R. Katoh, and M. Tachiya, "Mechanism of particle size effect on electron injection efficiency in ruthenium dye-sensitized TiO_2 nanoparticle films," *The Journal of Physical Chemistry C*, vol. 114, pp. 8135-8143, 2010.

[8] M.-J. Jeng, Y.-L. Wung, L.-B. Chang, and L. Chow, "Particle size effects of TiO_2 layers on the solar efficiency of dye-sensitized solar cells," *International Journal of Photoenergy*, vol. 2013, 2013.

[9] Z.-M. Wang, G. Yang, P. Biswas, W. Bresser, and P. Boolchand, "Processing of iron-doped titania powders in flame aerosol reactors," *Powder technology*, vol. 114, pp. 197-204, 2001.

[10] L. Li, J. Liu, Y. Su, G. Li, X. Chen, X. Qiu, and T. Yan, "Surface doping for photocatalytic purposes: relations between particle size, surface modifications, and photoactivity of SnO2: Zn2+ nanocrystals," *Nanotechnology*, vol. 20, p. 155706, 2009.

[11] G. Li, N. M. Dimitrijevic, L. Chen, T. Rajh, and K. A. Gray, "Role of Surface/Interfacial Cu2+ Sites in the Photocatalytic Activity of Coupled CuO− TiO2 Nanocomposites," *The Journal of Physical Chemistry C*, vol. 112, pp. 19040-19044, 2008.

[12] X. Qiu, M. Miyauchi, K. Sunada, M. Minoshima, M. Liu, Y. Lu, D. Li, Y. Shimodaira, Y. Hosogi, and Y. Kuroda, "Hybrid Cu x O/TiO2 Nanocomposites As Risk-Reduction Materials in Indoor Environments," *ACS nano*, vol. 6, pp. 1609-1618, 2012.

[13] G. Liu, C. Sun, X. Yan, L. Cheng, Z. Chen, X. Wang, L. Wang, S. C. Smith, G. Q. M. Lu, and H.-M. Cheng, "Iodine doped anatase TiO 2 photocatalyst with ultra-long visible light response: correlation between geometric/electronic structures and mechanisms," *Journal of Materials Chemistry*, vol. 19, pp. 2822-2829, 2009.

[14] H. Jensen, A. Soloviev, Z. Li, and E. G. Søgaard, "XPS and FTIR investigation of the surface properties of different prepared titania nano-powders," *Applied Surface Science*, vol. 246, pp. 239-249, 2005.

[15] A. Y. A. M.HEMA, P.TAMILSELVI and R.ANBARASAN, "Titania Nanoparticles Synthesized by Sol-Gel Technique," *Chem Sci Trans.*, vol. 1, 2013.

[16] A. Murashkevich, A. Lavitskaya, T. Barannikova, and I. Zharskii, "Infrared absorption spectra and structure of TiO 2-SiO 2 composites," *Journal of Applied Spectroscopy*, vol. 75, pp. 730-734, 2008.

[17] H. W. N. Slamet, E. Purnama, K. Riyani, and J. Gunlazuardi, "Effect of copper species in a photocatalytic synthesis of methanol from carbon dioxide over copper-doped titania catalysts," *World Applied Sciences Journal*, vol. 6, pp. 112-122, 2009.

[18] N. WON and N. Vit, "Cu-Doped TiO2 Nanopowders Synthesized by Sonochemical-assisted Process," *Sains Malaysiana,* vol. 42, pp. 175-181, 2013.

[19] S. Ratchahat, N. Viriya-empikul, K. Faungnawakij, T. Charinpanitkul, and A. Soottitantawat, "Synthesis of carbon microspheres from starch by hydrothermal process," 2010.

[20] J. Qian, P. Liu, Y. Xiao, Y. Jiang, Y. Cao, X. Ai, and H. Yang, "TiO2-Coated Multilayered SnO2 Hollow Microspheres for Dye-Sensitized Solar Cells," *Advanced Materials,* vol. 21, pp. 3663-3667, 2009.

[21] S. J. Gregg, K. S. W. Sing, and H. Salzberg, "Adsorption surface area and porosity," *Journal of The Electrochemical Society,* vol. 114, pp. 279C-279C, 1967.

[22] E. Bayatloo, E. Saievar-Iranizad, and S. S. Polkoo, "Performance enhancement of TiO2-based dye-sensitized solar cells by carbon nanospheres in photoanode," *arXiv preprint arXiv:1311.0415,* 2013.

[23] Dipal B. patel, "Effect of Electrode's Geometric shape, Thickness and Porosity on the Performance of Dye Sensitized Solar Cell," *IJTEMAS,* vol. III, january 2014 2014.

[24] G. K. Goh, S. K. Donthu, and P. K. Pallathadka, "Cracking and orientation of solution-deposited rutile TiO2 films," *Chemistry of materials,* vol. 16, pp. 2857-2861, 2004.

[25] R. K. Bordia and A. Jagota, "Crack growth and damage in constrained sintering films," *Journal of the American Ceramic Society,* vol. 76, pp. 2475-2485, 1993.

Chapter 7

Conclusions and Future Recommendations

7.1 Conclusions

- Titania and doped titania nanoparticles were successfully synthesized using sol-gel method as indicated by XRD, SEM/EDX, UV-Vis spectroscopy and FTIR results.
- Copper existed as amorphous CuO form in titania. Doping copper introduced structural defects in titania and initiated rutile phase formation.
- Copper doping into titania also shifted its absorption to visible region and reduced the crystallization temperature of titania.
- Optimization of doctor blade coating process for synthesis of titania and Cu doped titania thin films lead us to make thin coatings with remarkable control on crack density.
- Carbon microspheres were synthesized using hydrothermal method to include them into titania electrode as pore former. The pore formation enhanced the porosity of semiconductor and increased its surface area for greater adsorption of the dye molecules.
- 3wt% Cu doping rendered good properties to titania and it was observed that the cells fabricated by using 3 wt% Cu doped titania based photoanode showed better V_{oc} than that fabricated using undoped titania based electrodes. A 10% increase in V_{oc} and a 5% decrease in J_{sc} were observed.

7.2 Future Recommendations

To enable active commercialization of DSSCs, there is a need to enhance the efficiency of DSSCs beyond 12%. Listed below are some recommendations for the work to be done in near future on DSSCs in order to increase efficiency and reduce the cost of production.

7.2.1 Employing Use of Different Morphologies of Titaina

Different structures like nanorods, nanotubes etc. can be synthesized using different synthesis techniques and optimizing the synthesis conditions. Formation of photoanode using structures based nanoparticles can render better properties to photoanode and lead to enhanced dye adsorption, better conduction mechanism and efficient transport of electrons. These structures can be doped with different non-metals and metals to further improve their properties hence improving the performance and efficiency of the DSSc.

7.2.2 Optimization of Coating Processes

The low cost solution based coating techniques can be optimized to yield better films. Better properties and morphology of semiconductor thin films is beneficial for better working of the cell. Vacuum based techniques are expensive but they offer best compositional control of the films. Efforts should be made to improve the quality of the solution based coated thin films to match the quality of films coated by expensive methods. Optimization of electrochemical methods can be one option for better and low cost thin film coatings.

7.2.3 Steps Towards Better Stability of DSSCs

In-stability is a key disadvantage of a DSSC. This problem requires special attention as it is the biggest hurdle in commercialization of DSSCs. the instability mainly arises due to the use of volatile solvents in liquid electrolytes. The solvents evaporate and degrade with time and increasing temperature and ultimately short the cell. These electrolytes can be substituted with solid state electrolytes like hole conducting materials. Research should be done to improve the efficiency of solid-state DSSCs by optimizing the cell fabrication methods and using other materials that match te properties of such electrolytes.

7.2.4 Study of the Effects of Co-doping

TiO_2 can be co doped with metals to further enhance its properties for its application in DSSCs. co-doping has not been investigated extensively.

7.2.5 Use of Natural Sensitizers

Ru based sensitizers are very expensive. Most of the cost of a DSSC is due to use of artificial metal sensitizer. Many natural sensitizers are available like the juice of berries, extract of rose petals etc. the problem with these sensitizers is that they degrade with time and the cells are not long lasting. Research needs to be done on use of such sensitizers to open ways for further low cost DSSCs.

Sol-Gel Fabrication of TiO_2 Nanoparticles and Investigations on Cu Doping Effects for Application in Dye Sensitized Solar Cells

Sehar Shakir [*(a)], Abdur Rehman[(b)], Muhammad Akmal Rana[(a)], M N Akbar[(a)], Mustafa Anwar[(a)], Kamaal Mustafa[(a)], Zuhair S. Khan[(a)]

[(a)]Advanced Energy Materials and Fuel Cells Lab, Centre for Energy Systems, National University of Sciences and Technology, Sector H-12 Islamabad 44000, Pakistan.

[(b)] Mechanical engineering department, King Fhad University of Petroleum and Minerals, KSA.

[*]email: 12sehar_shakir@ces.nust.edu.pk; zskhan@ces.nust.edu.pk

Abstract: Dye Sensitized Solar Cells possess the novel properties of both organic as well as inorganic compounds. Scientists are especially attracted towards them as alternative devices to traditional silicon solar cells because they offer lower fabrication costs. Dye Sensitized Solar cells have reached an energy conversion efficiency of 12% and further efforts are being carried out to improve its efficiency. Scientists are devotedly working on Titania doping for its use in photovoltaic cells and photo-catalysis to enhance the capabilities of the semiconductor. In this work, titania nanoparticles have been synthesized using sol-gel route and doctor blade was used to apply thin film titania coatings on FTO coated glass substrates. Coating process was optimized and crack free titania films were successfully obtained. Furthermore, copper doped titania nanoparticles were also synthesized using sol-gel route. To analyze the structure and composition, synthesized nanoparticles were characterized with several instrumental techniques, including X-ray diffraction (XRD) and Scanning Electron Microscopy (SEM). Copper doping in Titania initiates rutile phase formation and structural defects into the semiconductor as evident by XRD pattern. The effect of Copper doing and annealing temperature on Titania nanoparticles in terms of crystal structure, phase change, morphology, UV-Vis absorption etc. has been studied in detail.

Keywords: Dye sensitized solar cells, sol-gel route, copper doped Titania, doctor blade, crack free film.

Introduction

The efficiency of Dye Sensitized Solar Cells (DSSC's) depends on various factors. The efficiency is very much related to the properties of semiconductor photoanode. Other cell -based efficiency depending factors are properties of dye, nature of redox couple, catalytic properties of counter electrode etc. In other words each and every layer of a DSSC affects the efficiency of the cell. Focusing on semiconductor photoanode, TiO_2 is most usable and attractive semiconductor material for DSSC's because of its chemical

stability and easy availability. The main downside of TiO_2 is that it only absorbs UV radiation form solar spectrum which makes only 4% of the electromagnetic radiations coming from sun [1, 2]. In order to enhance the absorption of solar radiation by TiO_2 we need to create oxygen deficiencies or structural defects in its structure to decrease the band gap. The reduction in band gap of TiO_2 (anatase =3.2ev) can lead to make it active in visible light.

Previous studies have shown that correctly doping TiO_2 by various metals can enhance some of the photovoltaic properties of the cell. Doping TiO_2 semiconductor render three main advantages in DSSCs, reduction in band gap thus enhancement in efficiency, reduction in photocatalytic activity of DSSCs and reduction in recombinations. For example Feng et al.[3] reported using Ta-doped TiO_2 nanowire arrays for DSSC's showed negative shifting of C.B of TiO_2 due to which increase in open circuit voltage (V_{oc}) was observed. M. Geetha et al. [4] reported improvements in photoelectric performance of DSSCs by using chromium doped TiO_2 semiconductor as photoanode. Maciej Zalas and Maciej Klein [5] studied the influence of rare earth metal doping on performance of DSSCs. These modified electrodes prevented back transfer of electrons and enhanced dye absorption ability Xujiye Lu et al. [6] and Lee et al. [7] studied niobium doped TiO_2 semiconductor based DSSC and reported an improvement in cell performance due to doping.

Copper is readily available in earth's crust and cheap metal with high electronic conductivity [8] which makes it an attractive metal for doping TiO_2 semiconductor photoanode of DSSCs. Doping copper in TiO_2 can create structural defects in TiO_2 lattice hence reducing its wide band gap. In this research we have studied the doping effects of copper on structure, crystallinity and morphology of undoped TiO_2 and discussed how doping copper shifts the absorption edge of TiO_2 to visible region. Meanwhile, thermal stability of semiconductor and doped semiconductor was also investigated.

Experimentation

Synthesis of nanoparticles

Pristine (undoped) titania nanoparticles and titania with 3wt% Cu were prepared by sol–gel method. The synthesis of pristine titania started with the addition of 25 ml of titanium isopropoxide (Sigma-Aldrich) was stirred for one hour in 50 ml ethanol. Isopropoxide chain was hydrolyzed by addition of 30ml water and 6 ml HCl and was stirred continuously for 3 hours. The sol was kept for 24 hours, dried and then annealed at 450℃ and 650℃ for 4 hours. To prepare Cu-doped Titania another solution was made containing $CuCl_2.5H_2O$, water and ethanol. This solution was added while hydrolyzing TTIP solution. This sol was also kept for 24 hours, dried and annealed at similar conditions as for pristine titania.

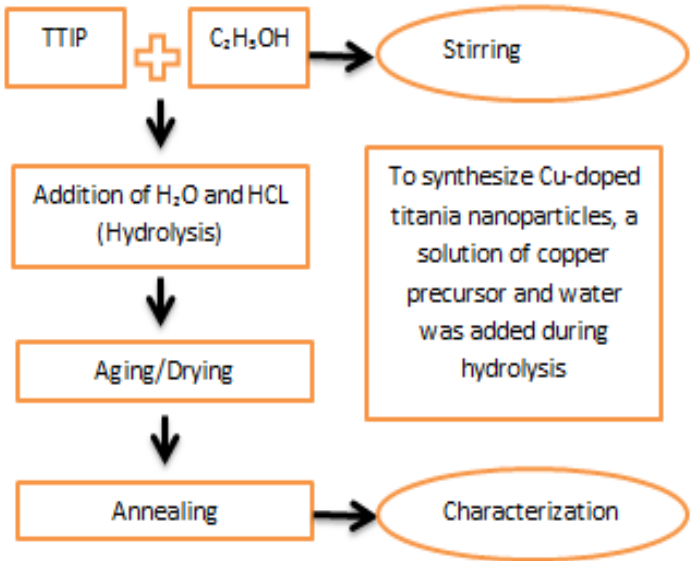

Fig. 1 Sol-gel preparation of pristine and doped titania nanoparticles.

The X-ray diffraction (XRD) pattern of the samples was obtained using a θ-θ STOE Germany X Ray diffractometer at room temperature irradiating X Rays from Cu-Kα for structure and phase analysis. XRD was operated at 40kV and 30 mA. The specimens were prepared. Powders were packed in glass holder and XRD graphs were collected at room temperature. The measurements were recorded in step of 0.04° and scan angle range of 10-80°. SEM and (EDX) of the samples were carried out using a JEOL 2300 scanning electron microscope at and operating voltage of 20kV with an EDX detector. The powder samples were coated with gold using sputter ion coater before putting them into machine. UV-VIS spectra of the samples were obtained using a BMS 2800 UV–Vis spectrophotometer with $BaSO_4$ powder as the standard reference sample and data was taken from range 300nm to 900nm. TG-DT analyses of the samples were performed using Perkin Elmer diamond TG/DTA version 2.0 with 2g sample weight each. Temperature range was set from room temperature to 500 °C.

Results and discussion

Doping Titania with other atoms influences its properties and causes change in light absorption, crystal structure, particle size and stability. The results and discussions elaborate the study of effect of doping Copper into Titania lattice at different annealing temperatures.

XRD analysis

Crystal phase of titania nanoparticles determine its functionality for various applications. The rutile phase of titania is recommended for its use in pigments [9] and anatase phase is recommended for photocatalytic applications [10]. Therefore, it is very

important to investigate the changes in crystal structure by incorporation of different dopants in titania lattice. Pristine and Cu-doped titania nanoparticles were prepared at the same conditions for comparisons. The similarity in ionic radius of Cu^{2+} (0.73 Å) to that of Ti^{4+} (0.64 Å) enables copper to substitutionally replace Titanium. Titania doped with Cu^{2+} initiates the formation of rutile phase along with anatase. Doping of Cu^{2+} introduces structural defects into titania as evident by XRD graphs. The XRD pattern of pristine and Cu-doped titania nanoparticles is shown in Figure 2. The diffraction pattern corresponds to the tetragonal anatase phase of titania (JCPDS-782486). Indeed, a small fraction of rutile phase is also present in between 27° and 36°, and at 40° (JCPDS-761934). Anatase is metastable phase of Titania and is usually formed at low temperature during solution-phase synthesis.[11]

As shown in Fig. 2a, when annealed at 450 °C, titania changes from amorphous to crystalline phase. At 450 °C pure anatase phase is formed. As the annealing Temperature increases to 650 °C pristine titania shows a small rutile phase shown at (110) rutile peak. It means the transformation of anatase to rutile in pristine Titania starts at temperatures above 650 °C. Whereas, introducing Cu^{2+} in Titania lattice initiates rutile phase as evident from Fig. 2b where rutile phase starts forming at 450 °C and a complete transformation of phase is been observed at 650 °C where all peaks corresponds to rutile phase of titania. Increase in rutile fraction with doping indicates inhibition of the formation of complete anatase phase due to incorporation of Cu on the titania lattice. The inclusion of copper in titania anatase creates a higher number of defects which results in quicker formation of rutile nuclei. During annealing, the replacement of Ti^{4+} by Cu^{2+} cause a decrease in free electron concentration and an increase in oxygen vacancy concentration. Anatase to rutile phase transition occurs because of this increase in oxygen vacancies created in crystal lattice [12]. The phase transformation results are consistent with DT analysis explained latter.

The effect of annealing temperature on pristine and Cu-doped titania is shown in Table. 1. The resultant sizes for pristine titania is 13.1nm and 43.1 nm annealed at temperatures 450 °C and 650 °C respectively and that for Cu-doped titania is 11.6 nm and 36.6 nm annealed at temperatures 450 °C and 650 °C respectively. Increasing annealing temperature increases the crystallite size. The addition of dopant affects the crystallite size of particles and decreases the crystallite size.

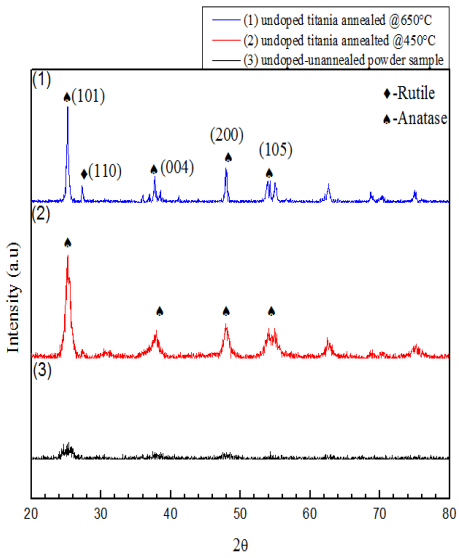

Fig. 2a XRD pattern of undoped titania at different annealing Temperature

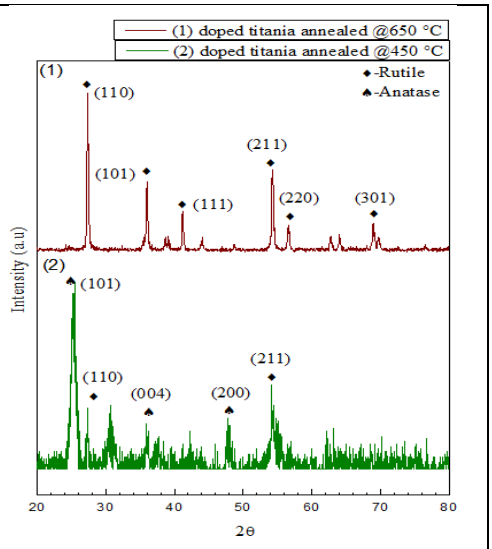

Fig. 2b XRD graphs of doped titania at 450 °C and 650 °C Temperature

Fig. 2 XRD patterns of doped and undoped titania at different annealing temperatures.

Table. 1 Crystallite sizes of undoped/3wt% Cu doped titania at 450 °C and 650 °C.

Sr no	Sample	Crystallite size (nm)
(1)	Undoped titania annealed @450 °C	13.1
(2)	3 wt% Cu-Doped titania annealed @ 450 °C	11.6
(3)	Undoped Titania annealed @650 °C	43.1
(4)	3 wt% Cu-doped titania annealed @650 °C	36.6

UV-VIS Analysis

The absorption spectra of the prepared undoped and doped samples annealed at 450 °C were determined by a diffusive reflectance spectroscopy measurement. The absorption spectrum of pristine and Cu-doped Titania is shown In Fig. 3. Doping Copper in titania lattice shows an absorbance shift towards the visible spectrum. Anatase Titania has Eg value 3.31 eV. Doped sample exhibit an absorption peak at 379 nm corresponding to the

maximum absorption when electrons are excited from the valence to the conduction band. Doped samples show shifting in the absorption peak to the visible region. The CB in titania comprises of Ti 3d states and VB comprises of O 2p states. The 379 nm absorption peak is due to electronic transition from O 2p to Ti 3d. The absorption between 400 and 500 nm appears as a result of charge transfer at the interface from the O 2p VB to the Cu (II) state attached to titania. These Cu (II) states may be present either as Cu (II) nanoclusters or in the form of amorphous oxide phase of CuO. Li et al. [13] demonstrated that Cu (II) does not show this absorption peak if it is present as CuO, but displays this absorption when it is present as Cu (II) ions attached to Titania. However, Qiu et al. [14] suggested that the absorption peak between 500 nm appears due to charge transfer from Titania to CuO clusters in CuO/Titania nanocomposite. Therefore, based on these observations, we can predict that the absorption appears due to charge transfer from O 2p to Cu (II) clusters or CuO amorphous phase. Hence it can be concluded that substitution of Ti^{4+} by Cu^{2+} atoms generates defect centers that cause the change in optical absorption.

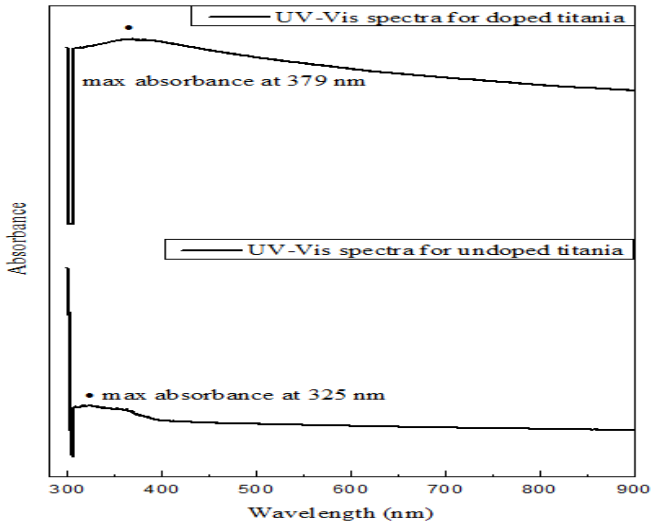

Fig. 3 UV-VIS spectra for pristine and 3wt% Cu-doped titania annealed at 450 °C.

Doping Titania with a transition metal leads to the reduction in the band gap energy which is attributed to the inclusion of copper ions into titania crystal lattice and formation of CuO on surface of the particles. It has been studied that doping titania with aliovalent ions changes the material properties and absorption properties because of the modification in local lattice symmetry and defects. When titania is doped with copper, Cu^{2+} ions either located on the surface sites or inside bulk titania. This causes lattice deformation due to rearrangement of adjoining atoms to neutralize charge deficiency. This lattice deformation and rearrangement modifies electronic structure and hence the band gap shift occurs [15]. Also, oxygen vacancies are created due to presence of small amounts of Cu^{2+} dopant in the lattice sites of titania [12, 16]. These are created due to

charge compensation effect. It is, therefore, possible to control band gap shift and absorption of the doped nanoparticles controlled by lattice strain and doping-induced vacancies. It can be concluded that the copper doped titania structure extends its absorption to the visible spectrum of sunlight (400-700 nm) effectively.

TG-DT Analysis

Fig. 4 show the TG/DTA curves of pristine and 3wt% Cu-doped Powders. Looking at TG curves of both powders, first weight loss is being observed at temperatures below 100 °C. This weight loss indicates the removal of water and ethanol from powders. At temperatures from 100 °C to 300 °C, a weight loss of 17% for pristine titania powder and 15% for doped titania powder is being observed. This loss can be attributed to the removal of un-hydrolyzed isopropoxide ligands in titania. A total of 18% weight loss for pristine powder and 17.5% weight loss for Cu-doped titania powders has been observed which is approximately same for both the powders. Weight loss tends to seize after 400 °C.

From DTA curves, we can observe one sharp exothermic reaction peaks in both the graphs. For pristine titania the exothermic peak appears at 399 °C and for doped titania it appears at 310 °C. these exothermic peaks indicates a phase change of powders from amorphous to crystalline. These results are consistent with XRD results. Undoped titania powders need more heat to crystallize since they possess smaller crystallite size of particles. Transformation from amorphous to anatase crystal structure for Cu-doped titania at lower temperature is because it contains comparatively larger crystallize size that required less heat to crystallize. It is evident from DT curves that doped titania powder shows crystallization at lower temperature than pristine titania. Incorporation of Cu dopant in titania reduces its crystallization temperature. This corresponds to the XRD graphs which showed formation of rutile phase in doped titania powder at lower Temperature (650 °C Fig. 2b). In Fig. 4b origin of new peak can be observed at 480 °C which may be attributed towards the phase shift from anatase to rutile.

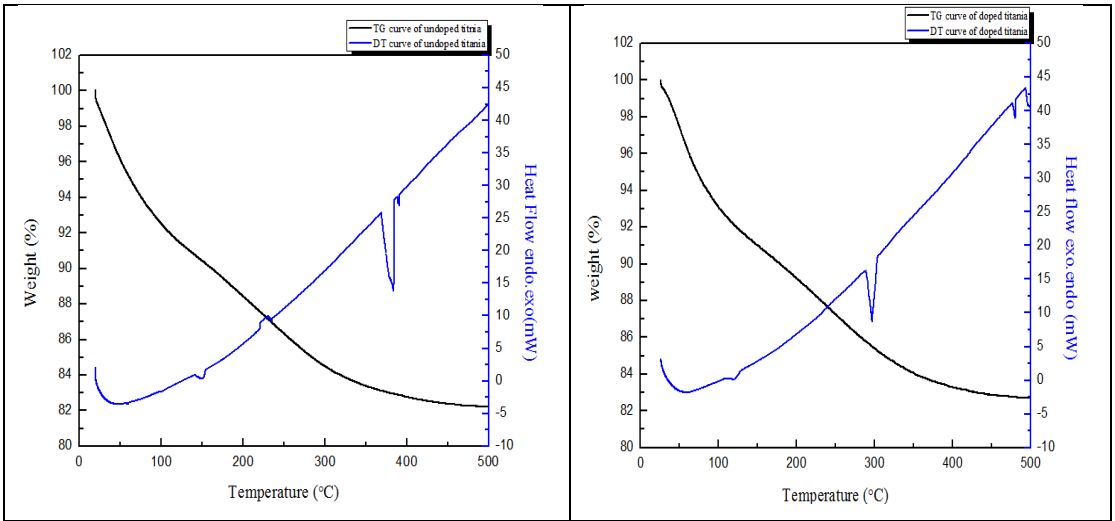

Fig. 4 TG-DT curves of (a) undoped and (b) doped titania up to 500 °C

SEM/EDX Analysis

The high-resolution Scanning Electron Microscope images of pristine and 3wt% Cu-doped Titania nanoparticles annealed at 450 °C and 650 °C are shown in Fig. 5. Fig. 5a shows that the particles are spherical in shape with some amount of agglomeration. While other figure shows arbitrary cubical shape. The particle size distribution shows that the average numbers of particles have a size of 71, 68.64, 61.84 and 60.50 for pristine and Cu-doped Titania annealed at 450 °C and 650 °C respectively. Increasing Annealing temperature decreased the particle size of titania as shown in Table. 2. Doping also affected the size of Titania nanoparticles.

Table. 2 Summary of SEM/EDX results.

Sr no	Sample	Mass%			Atom%			Average Particle Size
		Ti	O	Cu	Ti	O	Cu	
(1)	Undoped Titania annealed @450 °C.	57.94	42.06	0	31.51	68.49	0	71.27
(2)	Undoped Titania annealed @650 °C.	56.31	43.69	0	30.10	69.90	0	68.64
(3)	Cu-Doped Titania annealed @450 °C.	52.66	44.25	3.09	28.08	70.67	1.24	61.84
(4)	Cu-Doped Titania annealed @650 °C.	59.61	38.65	3.08	33.74	65.51	0.74	60.50

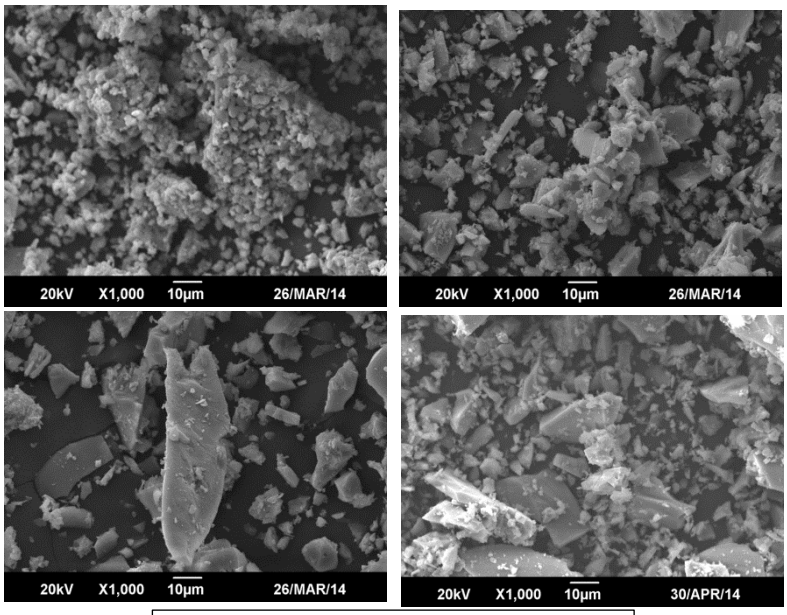

Fig.5 SEM images of particles

Hence addition of dopant and its concentration can be used to tailor the particle size of copper doped titania.

Conclusions

Titania and Cu-doped titania nanoparticles have been successfully formed using sol-gel method. Introducing Cu^{2+} in titania lattice initiates rutile phase formation. Doping Copper in titania lattice showed absorbance shift toward the visible spectrum. Incorporation of Cu dopant in titania reduces its crystallization temperature. The particle size of the Cu-doped titania can be controlled by manipulating the dopant concentration and annealing temperature**.** Based on above results, incorporating copper doped titania based photoanode in DSSC can enhance some of the photovoltaic properties of the cell.

Acknowledgment

We would like to thank SCME-NUST and Research/PGP Directorates of NUST Islamabad for their kind support.

References

[1] Sahu, M. and P. Biswas, *Single-step processing of copper-doped titania nanomaterials in a flame aerosol reactor.* Nanoscale research letters, 2011. **6**(1): p. 1-14.

[2] Ni, Y., Y. Zhu, and X. Ma, *A simple solution combustion route for the preparation of metal-doped TiO 2 nanoparticles and their photocatalytic degradation properties.* Dalton Transactions, 2011. **40**(14): p. 3689-3694.

[3] Feng, X., et al., *Tantalum-Doped Titanium Dioxide Nanowire Arrays for Dye-Sensitized Solar Cells with High Open-Circuit Voltage.* Angewandte Chemie, 2009. **121**(43): p. 8239-8242.

[4] Geetha, M., K. Suguna, and P. Anbarasan, *Photoanode Modification in DSSC Using Chromium Doped TiO2 nanoparticles by sol-gel method.* Archives of Physics Research, 2012. **3**(4): p. 303-308.

[5] Zalas, M. and M. Klein, *The Influence of Titania Electrode Modification with Lanthanide Ions Containing Thin Layer on the Performance of Dye-Sensitized Solar Cells.* International Journal of Photoenergy, 2012. **2012**.

[6] Lü, X., et al., *Improved-Performance Dye-Sensitized Solar Cells Using Nb-Doped TiO2 Electrodes: Efficient Electron Injection and Transfer.* Advanced Functional Materials, 2010. **20**(3): p. 509-515.

[7] Lee, S., et al., *Nb-doped TiO2: a new compact layer material for TiO2 dye-sensitized solar cells.* The Journal of Physical Chemistry C, 2009. **113**(16): p. 6878-6882.

[8] Cao, F.-F., et al., *Wet chemical synthesis of Cu/TiO 2 nanocomposites with integrated nano-current-collectors as high-rate anode materials in lithium-ion batteries.* Physical Chemistry Chemical Physics, 2011. **13**(6): p. 2014-2020.

[9] dos Santos, J., T. Ogasawara, and R. Corrêa, *Synthesis of mesoporous titania in rutile phase with pore-stable structure.* Brazilian Journal of Chemical Engineering, 2009. **26**(3): p. 555-561.

[10] Li, Y.-F. and Z.-P. Liu, *Particle size, shape and activity for photocatalysis on titania anatase nanoparticles in aqueous surroundings.* Journal of the American Chemical Society, 2011. **133**(39): p. 15743-15752.

[11] Choudhury, B., M. Dey, and A. Choudhury, *Defect generation, dd transition, and band gap reduction in Cu-doped TiO2 nanoparticles.* International Nano Letters, 2013. **3**(1): p. 1-8.

[12] Nair, J., et al., *Microstructure and phase transformation behavior of doped nanostructured titania.* Materials research bulletin, 1999. **34**(8): p. 1275-1290.

[13] Li, G., et al., *Role of Surface/Interfacial Cu2+ Sites in the Photocatalytic Activity of Coupled CuO− TiO2 Nanocomposites.* The Journal of Physical Chemistry C, 2008. **112**(48): p. 19040-19044.

[14] Qiu, X., et al., *Hybrid Cu x O/TiO2 Nanocomposites As Risk-Reduction Materials in Indoor Environments.* ACS nano, 2012. **6**(2): p. 1609-1618.

[15] Li, L., et al., *Surface doping for photocatalytic purposes: relations between particle size, surface modifications, and photoactivity of SnO2: Zn2+ nanocrystals.* Nanotechnology, 2009. **20**(15): p. 155706.

[16] Liu, G., et al., *Iodine doped anatase TiO 2 photocatalyst with ultra-long visible light response: correlation between geometric/electronic structures and mechanisms.* Journal of Materials Chemistry, 2009. **19**(18): p. 2822-2829

Review on the Effects of Metal Doping on TiO_2 Properties and Its Influence on Performance of Dye Sensitized Solar Cells

Sehar Shakir [*(a)], Hafiz M. Abd-ur-Rehman [(b)], Zuhair S. Khan[(a)]
[(a)]Advanced Energy Materials and Fuel Cells Lab, Centre for Energy Systems, National University of Sciences and Technology, Sector H-12 Islamabad 44000, Pakistan.
[(b)] Department of Mechanical Engineering, King Fahd University of Petroleum and Minerals, Dhahran, Saudi Arabia.
[*]email: 12sehar_shakir@ces.nust.edu.pk; zskhan@ces.nust.edu.pk

Abstract: Titanium dioxide (TiO_2) represents an effective semiconductor material for anode in Dye Sensitized Solar Cells (DSSCs). It is a chemically stable and relatively reactive semiconductor. It acts as a photo-catalyst under ultraviolet light that has wavelength less than visible light and photon energy from 3eV to 124 eV. The development of photo-catalysts exhibiting high reactivity under visible light (400 nm) should allow the main part of the solar spectrum to be used. Visible light-activated TiO_2 can be formed by doping it with a metal. The working of DSSCs is based on adsorption of photon by dye and its transfer to TiO_2 electrodes. The properties and structure of TiO_2 electrodes have a direct influence on the fabrication of high efficiency dye sensitized solar cells. The aim of this comprehensive review is to give an overview of the DSSCs technology, working principles, different methods for preparation of metal doped titania nanoparticles, and its application in DSSCs. The enhancement of conversion efficiency and effective electron transport using metal doped titania in DSSCs have been discussed. The effect of using doped titania anode on recombination rate and photo catalytic activity in DSSCs have also been summarized using metals like copper (Cu), iron (Fe), Neodymium (Nb), etc.

Keywords—*DSSC, Metal doping, Titania, Cell performance*

1. Introduction

Photovoltaic devices work on the phenomena of charge separation occurring at interface of two different materials. These materials have different conduction mechanism. Photovoltaic has been dominated by p-n junction devices which are usually made up of silicon but emergence of third generation solar cells challenged this dominance of solid state junction devices [1]. There are three generations of solar cells. The first generation consists of high cost-high efficiency crystalline silicon solar cell technology. These cells have achieved efficiencies beyond 24.4 %. Though cost of production has decreased over the passage of time but first generation solar cells are still more costly than fossil fuels as these solar cells are manufactured by expensive wafer processes involving many energy extensive steps [2]. Second generation consist of thin film solar cell technology including amorphous silicon solar cells, Cadmium Telluride (CdTe), micro morph tandem solar cells, and Copper Indium Gallium Diselenide (CIS or CIGS). Second generation solar cells are considered as low efficiency-low cost solar cells but recently their efficiency has been enhanced up to 20 % [3-5].

Hence to compete with fossil fuels and fulfill the increasing demand of energy there is a need to develop low cost-high efficiency solar cells. Third generation solar cells can fulfill this need. Third generation of solar cells consists of quantum dot solar cells and Dye Sensitized Solar Cells having efficiency up to 14 %.

2. Importance of Titania in Dye Sensitized Solar Cells

DSSCs are technical and economical alternatives for expensive p-n junction solar cells [1]. DSSCs allow using less purified starting materials as they are not much sensitive to the impurities and defects whereas solid junction solar cells require high purity materials. This makes production of DSSCs less costly and the energy payback period is shorter [6]. DSSCs have reached photo conversion efficiencies for small laboratory cells up to 12 % and for solar modules they have reached to about 9 % [7].

The working of DSSCs begins with the absorption of incident light by dye molecule. An electron in the dye molecule gets excited from its ground to excited state. This excited electron is injected to the conduction band of semiconductor of photoanode usually made up of titania and consequently the dye gets oxidized. Semiconductor layer is a porous layer and electron from this layer travels to Transparent Conducting Oxide TCO and follows its path towards external circuit to the counter electrode. As the dye molecule is in unstable state the electron, instead of moving towards external circuit, can recombine back. In order to limit this recombination, an electron is provided to the dye molecule by the electrolyte (redox couple). As a result, dye molecule is reduced and redox couple gets oxidized. The generated electron, after completing its path from external circuit, reach counter electrode and reduce the redox couple and DSSC working cycle is completed. Ideally this whole process should take place without permanent transformation and consumption of chemicals but in real systems there are some undesirable recombination's that occur in the cycle causing a reduction in cell efficiency [1, 8].

Different semiconductors other than titania like Nb_2O_5 [9], ZnO [10, 11], SnO_2 [12], and $SrTiO_3$ [13] have been studied for their use in DSSCs as photoanode material. Studies revealed TiO_2 to be the best material for photoanode due to its low cost, high availability, and chemical stability. In DSSCs, there are three major roles played by TiO_2:

(iv) It provides a medium for the adsorption.
(v) It accepts the excited electrons from the dye molecule into conduction band.
(vi) It transports the electron towards the TCO for its injection in external circuit.

TiO_2 is an inexpensive, chemically stable, nontoxic, and biocompatible material with interesting photocatalytic activities and high dielectric constant [14]. Nanoscale titania is a multifunctional material that has its applications as anode material in DSSCs and many other fields [15]. Titania is an n-type semiconductor because of presence of oxygen deficiency [14]. It has three polymorphs: brookite (orthorhombic), rutile (tetragonal), and anatase (tetragonal). The band gap of brookite is approximately

3.2eV, rutile has a band gap of 3.0eV, and band gap of anatase is 3.2eV. Anatase and rutile are the main polymorphs [16].

The photocatalytic mechanism in titania starts with the absorption of photon. The excitation occurs when the photons with energy equal to or greater than the band gap of titania is absorbed. This allows the formation of an electron-hole pair on the surface of TiO_2 molecule. A hole (positive) is created in Valence band (VB) and an excited electron is promoted to the Conduction Band (CB). The electrons in Excited-state can get trapped in metastable states on surface, dissipate the input energy as heat due to recombination or react with electron acceptors/donors on semiconductor surface [17]. Anatase possesses the energy band 3.2 eV, which corresponds to 400 nm in electromagnetic spectra. The wide band gap of pristine (undoped TiO_2) is its main drawback. The electron in pristine gets excited when irradiated to photons in UV region which constitutes only 4 % of total solar spectrum and about 40 % solar photons belongs to visible region. Also material efficiency is reduced due to recombination [18]. Scientists have been trying to induce visible light activity and enhance generated carrier separation efficiency by introducing different changes in titania like incorporating nonmetals, transition metals, rare earth metals, creating oxygen vacancies and introducing structural defects [19, 20]. The incorporation of dopants and defects create sub band states in titania band gap and enhance their visible light photoactivity by shifting the absorption edge towards visible region. Several methods have been reported in literature to enhance the visible light photoactivity of titania.

1) To enhance spectral response of titania it has been doped by metals (Cu, Fe, Mg, Cr etc.) and nonmetal impurities (B, N etc.). Doping generates an intermediate energy level between valence band and conduction band of titania. Therefore metal doped titania shows enhanced visible photoactivity due to formation of new energy level in band gap of titania formed by scattering of metal nanoparticles in titania lattice [21]. When titania is doped with non-metals, three different modification mechanisms have been suggested, formation of impurity energy levels, narrowing of band gap and oxygen vacancies[21].

2) To enhance the separation of generated carriers, TiO_2 nanotubes have been reported to be beneficial [15].

3) It has been found that noble metal and TiO_2 heterogeneous materials have excelled titania nanotubes and doped titania in properties as these heterogeneous materials inhibits the recombination's and enhances visible light absorption [22, 23].

4) To decrease recombination's and enhance photocatalytic efficiency coupled semiconductors like $Bi_2S_3TiO_2$, ZnO/TiO_2 and CdS/TiO_2 has been reported [24-26].

There are many ways to dope titania like ion assisted Sputtering, ion implantation, CVD etc. But these processes are very expensive. Solution based processes for doping like sol-gel and other hydrothermal processes contribute cost effective and large scale production [21, 27].

3. Discussion on Effects of Metal Doping of Titania on Performance of DSSCs

When TiO_2 is doped with metals, the dispersion of metal nanoparticles in titania matrix produces a new energy level. The electrons need less energy to excite from defect state to CB of TiO_2 as compared to the photon energy required in exciting electrons in undoped titania. Metal doping offers reduction in electron-hole recombinations by improved trapping of electrons and enhanced photocatalytic activity [21]. Considering crystal structure of titania, it is difficult to substitute O^- with any other anion than to replace Ti^{4+} with another cation because of the difference in ionic radii and charge states.

Cationic doping of TiO_2 with rare earth metals and transition metals (such as Sm, Cu, Nd, Zr, Gb, Zn, Pr , Co, Er, Ni, Ce, Cr, La, Mn, Pt, Mo, Ag, Nb, Au, V, Sn, Fe, Ru or W) has been extensively studied. Researchers have found that doping titania with transition metal increase thermal stability, decrease photothreshold energy of titania. A decrease in lifetime of carriers has also been indicated [14]. This limits the overall conversion efficiencies. Sometimes transition metals in TiO_2 behave as trapping sites for generated electron-hole pairs and hence the inclusion of these metals in titania leads to lowering of quantum efficiency. In anatase phase, they can also cause thermal instability. Despite doping metals in TiO_2, a reduction in band gap energy has been attained by researchers, but an exceptional enhancement in photocatalytic activity has not been observed [15, 16].

Doping the titania semiconductor of photoanode render three main advantages in DSSCs: reduction in the photocatalytic activity of DSSCs, reduction in band gap thus enhancement in efficiency and reduction in recombination rate. Some researcher have studied and reported better device performances when utilizing doped semiconductor as compared to performance of cells based on undoped semiconductor. Several dopants have been doped in titania semiconductor of DSSCs but none of them could enhance the open circuit voltage (V_{oc}) and short-circuit current density (J_{sc}) together at the same device.

Feng et al. [28] prepared Ta-doped titania nanowire arrays for DSSCs and found a considerable increase in open circuit voltage (V_{oc}) due to negative shifting of CB of titania. A decrease in photoconductivity of chromium doped TiO_2 has been indicated. The decrease is due to presence of Cr^{3+} ions in lattice displacing Ti^{4+} ions [29] . Whereas, M. Geetha et al. [30] reported doping chromium showed improvement in photoelectric performance of dye sensitized

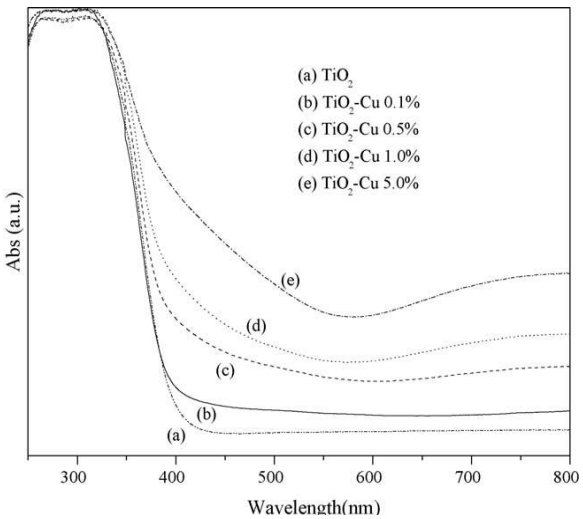

Fig. 1 UV-Vis spectra for pristine and Cu-doped TiO_2 semiconductors [37].

solar cells. They found an enhancement of light to electric conversion efficiency by a factor of 2.33 with 0.05 mol % Cr doping in titania photoanode. Tran van nam et al. [31] found doping magnesium caused a negative shift of the CB edge 1.142 and -1.16 eV for surface and bulk respectively. They also observed shift of Fermi level to negative energy. These effects improved J_{sc} but decreased the V_{oc} of DSSCs. Yandong Duan et al. [15] studied the effect of Sn doping in titania photoanode of DSSCs and found 12.1 % increase in efficiency compared with efficiency of cell containing pure titania based photoanode. Maciej Zalas and Maciej Klein [7] studied the influence of rare earth metal doping on performance of DSSCs. They found doping had no effect on crystal structure of electrode but strongly affect properties of DSSCs and a change in electronic properties was reported. These modified electrodes prevented back transfer of electrons and enhanced dye absorption ability. The best device performance was obtained in devices which used Ce and Yb as dopants. But many of rare earth metals modifications in DSSCs (like Tm, Gd, Eu, Y, etc.) decreased photoconversion of DSSCs. An enhancement in efficiency has been indicated by using vanadium doped TiO_2 as photoanode in DSSCs [32]. Xi Xang et al. indicated improvement in J_{sc} due to reduction in charge recombination, amelioration in electron lifetime and increase in power conversion efficiency in DSSCs fabricated using W-doped TiO_2 as photoanode [33]

Effect of co-doping has also been studied. Ko et al. [34]. They found enhancement in device efficiency when the semiconductor was co-doped with tungsten and aluminum. Qiuping Liu et al. [35] investigated cell made by using Zn and Mg co-doped titania electrode and found 26.7 % increase in conversion efficiency as compared to undoped titania based DSSCs.

Copper doped nanoparticles are usually synthesized by easy and cost effective sol-gel process [36-39]. Zhao et al. [40] reported a novel one step self-assemble method of doping copper into titania lattice. It has been reported that doping copper in titania enhan ces the photo-catalytic activity [36-38] and reduce the band gap of titania. The enhancement of the photo-catalytic activity was discussed as an effect due to the Cu content as well as to the formation of stable Cu (I) in the Cu-doped TiO_2 semiconductors. Doped samples show shifting of absorption peak in UV spectra to visible region or longer wavelengths [38, 39] . Two absorption peaks shifting in spectra have been seen for doped samples when compared to spectra of un-doped samples as shown in **Fig. 1** [37] and **Fig. 2** [39]. One of the shifts is at 400 nm and other at around 500-900 nm. The first shifting is due to presence of Cu(II) states which exists either as

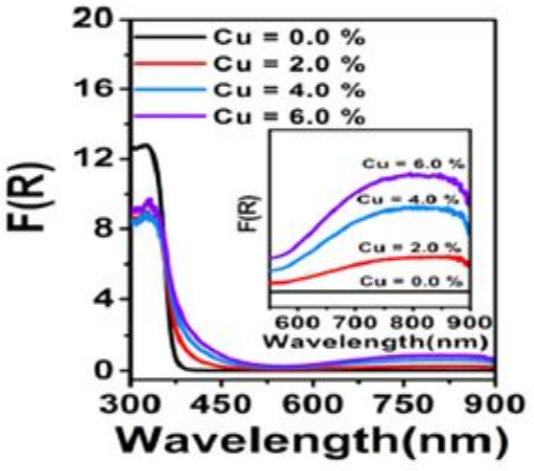

Fig. 2 UV-Vis spectra of pure and Cu-doped TiO_2 nanoparticles [39].

Cu(II) nano-clusters ions attached to TiO_2 [39] or in form of amorphous oxide phase of CuO (3,5,4,6). The second shift is due to d-d transitions or $2E_g$-$2T_{2g}$ of Cu^{2+} in crystalline environment of TiO_2. The Jahn-Teller distortion splits the 2Eg and 2T2g state of Cu^{2+} into several d states. Interaction of light excites the electron from ground to several of the excited states and gives the visible absorption peaks in the framework of TiO_2 [39].

Table 1 Band gap and average crystallite size of copper doped titania samples [37].

TiO_2-Cu (wt%)	Crystallite Size (nm)	E_g(eV)
0	40.5	3.28
0.1	30.4	3.19
0.5	29.7	3.13
1.0	26.7	3.05
5.0	29.0	2.81

These Cu^{2+} d states and oxygen defects create band states, thereby favoring electronic transition to these levels and resulting in lowering of band gap of TiO_2. As summarized in **Table 1** [37] decrease in band gap and crystallite size has been reported by increasing copper concentration, [37, 39, 41]. Maeda et al. [38] reported copper doping had no effect on crystallinity of titania whereas Vidyasagar et al. [42] stated that Cu doping in titania alter crystallinity but remains unaffected towards crystal structure of nanoparticles**.** Incorporation of copper in titania lattice initiates the formation of brookite phase and inhibit complete anatase formation [39, 43]. Whereas Teleiki et al. [44] reported that addition of copper initiated anatase to rutile formation and enhanced grain growth. A shift in 2 theta in XRD pattern of 101 peak has been observed indicating incorporation copper species in titania network. F.J.Navas et al. [41] fabricated the cell using paste coating of doped and un-doped nanoparticles on FTO substrates to develop photoanode, N3 dye, electrolyte and platinum counter electrode and reported 10% increase in V_{oc} of cell. The increase in V_{oc} of DSSCs is due to reduction in band gap

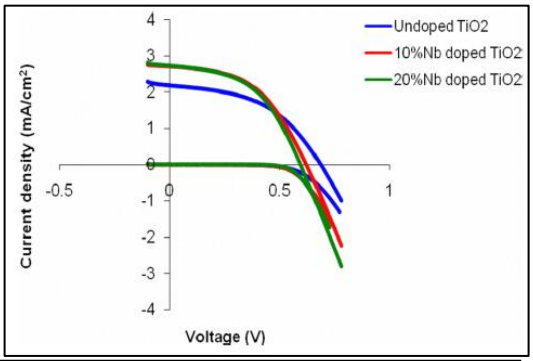

Fig. 3 Current density-voltage curves of Niobium doped and undoped Titania based DSSC [46].

Several methods have been reported to synthesize niobium doped titania nanoparticles. The most common of which is

sol-gel [45]. Others being flame spray pyrolysis[44] , hydrothermal method [46, 47]. Wang et al. [48] claims to synthesize Nb doped nanoparticles by a novel polymer assisted sol-gel process and M Hirano et al. [49] synthesized Photoactive and Adsorptive Niobium-Doped Anatase (TiO_2) by changing Hydrothermal Conditions. The crystalline structure of titania is not altered even when large amounts of dopant (20 wt %) has been doped . XRD peaks show a slight shifting towards left that indicates the inclusion if niobium in titania lattice because Ti^{+4} has smaller radius (0.61 Å) as compared to Nb^{+5} (0.64 Å). Larger shift of peaks has been observed when higher amount of dopant has been incorporated [46, 49]. While increasing niobium loading, the onset of absorption shifts towards longer wavelengths. A red shift has been observed in UV-vis spectra for 10 wt % doping as compared to undoped titania and allows doped titania to absorb 40 % more light than pristine [45, 49]. Decrease in bandgap by Nb doping in titania has also been reported by Salvador et al. [50]. They performed electrochemical measurements and found photocurrent quantum efficiency to calculate the bandgap (Eg). They varied quantum efficiency with photon energy to determine value of Eg experimentally. They report highest band gap reduction (Eg=2.9eV) and highest quantum efficiency by 0.2 wt % doping of niobium. Increasing Nb content further increased band gap which was an indication of segregation of Nb_2O_5. band gap reduction. Reported by X Lu et al. [47] cell consisting photoanode made from Nb doped titania nanoparticles (5 mol %) showed 18.2 % more energy conversion efficiency and enhanced conductivity than cell consisting photoanode made from undoped titania nanoparticles. As indicated in **Fig. 3** [46] and **Fig. 4** [47], an enhancement in opto-electronic properties and device efficiency of cell containing niobium doped titania photoanode has been observed [51]. A decrease in V_{oc} was observed when dopant concentration was increased. This is due to the positive shifting of V_{fb}. Lowering of V_{oc} can be avoided and photocurrent density can be improved by optimizing and carefully selection of electrolyte, dye and photo-anode material.

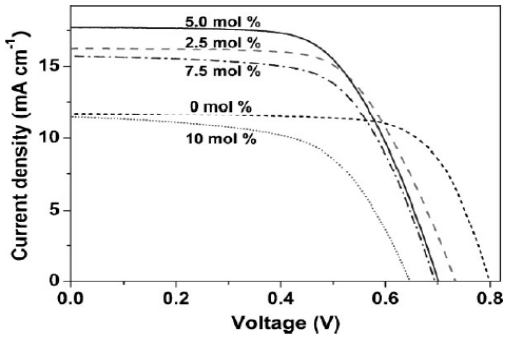

Fig. 4 Current-voltage curves of Niobium doped and undoped Titania based DSSC [47].

Iron can be doped in titania using different methods including sol-gel [38, 52, 53], wet impregnation [54] and oxidative pyrolysis [55]. Photo-anode for DSSCs can be made out of these doped nanoparticles using doctor blade coating technique. When opting sol-gel technique, sol can be directly coated on substrate using spin coating or dip coating. The ionic radius of Ti^{4+} (0.0605 nm) and that of Fe^{3+} makes the substitution of dopant in titania lattice possible. Due to doping iron in titania lattice and iron ion radius being smaller than Ti^{4+} ion, compaction of titania lattice is observed and denser phase is formed [55]. Iron exists as its oxide form in titania matrices and the crystallinity of TiO_2 is hardly affected by iron doping [53]. It was reported that the presence of iron as dopant in titania lattice initiates the formation of rutile phase. The formation of rutile phase increases with increase in iron loading. An increase in wt % of rutile phase has

been indicated from 14% (pristine) to 23% (doped). Changing different concentrations of iron dopant in titania, a reduction in band gap has been seen up to 2.9 eV and this make photoresponse of doped titania possible in visible region. The impurity levels formed by doped metal oxides not only act as absorption centers of VIS-light but also act as recombination centers of electron/hole pairs. It is found that the recombination of the photogenerated electron/hole pairs take place quickly in the Fe-doped TiO_2 films [38] whereas Wang X et al. [55] observed a decrease in recombination's of generated carriers. A decrease in photocatalytic activity has been observed by presence of Fe ions [53]. Iron doped titania showed higher specific surface area when compared to undoped titania.

4. Conclusions

In this review we discussed electrode properties of doped and undoped titania and its effect on efficiency of Dye Sensitized Solar Cells (DSSCs). The enhancement of conversion efficiency and effective electron transport using metal doped titania in DSSCs have been discussed. A review on effect of using doped titania anode on recombination rate and photo catalytic activity in DSSCs has also been summarized. Doping the titania semiconductor of photoanode rendered three main advantages that are reduction in the photocatalytic activity of DSSCs, reduction in band gap thus enhancement in efficiency, and reduction in recombination rate. Better performances of cells have been observed by utilizing doped semiconductor as compared to undoped semiconductor. Although extensive studies have been made on doping TiO_2 and its use as a photoanode in DSSCs, none of these are able to enhance both the short-circuit current density and open-circuit voltage. Therefore, there is a need to investigate thoroughly and more deeply in this area to obtain commendable outcomes.

Acknowledgement

The authors would like to thank Research and PGP Directorates of NUST Islamabad for their support for research on photovoltaic technologies.

References

[1] M. Grätzel, "Dye-sensitized solar cells," Journal of Photochemistry and Photobiology C: Photochemistry Reviews, vol. 4, pp. 145-153, 2003.

[2] J. Zhao, A. Wang, M. A. Green, and F. Ferrazza, "19.8% efficient “honeycomb” textured multicrystalline and 24.4% monocrystalline silicon solar cells," Applied Physics Letters, vol. 73, pp. 1991-1993, 1998.

[3] P. Jackson, D. Hariskos, E. Lotter, S. Paetel, R. Wuerz, R. Menner, W. Wischmann, and M. Powalla, "New world record efficiency for Cu (In, Ga) Se2 thin-film solar cells beyond 20%," Progress in Photovoltaics: Research and Applications, vol. 19, pp. 894-897, 2011.

[4] M. Xu, D. Xia, and Y. Sheng, "Thin-film solar cells," Mater Rev, vol. 20, pp. 109-111, 2006.

[5] A. G. Aberle, "Thin-film solar cells," Thin Solid Films, vol. 517, pp. 4706-4710, 2009.

[6] B. Li, L. Wang, B. Kang, P. Wang, and Y. Qiu, "Review of recent progress in solid-state dye-sensitized solar cells," Solar Energy Materials and Solar Cells, vol. 90, pp. 549-573, 2006.

[7] M. Zalas and M. Klein, "The Influence of Titania Electrode Modification with Lanthanide Ions Containing Thin Layer on the Performance of Dye-Sensitized Solar Cells," International Journal of Photoenergy, vol. 2012, 2012.

[8] M. Grätzel, "Conversion of sunlight to electric power by nanocrystalline dye-sensitized solar cells," Journal of Photochemistry and Photobiology A: Chemistry, vol. 164, pp. 3-14, 2004.

[9] A. Le Viet, R. Jose, M. Reddy, B. Chowdari, and S. Ramakrishna, "Nb2O5 photoelectrodes for dye-sensitized solar cells: choice of the polymorph," The Journal of Physical Chemistry C, vol. 114, pp. 21795-21800, 2010.

[10] A. B. Martinson, J. W. Elam, J. T. Hupp, and M. J. Pellin, "ZnO nanotube based dye-sensitized solar cells," Nano letters, vol. 7, pp. 2183-2187, 2007.

[11] M. Quintana, T. Edvinsson, A. Hagfeldt, and G. Boschloo, "Comparison of dye-sensitized ZnO and TiO2 solar cells: studies of charge transport and carrier lifetime," The Journal of Physical Chemistry C, vol. 111, pp. 1035-1041, 2007.

[12] A. Birkel, Y.-G. Lee, D. Koll, X. Van Meerbeek, S. Frank, M. J. Choi, Y. S. Kang, K. Char, and W. Tremel, "Highly efficient and stable dye-sensitized solar cells based on SnO2 nanocrystals prepared by microwave-assisted synthesis," Energy & Environmental Science, vol. 5, pp. 5392-5400, 2012.

[13] S. Yang, H. Kou, J. Wang, H. Xue, and H. Han, "Tunability of the band energetics of nanostructured SrTiO3 electrodes for dye-sensitized solar cells," The Journal of Physical Chemistry C, vol. 114, pp. 4245-4249, 2010.

[14] A. N. Banerjee, "The design, fabrication, and photocatalytic utility of nanostructured semiconductors: focus on TiO2-based nanostructures," Nanotechnol Sci Appl, vol. 4, p. 35, 2011.

[15] Y. Duan, N. Fu, Q. Liu, Y. Fang, X. Zhou, J. Zhang, and Y. Lin, "Sn-doped TiO2 photoanode for dye-sensitized solar cells," The Journal of Physical Chemistry C, vol. 116, pp. 8888-8893, 2012.

[16] M. Pelaez, N. T. Nolan, S. C. Pillai, M. K. Seery, P. Falaras, A. G. Kontos, P. S. Dunlop, J. W. Hamilton, J. A. Byrne, and K. O'Shea, "A review on the visible light active titanium dioxide photocatalysts for environmental applications," Applied Catalysis B: Environmental, vol. 125, pp. 331-349, 2012.

[17] M. R. Hoffmann, S. T. Martin, W. Choi, and D. W. Bahnemann, "Environmental applications of semiconductor photocatalysis," Chemical reviews, vol. 95, pp. 69-96, 1995.

[18] A. K. Chandiran, F. Sauvage, M. Casas-Cabanas, P. Comte, S. Zakeeruddin, and M. Graetzel, "Doping a TiO2 Photoanode with Nb5+ to Enhance Transparency and Charge Collection Efficiency in Dye-Sensitized Solar Cells," The Journal of Physical Chemistry C, vol. 114, pp. 15849-15856, 2010.

[19] F. Meng, Z. Hong, J. Arndt, M. Li, M. Zhi, F. Yang, and N. Wu, "Visible light photocatalytic activity of nitrogen-doped La2Ti2O7 nanosheets originating from band gap narrowing," Nano Research, vol. 5, pp. 213-221, 2012.

[20] G. Liu, H. G. Yang, X. Wang, L. Cheng, H. Lu, L. Wang, G. Q. Lu, and H.-M. Cheng, "Enhanced photoactivity of oxygen-deficient anatase TiO2 sheets with dominant {001} facets," The Journal of Physical Chemistry C, vol. 113, pp. 21784-21788, 2009.

[21] A. Zaleska, "Doped-TiO2: a review," Recent Patents on Engineering, vol. 2, pp. 157-164, 2008.

[22] X. Chen and S. S. Mao, "Titanium dioxide nanomaterials: synthesis, properties, modifications, and applications," Chemical reviews, vol. 107, pp. 2891-2959, 2007.

[23] I. Tanabe, K. Matsubara, N. Sakai, and T. Tatsuma, "Photoelectrochemical and optical behavior of single upright Ag nanoplates on a TiO2 film," The Journal of Physical Chemistry C, vol. 115, pp. 1695-1701, 2010.

[24] H. Yu, J. Huang, H. Zhang, Q. Zhao, and X. Zhong, "Nanostructure and charge transfer in Bi2S3-TiO2 heterostructures," Nanotechnology, vol. 25, p. 215702, 2014.

[25] N. Ghows and M. Entezari, "A novel method for the synthesis of CdS nanoparticles without surfactant," Ultrasonics sonochemistry, vol. 18, pp. 269-275, 2011.

[26] G. Marci, V. Augugliaro, M. J. Lopez-Munoz, C. Martin, L. Palmisano, V. Rives, M. Schiavello, R. J. Tilley, and A. M. Venezia, "Preparation characterization and photocatalytic activity of polycrystalline ZnO/TiO2 systems. 1. Surface and bulk characterization," The Journal of Physical Chemistry B, vol. 105, pp. 1026-1032, 2001.

[27] R. Asahi, T. Morikawa, T. Ohwaki, K. Aoki, and Y. Taga, "Visible-light photocatalysis in nitrogen-doped titanium oxides," science, vol. 293, pp. 269-271, 2001.

[28] X. Feng, K. Shankar, M. Paulose, and C. A. Grimes, "Tantalum-Doped Titanium Dioxide Nanowire Arrays for Dye-Sensitized Solar Cells with High Open-Circuit Voltage," Angewandte Chemie, vol. 121, pp. 8239-8242, 2009.

[29] H. P. Maruska and A. K. Ghosh, "Transition-metal dopants for extending the response of titanate photoelectrolysis anodes," Solar Energy Materials, vol. 1, pp. 237-247, 1979.
[30] M. Geetha, K. Suguna, and P. Anbarasan, "Photoanode Modification in DSSC Using Chromium Doped TiO2 nanoparticles by sol-gel method," Archives of Physics Research, vol. 3, pp. 303-308, 2012.
[31] T. VAN NAM, N. T. TRANG, and B. T. CONG, "Mg-DOPED TiO2 FOR DYE-SENSITIVE SOLAR CELL: AN ELECTRONIC STRUCTURE STUDY," in Proc. Natl. Conf. Theor. Phys, 2012, pp. 233-242.
[32] J. Liu, Y. Duan, X. Zhou, and Y. Lin, "Influence of VB group doped TiO2 on photovoltaic performance of dye-sensitized solar cells," Applied Surface Science, vol. 277, pp. 231-236, 2013.
[33] X. Zhang, F. Liu, Q.-L. Huang, G. Zhou, and Z.-S. Wang, "Dye-sensitized W-doped TiO2 solar cells with a tunable conduction band and suppressed charge recombination," The Journal of Physical Chemistry C, vol. 115, pp. 12665-12671, 2011.
[34] K. H. Ko, Y. C. Lee, and Y. J. Jung, "Enhanced efficiency of dye-sensitized TiO< sub> 2</sub> solar cells (DSSC) by doping of metal ions," Journal of colloid and interface science, vol. 283, pp. 482-487, 2005.
[35] Q. Liu, Y. Zhou, Y. Duan, M. Wang, and Y. Lin, "Improved photovoltaic performance of dye-sensitized solar cells (DSSCs) by Zn+Mg co-doped TiO2 electrode," Electrochimica Acta, vol. 95, pp. 48-53, 2013.
[36] G. Colon, M. Maicu, M. s. Hidalgo, and J. Navio, "Cu-doped TiO< sub> 2</sub> systems with improved photocatalytic activity," Applied Catalysis B: Environmental, vol. 67, pp. 41-51, 2006.
[37] R. López, R. Gómez, and M. E. Llanos, "Photophysical and photocatalytic properties of nanosized copper-doped titania sol–gel catalysts," Catalysis Today, vol. 148, pp. 103-108, 2009.
[38] M. Maeda and T. Yamada, "Photocatalytic activity of metal-doped titanium oxide films prepared by sol-gel process," in Journal of Physics: Conference Series, 2007, p. 755.
[39] B. Choudhury, M. Dey, and A. Choudhury, "Defect generation, dd transition, and band gap reduction in Cu-doped TiO2 nanoparticles," International Nano Letters, vol. 3, pp. 1-8, 2013.
[40] P.-J. Zhao, R. Wu, J. Hou, A.-M. Chang, F. Guan, and B. Zhang, "One-step Self Assemble of Cu-TiO2 Heterogeneous Nanoparticles Using a Soft Template," 无机材料学报, vol. 27, 2012.
[41] J. Navas, C. Fernández-Lorenzo, T. Aguilar, R. Alcántara, and J. Martín-Calleja, "Improving open-circuit voltage in DSSCs using Cu-doped TiO2 as a semiconductor," physica status solidi (a), vol. 209, pp. 378-385, 2012.
[42] C. Vidyasagar, Y. A. Naik, T. Venkatesha, and R. Viswanatha, "Optical properties of Dye Sensitized Anatase Cu-TiO2 Nanoparticles," 2011.
[43] W. W. So, S. B. Park, K. J. Kim, C. H. Shin, and S. J. Moon, "The crystalline phase stability of titania particles prepared at room temperature by the sol-gel method," Journal of materials science, vol. 36, pp. 4299-4305, 2001.

[44] A. Teleki, N. Bjelobrk, and S. Pratsinis, "Flame-made Nb- and Cu-doped TiO2 sensors for CO and ethanol," Sensors and Actuators B: Chemical, vol. 130, pp. 449-457, 2008.

[45] A. Mattsson, M. Leideborg, K. Larsson, G. Westin, and L. Österlund, "Adsorption and solar light decomposition of acetone on anatase TiO2 and niobium doped TiO2 thin films," The Journal of Physical Chemistry B, vol. 110, pp. 1210-1220, 2006.

[46] M. Siddiki, D. Munoz-Rojas, J. Oro, J. Li, Q. Qiao, D. Galipeau, and M. Lira-Cantu, "Synthesis and characterization of Nb doped titania for dye sensitized solar cells," in Photovoltaic Specialists Conference (PVSC), 2009 34th IEEE, 2009, pp. 000685-000689.

[47] X. Lü, X. Mou, J. Wu, D. Zhang, L. Zhang, F. Huang, F. Xu, and S. Huang, "Improved-Performance Dye-Sensitized Solar Cells Using Nb-Doped TiO2 Electrodes: Efficient Electron Injection and Transfer," Advanced Functional Materials, vol. 20, pp. 509-515, 2010.

[48] Y. Wang, B. M. Smarsly, and I. Djerdj, "Niobium Doped TiO2 with Mesoporosity and Its Application for Lithium Insertion," Chemistry of materials, vol. 22, pp. 6624-6631, 2010.

[49] M. Hirano and K. Matsushima, "Photoactive and Adsorptive Niobium-Doped Anatase (TiO2) Nanoparticles: Influence of Hydrothermal Conditions on their Morphology, Structure, and Properties," Journal of the American Ceramic Society, vol. 89, pp. 110-117, 2006.

[50] P. Salvador, "The influence of niobium doping on the efficiency of n-TiO< sub> 2</sub> electrode in water photoelectrolysis," Solar Energy Materials, vol. 2, pp. 413-421, 1980.

[51] A. V. Emeline, Y. Furubayashi, X. Zhang, M. Jin, T. Murakami, and A. Fujishima, "Photoelectrochemical behavior of Nb-doped TiO2 electrodes," The Journal of Physical Chemistry B, vol. 109, pp. 24441-24444, 2005.

[52] M. Li, "The research and development of Fe doped TiO2," Research of Materials Science, vol. 2, 2013.

[53] J. A. Navío, G. Colón, M. Macías, C. Real, and M. I. Litter, "Iron-doped titania semiconductor powders prepared by a sol–gel method. Part I: synthesis and characterization," Applied Catalysis A: General, vol. 177, pp. 111-120, 1999.

[54] A. Di Paola, G. Marci, L. Palmisano, M. Schiavello, K. Uosaki, S. Ikeda, and B. Ohtani, "Preparation of polycrystalline TiO2 photocatalysts impregnated with various transition metal ions: characterization and photocatalytic activity for the degradation of 4-nitrophenol," The Journal of Physical Chemistry B, vol. 106, pp. 637-645, 2002.

[55] X. Wang, J.-G. Li, H. Kamiyama, M. Katada, N. Ohashi, Y. Moriyoshi, and T. Ishigaki, "Pyrogenic iron (III)-doped TiO2 nanopowders synthesized in RF thermal plasma: phase formation, defect structure, band gap, and magnetic properties," Journal of the American Chemical Society, vol. 127.

Synthesis of Cu Doped Titania Nanoparticles and Studies on its Structural and Thermal Performance for Dye Sensitized Solar Cells

Sehar Shakir [*(a)], Abd-ur-Rehman[(b)], Muhammad Akmal Rana[(a)], M N Akbar[(a)], Mustafa Anwar[(a)], Kamaal Mustafa[(a)], Zuhair S. Khan[(a)]

[(a)]Advanced Energy Materials and Fuel Cells Lab, Centre for Energy Systems, National University of Sciences and Technology, Sector H-12 Islamabad 44000, Pakistan.

[(b)] Mechanical engineering department, King Fhad University of Petroleum and Minerals, KSA.

[*]email: 12sehar_shakir@ces.nust.edu.pk; zskhan@ces.nust.edu.pk

Abstract: Photoanode is one of the most important components in DSSCs for which oxide ceramics such as titania is one of the top choices. In this work, we have synthesized undoped and doped titania nanoparticles by simple and reliable sol-gel route. Metal doping can introduce structural defects in titania lattice that can result in increase in photo-absorption of solar cells. There was an indication in literature that Cu could initiate phase transformation in titania at lower temperature supportive to cell performance. Furthermore, Cu offers its candidature due to being relatively inexpensive and easily available. However, there is not enough data available in literature on performance of DSSCs based on Cu doped titania photoanode. Therefore, we are presenting herein systematic studies on Cu doped titania nanoparticles. Meanwhile, thin film coatings of titania and doped titania were made on FTO coated glass by assortment of methods like spin coating, doctor blade coating, etc. Various process routes such as effects of annealing temperature, Cu concentration, pore former, etc. were used in this study. Structural and thermal performance of materials and thin films were carried out using diversified techniques such as X-ray diffraction, Scanning electron Microscopy, TG-DT analysis, etc. Studies have revealed that dopant existed in the form of CuO in nanoparticles and thin films. Cu doping assisted in reduction in particle size and band gap which was further verified by red absorption shift. Films with almost negligible crack were successfully made on FTO coated glass and it was found that crack density reduced with reducing drying time, increasing stirring time and adding HNO_3 along with water and ethanol as a precursor solvent. The inclusion of carbon microspheres formed cavities into the pellets of titania and Cu:Titania and increased the porosity and surface area for greater dye adsorption. It was found that porosity increased from 31% to 42% by adding 2.5 wt% carbon microspheres in 3wt% Cu doped titania thin films. IV measurements of the cells fabricated using Cu doped titania photoanode N3 dye, I^-/I_3^- electrolyte and gold coated FTO glass as counter electrode revealed a 11% increase in V_{oc} when compared to V_{oc} of cells made with similar components but using undoped titania photoanode

Keywords: Doped titania nanoparticles, doctor blade coating, DSSCs, carbon microsphere, Titania thin films.

To be submitted to “International Journal of Nanotechnology” by Oct, 2014.

Introduction

The efficiency of Dye Sensitized Solar Cells (DSSC's) depends on various factors. The efficiency is very much related to the properties of semiconductor photoanode. Few other cell -based efficiency depending factors are properties of dye, nature of redox couple, catalytic properties of counter electrode etc. In other words each and every layer of a DSSC affects the efficiency of the cell. Focusing on semiconductor photoanode, titania is the most usable and attractive semiconductor material for DSSC's because of its chemical stability and easy availability. The main downside of titania is that it only absorbs UV radiation form solar spectrum which makes only 4% of the electromagnetic radiations coming from sun [1, 2]. In order to enhance the absorption of solar radiation by titania we need to create oxygen deficiencies or structural defects in its structure to decrease the band gap. The reduction in band gap of titania (anatase =3.2ev) can lead to make it active in visible light. Moreover, forming pores in titania layer of photoanode can lead to enhanced adsorption of dye and hence greater absorption of incident light. Homogenous thin films of titania formed using a low cost solution based technique can offer price control over the cells as well as better films lead to better performance of cells.

Previous studies have shown that correctly doping titania by various metals can enhance some of the photovoltaic properties of the cell. Doping titania semiconductor render three main advantages in DSSCs, reduction in band gap thus enhancement in efficiency, reduction in photocatalytic activity of DSSCs and reduction in recombinations. For example Feng et al.[3] reported using Ta-doped Titania nanowire arrays for DSSC's showed negative shifting of C.B of titania due to which increase in open circuit voltage (V_{oc}) was observed. M. Geetha et al. [4] reported improvements in photoelectric performance of DSSCs by using chromium doped titania semiconductor as photoanode. Maciej Zalas and Maciej Klein [5] studied the influence of rare earth metal doping on performance of DSSCs. These modified electrodes prevented back transfer of electrons and enhanced dye absorption ability Xujiye Lu et al. [6] and Lee et al. [7] studied niobium doped Titania semiconductor based DSSC and reported an improvement in cell performance due to doping.

Copper is readily available in earth's crust and cheap metal with high electronic conductivity [8] which makes it an attractive metal for doping Titania semiconductor photoanode of DSSCs. Doping copper in titania can create structural defects in titania lattice hence reducing its wide band gap.

In this research we have studied the doping effects of copper on structure, crystallinity and morphology of undoped titania and discussed how doping copper shifts the absorption edge of titania to visible region. Meanwhile, thermal stability of semiconductor and doped semiconductor was also investigated. Efforts were made to enhance the performance of photoanode by increasing its porosity, absorption of light and optimizing coating process.

Experimentation

Undoped titania nanoparticles and titania with 1wt% and 3wt% Cu were prepared by sol–gel method. The synthesis of doped titania nanoparticles was done using sol-gel method in which 25 ml of titanium isopropoxide (Sigma-Aldrich) was stirred for one hour in 50 ml ethanol. Isopropoxide chain was hydrolyzed by addition of 30ml water and 6 ml HCl and was stirred continuously for 3 hours. The sol was kept for 24 hours, dried and then annealed at 450℃ and 650℃ for 4 hours. To prepare Cu-doped titania another solution was made containing $CuCl_2.5H_2O$, water and ethanol. This solution was added while hydrolyzing TTIP solution. This sol was also kept for 24 hours, dried and annealed at similar conditions as for undoped titania.

Paste was formed by adding 15 mL ethanol, 1 mL distilled water, $1/3^{rd}$ mL HNO_3 in 2g Cu-doped titania (3 wt% doped Cu) and 2g PEG and stirred for 4 hours to make an homogenous paste. To deposit undoped titania layer on glass slide, undoped titania powder was used. The pores were formed into photoanode by including 0wt% and 2.5 wt% hydrothermally synthesized carbon microspheres in this paste. The paste was coated on the conductive side of FTO coated glass substrates using a doctor blade coater. The coated films were dried at room temperature for several hours and then annealed at 450 °C. The cells were fabricated using N3 dye adsorbed on photoanode, I_3/I_3^- redox electrolyte and gold counter electrode.

The X-ray diffraction (XRD) pattern of the samples was obtained using a θ-θ STOE Germany X Ray diffractometer at room temperature irradiating X Rays from Cu-Kα for structure and phase analysis. XRD was operated at 40kV and 30 mA. The measurements were recorded in step of 0.04° and scan angle range of 10-80°. SEM and (EDX) of the samples were carried out using a JEOL 2300 scanning electron microscope at and operating voltage of 20kV with an EDX detector. UV-VIS spectra of the samples were obtained using a BMS 2800 UV–Vis spectrophotometer with $BaSO_4$ powder as the standard reference sample and data was taken from range 300nm to 900nm. TG-DT analyses of the samples were performed using Perkin Elmer diamond TG/DTA version 2.0 with 2g sample weight each. Temperature range was set from room temperature to 500 °C. Thickness of film was determined using JEOL 2300 scanning electron microscope at an operating voltage of 20kV. Optical Microscopic Images of coatings were obtained using Optika B-600 MET with camera Optika 40. IV characteristics of DSSCs were obtained using Biological VSP (potentiostat system).

Results and Discussion

Effect of Annealing Temperature and Cu Concentration on Crystal Structure of Nanoparticles (XRD Analysis)

The similarity in ionic radius of Cu^{2+} (0.73 Å) to that of Ti^{4+} (0.64 Å) enables copper to substitute titanium. Titania doped with Cu^{2+} initiates the formation of rutile phase along with anatase. As shown in Fig. 1 (a), when annealed at 450 °C, titania changes from amorphous to crystalline phase. At 450 °C pure anatase phase is formed corresponding to JCPDS card# 78-2486. Anatase is metastable phase of Titania and is usually formed at low temperature during solution-phase synthesis [9]. As the annealing Temperature increases to 650 °C undoped titania shows a small rutile phase peak (110). It means at

higher temperature rutile phase starts forming. Fig. 1 (b) shows the XRD patterns of 1wt% Cu doped titania. Sample annealed at 450 °C completely show anatase phase and no other peak is being observed and sample annealed at 650 °C show a little peak of rutile phase. The reason for no prominent change when compared with XRD patterns of undoped titania samples might be low concentration of dopant. Therefore it can be concluded inclusion of impurities at this concentration didn't affect the crystal structure of titania.

Whereas, introducing 3 wt% copper in titania lattice initiates rutile phase as evident from Fig. 1 (c) where peak of rutile phase can be observed when the sample for annealed at 450 °C and a complete transformation of phase is been shown at 650 °C where all peaks corresponds to rutile phase of titania (JCPDS card# 76-1934). Increase in rutile fraction with doping indicates inhibition of the formation of complete anatase phase due to incorporation of Cu on the titania lattice. The inclusion of copper in titania anatase creates a higher number of defects which results in quicker formation of rutile nuclei. During annealing, the replacement of Ti^{4+} by Cu^{2+} cause a decrease in free electron concentration and an increase in oxygen vacancy concentration. Anatase to rutile phase transition occurs because of this increase in oxygen vacancies created in crystal lattice [10]. The phase transformation results are consistent with DT analysis explained latter. No peaks of copper are being observed in XRD of the doped Cu titania particle due to very low concentration of the dopant.

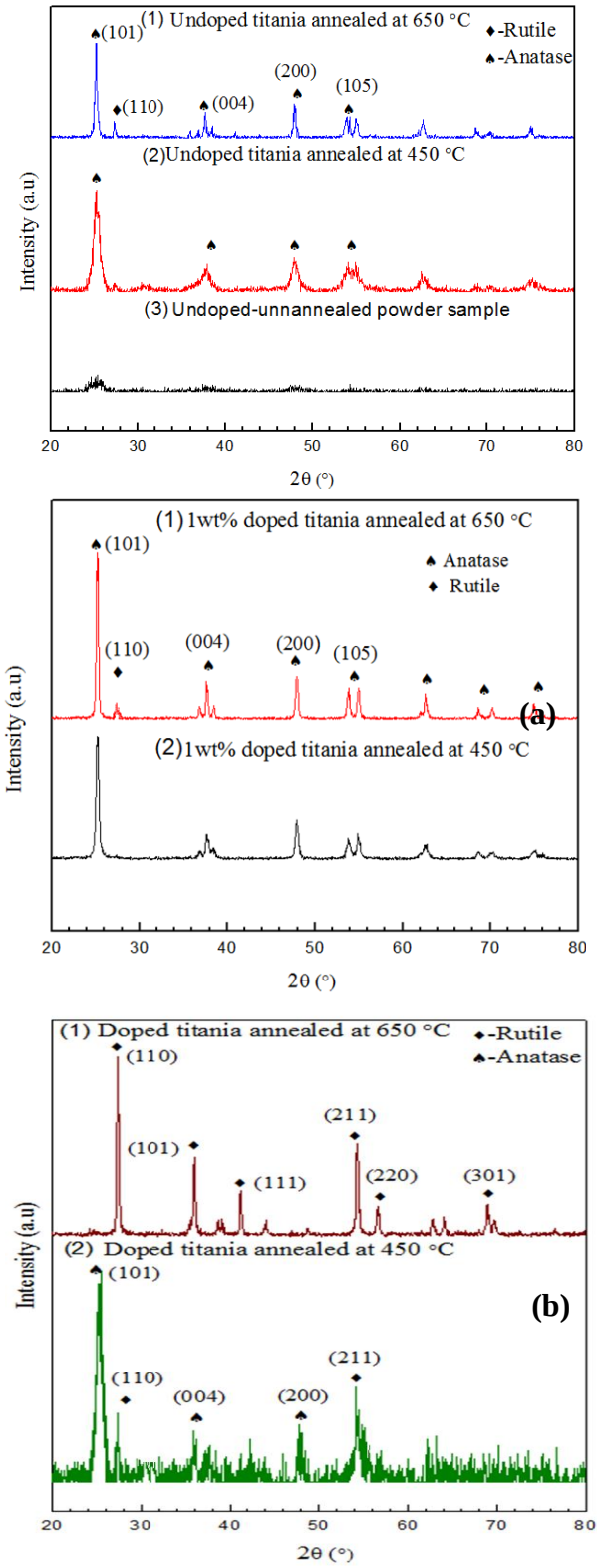

Fig. 37 XRD pattern of (a) undoped (b) 1wt% Cu doped and (c) 3wt% Cu doped titania nanoparticles at different annealing temperatures.

The crystallite sizes for undoped titania is 13.1nm and 43.1 nm annealed at temperatures 450 °C and 650 °C

respectively and that for 3wt% Cu-doped titania is 11.6 nm and 36.6 nm annealed at temperatures 450 °C and 650 °C respectively. The trend in crystallite size due to annealing and doping has been shown in table 6.2 and it shows increasing annealing temperature increases the crystallite size. The increase is due to increase in crystallinity of particles. Greater crystallite size indicates greater crystallinity of nanoparticles [11]. So adding dopant decr eased the crystallite size and crystallinity of the particles when compared with undoped samples at their respective temperatures. This means copper might exist in amorphous form (later confirmed by FTIR results). These results show that incorporation of dopants in host nanomaterials modified the crystal phase.

Table 9 Crystallite sizes of undoped, 1wt% and 3wt% Cu-doped titania at 450 °C and

Sr no	Sample	Annealing Temperature (°C)	Crystallite Size (nm)
1)	Undoped Titania	450	13.1
2)	Undoped titania	650	43.1
3)	1wt% Cu doped titania	450	12.9
4)	1wt% Cu doped titania	650	13
5)	3wt% Cu doped titania	450	11.6
6)	3wt% Cu doped titania	650	36.6

Anatase allows more absorption of dye and hence performs better when compared to other phases. But studies have shown that co-presence of anatase and rutile crystallites can enhance charge separation, photocatalytic activity and transfer of photo-generated electrons and holes [12]. DSSCs made with P25 (Degussa) showed higher efficiency and better photocatalytic performance. P25 is composed of anatase and rutile crystallites, anatase being the major phase and rutile being the minor (in rations 70:30 or 80:20).These results showed that doping titania with 3wt% copper caused oxygen deficiency and created defects. While doping titania with 1wt% copper hardly had any effect on crystal structure. Therefore, other techniques were used to probe deeply into the effects of inclusion on 3wt% copper dopant in titania.

Effect of Annealing Temperature and Cu Addition on Morphology, Composition and Particle Size of Nanoparticles (SEM/EDX Analysis)i

The high-resolution SEM micrographs of undoped and 3wt% Cu-doped titania nanoparticles annealed at 450 °C and 650 °C are shown in Fig. 2.

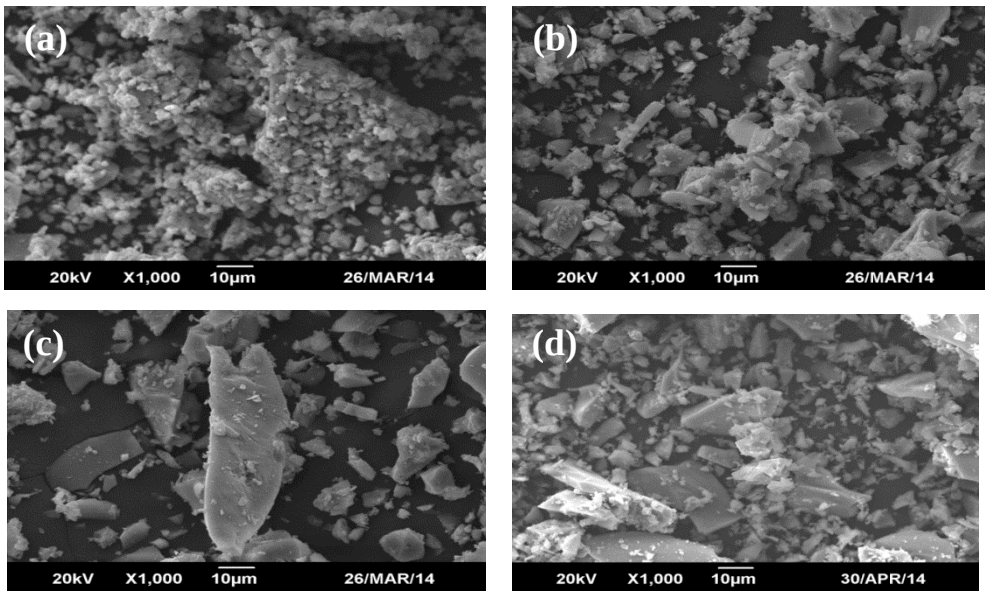

Fig. 2 SEM images (a) undoped titania particles annealed at 450 °C, (b) undoped titania particles annealed at 650 °C, (c) 3wt% Cu-doped titania particles annealed at 450 °C and (d) 3wt% Cu-doped titania particles annealed at 650 °C.

Fig. 2 shows that the particles are of arbitrary shape. With increasing annealing temperature of undoped titania nanoparticles from 450 °C to 650 °C, growth of particles can be seen in Fig. 2 (a) and (b). In Fig. 2 (c) and (d) we can see an accumulation of some substance appearing lighter in images. The substance accumulation is increasing with increasing annealing temperature. This can be attributed to the formation of oxide with doping and increasing temperature. The particle size distribution shows that the average particle size of undoped titania is 68.64 nm and 71 nm annealed at 450 °C and 650 °C respectively and that of 3wt% Cu doped nanoparticles is 61.84 nm and 60.50 nm annealed at 450 °C and 650 °C respectively. Increasing Annealing temperature decreased the average particle size of titania as shown in Table 2. Small particles offer large surface areas allowing better light absorption. Current density can be more than doubled by controlling particle size [13]. Large particles allows strong light scattering [14].

The decrease in average particle size of 3wt% Cu doped samples can be observed. It is due addition of dopant cause inhibition of the growth and hence decrease in particle size. We observed a decrease in crystallinity in our XRD results as well. These results reported by Wang et al. [15] are consistent with our Cu-doped titania results. He observed a decrease in grain size and formation of amorphous crystal structure with doping iron and reported further decrease in particle size with increasing dopant concentration. Li et al. [16] studied Zn-doped SnO_2 nanomaterials and also reported a decrease in particle size. The change in grain size with addition of dopant is basically

very important phenomenon for change in electronic structure. Hence addition of dopant and its concentration can be used to tailor the particle size of copper doped titania.

Table 2 Summary of SEM/EDX results.

Sample	Annealing Temperature (°C)	Atom%			Particle Size (nm)
		Ti	O	Cu	
Undoped titania	450	31.51	68.49	0	68.64
Undoped titania	650	31.10	68.90	0	71.27
3wt% Cu doped titania	450	28.08	70.67	1.24	61.84
3wt% Cu doped Titania	650	24.74	71.51	0.74	60.50

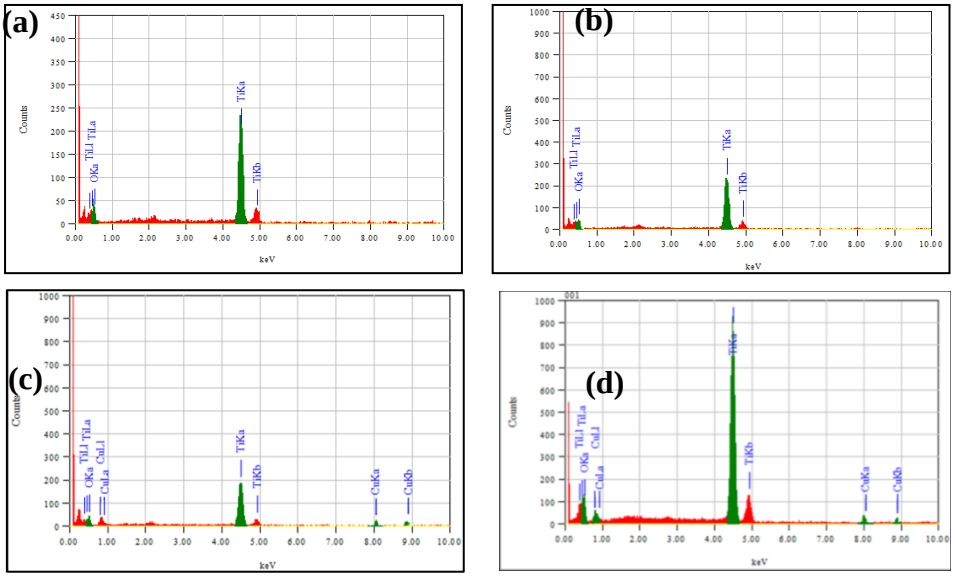

Fig. 3 EDX pattern of (a) undoped titania annealed at 450 °C (b) undoped titania annealed at 650 °C (c) 3wt% Cu doped titania annealed at 450℃ and (d) 3wt% Cu-doped titania annealed at 650 °C.

Fig. 3 shows the EDX pattern of the undoped and 3wt% Cu-doped titania nanoparticles, showing the presence of Cu, Ti, and O in the nanoparticles. No impurities can be observed. The results are summarized in Table 2. In Fig. 3 (c) and (d) presence of copper (~3 wt%) confirms the doping of the copper in titania and the result is consistent with results of XRD and FTIR spectroscopy.

UV-Vis Analysis of 3wt% Cu Doped Titania Nanoparticles

Anatase titania has Eg value 3.31 eV and exhibits absorption peaks in UV region of electromagnetic radiations. The absorption spectrum of undoped and 3wt% C u-doped titania is shown In Fig. 4, doping copper in titania lattice shows an absorbance shift towards the visible spectrum. Undoped titania particles exhibits maximum absorption at 325 nm whereas, doped sample exhibits maximum absorption at 379 nm. The absorption peaks corresponds to the maximum absorption when electrons are excited from the valence to the conduction band. Doped sample shows a shift in the absorption towards visible region. The CB in titania comprises of Ti 3d states and VB comprises of O 2p states. The 325 nm absorption peak is due to electronic transition from O 2p to Ti 3d. The absorption shift to 379 nm appears as a result of charge transfer at the interface from the O 2p VB to the Cu (II) state attached to titania. These Cu (II) states may be present either as Cu (II) nanoclusters or in the form of amorphous oxide phase of CuO. Li et al. [11] demonstrated that Cu (II) does not show this absorption peak if it is present as CuO, but displays this absorption when it is present only as Cu (II) ions attached to titania. However, Qiu et al. [12] suggested that the absorption peak shift appears due to charge transfer from titania to CuO clusters in CuO/Titania nanocomposite. Therefore, based on these observations, we can predict that the absorption appears due to charge transfer from O 2p to Cu (II) clusters or CuO amorphous phase. Hence it can be concluded that substitution of Ti^{4+} by Cu^{2+} atoms generates defect centers that cause the change in optical absorption. These results were later affirmed by FTIR analysis results which showed that in our case, copper existed as CuO form

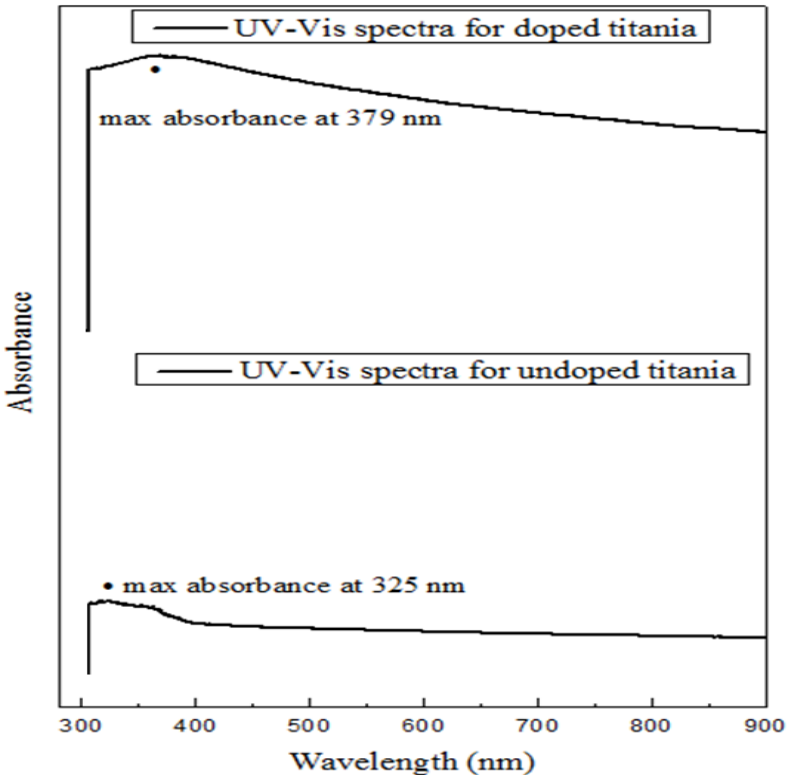

Fig. 4 UV-VIS spectra for undoped and 3wt% Cu-doped titania annealed at 450 °C.

Doping titania with a transition metal leads to the reduction in the band gap energy which is attributed to the inclusion of copper ions into titania crystal lattice and/or formation of CuO on surface of the particles. It has been studied that doping titania with aliovalent ions changes the material properties and absorption properties because of the modification in local lattice symmetry and defects. When titania is doped with copper,

Cu^{2+} ions either locate themselves on the surface sites or inside bulk titania. This causes lattice deformation due to rearrangement of adjoining atoms to neutralize charge deficiency. This lattice deformation and rearrangement modifies electronic structure and hence the band gap shift occurs [17]. Also, oxygen vacancies are created due to presence of small amounts of Cu^{2+} dopant in the lattice sites of titania [10,19]. These are created due to charge compensation effect. It is, therefore, possible to control band gap shift and absorption of the doped nanoparticles controlled by lattice strain and doping-induced vacancies.

Thermal Analysis of Undoped and 3wt% Cu Doped Titania Nanoparticles Using TG/DT Setup

Fig. 5 shows the TG/DTA curves of doped and 3wt% Cu-doped titania nanoparticles. Looking at TG curves of both samples, initial weight loss is being observed at temperatures below 100 °C. This weight loss indicates the removal of water and ethanol from powders. At temperatures from 100 °C to 300 °C, a weight loss of 17% for undoped titania powder and 15% for doped titania powder is being observed. This loss can be attributed to the removal of un-hydrolyzed isopropoxide ligands in titania. A total of 18% weight loss for pristine powder and 17.5% weight loss for Cu-doped titania powders has been observed which is approximately same for both the powders. Weight loss tends to seize after 400 °C.

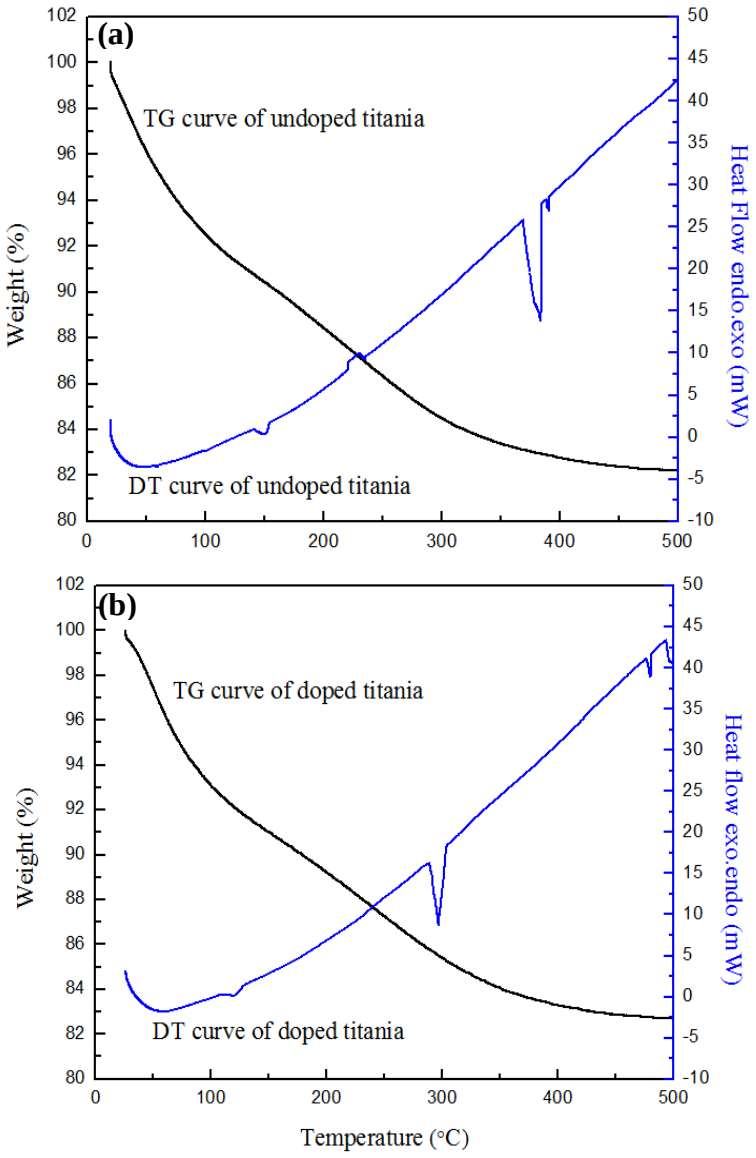

Fig. 5 TG-DT curves of (a) undoped and (b) 3wt% doped titania up to 500 °C.

From DTA curves, we can observe one sharp exothermic reaction peaks in both the graphs. For undoped titania, the exothermic peak appears at 399 °C and for doped titania it appears at 310 °C. These exothermic peaks indicate a phase change of samples from amorphous to crystalline. These results are consistent

with XRD results. Undoped titania powders need more heat to crystallize since they possess smaller crystallite size of particles. It is evident from DT curves that doped titania sample shows crystallization at lower temperature than undoped titania. Incorporation of Cu dopant in titania reduces its crystallization temperature. This corresponds to the XRD results which indicated formation of rutile phase in doped titania powder at lower temperature (650 °C Fig.1). In Fig. 5(b) formation of new peak can be observed at 480 °C which may be attributed towards the phase shift from anatase to rutile in 3wt% Cu doped sample.

FTIR Analysis

Infrared spectroscopy was done to investigate the surface properties of the prepared doped and undoped titania nano-powders. Chemical bonding of elements was explored by correlating the obtained peaks in spectra with the stretching or vibration of different functional groups. The spectra were used to probe presence of carbon and OH groups in samples and also to examine the chemical state of copper in doped powder samples. Fig. 6 shows the FTIR spectra of undoped and doped titania powder samples at different annealing temperatures respectively. The common peaks at 3200-3600 cm^{-1} correspond to the stretching vibration of OH bond and peaks at 1630 cm^{-1} correspond to the bending vibration of surface OH bond [20]. It is reported in literature hydrolysis reaction in sol-gel synthesis of nanoparticles is responsible for the presence of TiO_2-OH bonds, but chemically and physically adsorbed water on the surface of titania can also be the reason for the presence of this bond. From the figures a decrease in intensity of OH bonds can be clearly observed with increasing annealing temperature and lowest amount of surface OH groups are present in powders annealed at 650 °C due to dehydration

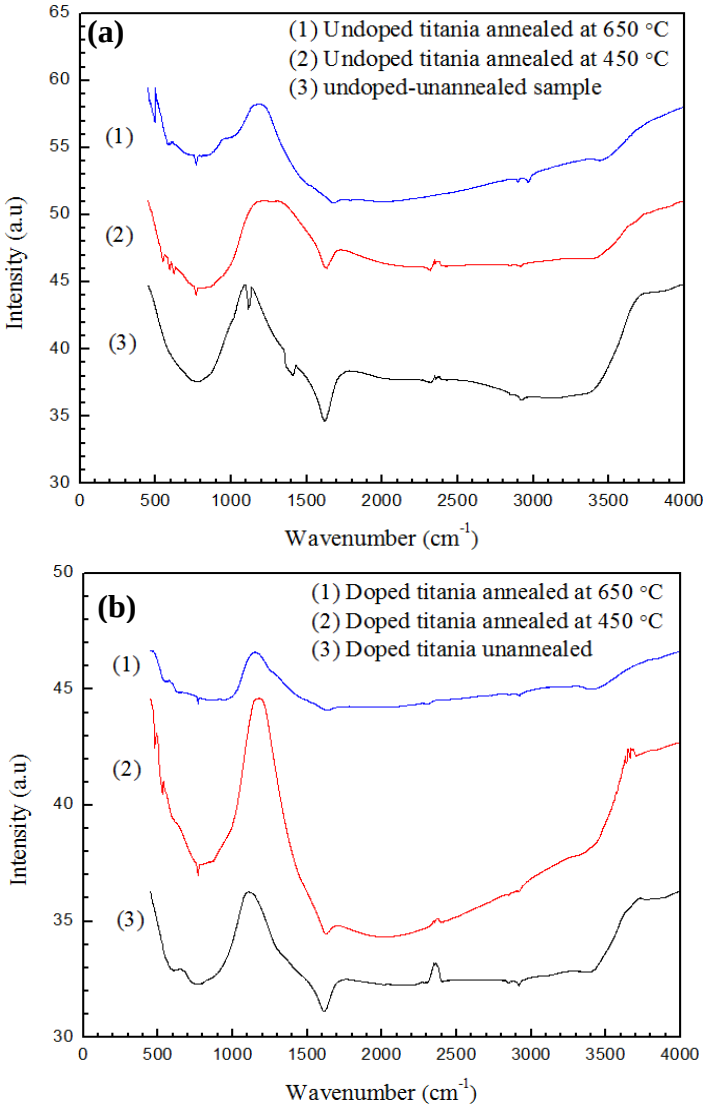

Fig. 6 FTIR spectra of (a) undoped titania and (b) doped titania at different annealing temperatures.

during annealing. The surface hydroxyl content is directly proportional to photocatalytic activity. Increase in hydroxyl content enhances the photocatalytic activity. The reason is that the hydroxyl group can behave as a center for capturing the photo-excited electron [21].

For annealed samples appearance of bands at 621 cm^{-1}, 594-549 cm^{-1}, 412 cm^{-1} are attributed towards the Ti-O vibrations. The peak at 768 cm^{-1} is characteristic feature of crystalline titania (anatase/rutile) spectrum. This peak corresponds to the stretching vibration of Ti-O bonds in TiO_4 tetrahedral geometry [22].

The presence of peaks in un-annealed samples at 1045 cm^{-1} and 1114 cm^{-1} show the presence of carbon group (Ti-O-C). This can be attributed to the presence of alkoxy group formed in sol-gel process which is removed during annealing process. These results are in exact accordance with TG analysis.

In Fig. 6 (b) new peaks are observed at 480-529 cm^{-1} in powder samples annealed at certain temperatures which correspond to the stretching mode of Cu-O bond [23] [24]. This result along with EDX spectra confirms the incorporation and doping of copper in titania lattice and its existence as CuO. Peaks at 2300-2500 cm^{-1} can be attributes to CO_2 resulting from surrounding conditions.

Discussion on Inclusion of Carbon Microspheres in photoanode:

Fig. 7 shows the XRD pattern of synthesized carbon microspheres. The pattern corresponds to the XRD pattern of carbon referring to JCPDS card# 50-1086. No peak of any impurity is visible. This pattern was achieved after annealing the as received sample at 350 ° for 10h. EDX was also performed on carbon microspheres which showed that the main component of is carbon (61 atomic%). The presence of oxygen component is because of the water molecules absorbed in the porous structure [25].

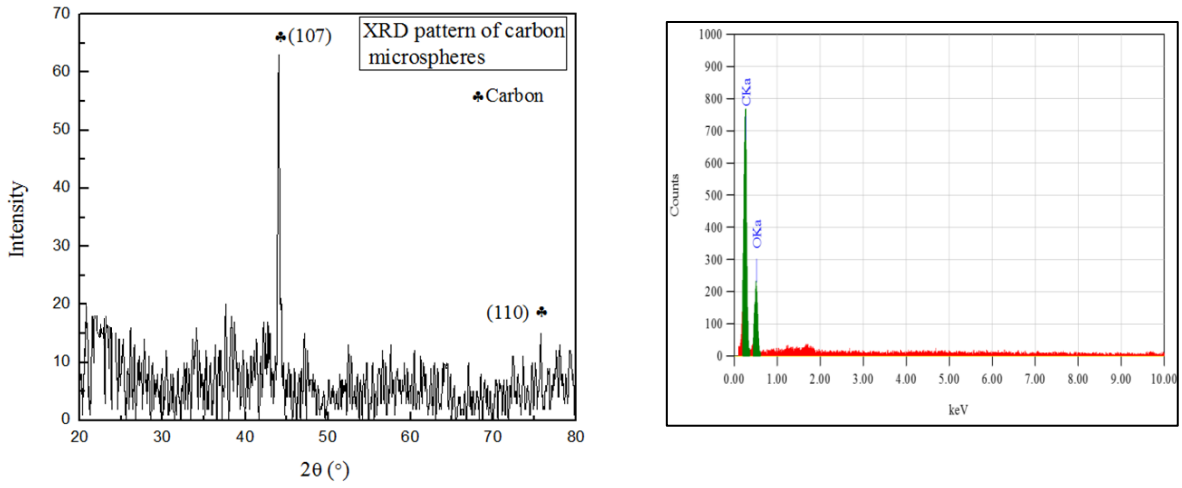

Fig. 7 (a) XRD pattern (b) EDX pattern of carbon microspheres annealed at 350 °C for 4h.

Carbon microspheres are removed at around 430 °C [26] during annealing and leads to the formation of pores. These pores are responsible for enhancing porosity, light scattering and surface area for dye adsorption and hence enhance performance of Dye sensitized solar Cells. Fig. 8 shows the isotherms of sample with and without the inclusion of carbon microsphere. The isotherms represents type IV which indicates the presence of the mesopores in the samples [27]. Other factors like pore size, BET surface area and porosity have been shown in Table 3. It is clear from the values of BET surface area that inclusion of microspheres increased the surface area for enhanced adsorption of dye. This leads to higher photovoltaic performance of the cells due to enhancement of light absorption [28]. The sample with carbon microspheres also showed enhanced porosity, pore volume and pore size. The optimized porosity for best performance of solar cells with thickness of photoanode around 20-25 µm is 40% as reported in the literature [29]. The sample showing porosity near to the optimized is the one that has pores due to carbon microsphere inclusion. Enhanced pore size aids the access of electrolyte and molecules of the dye to the surface of titania improving J_{sc} of the cells. Hence, to enhance the performance of photoanode and consequently, the performance of the cell, it is advisable to include carbon microspheres in the titania layer of photoanode.

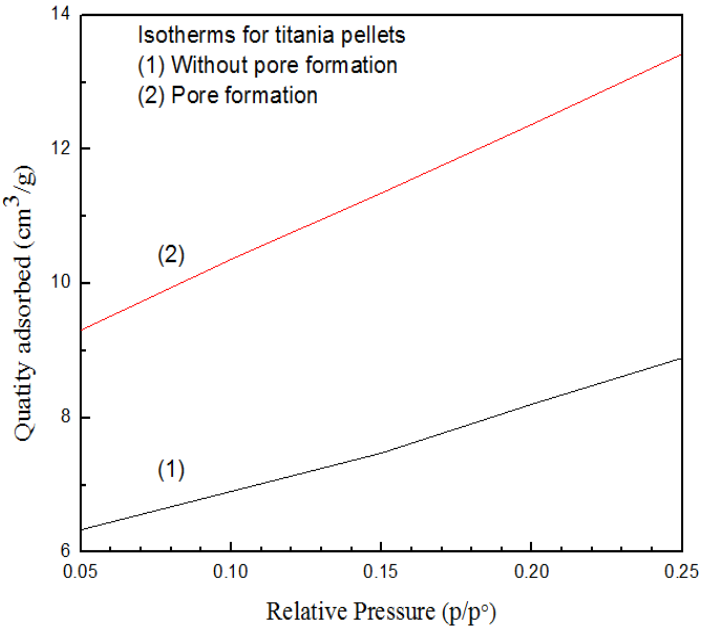

Fig. 8 N_2-sorption isotherm for titania with and without inclusion of carbon microspheres.

Table 3 Summary of the results of N2-sorption.

Sr no	Sample	Pore size (Å)	Pore volume (cm3/g)	Porosity (%)
1)	Photoanode without carbon microsphere	16.5126	0.2498660	31
2)	Photoanode with carbon microspheres	20.5062	0.3014512	42

Increase in V_{oc} of 3wt% Cu Doped Titania Based Dye Sensitized Solar Cells

IV characteristics of the cells are shown in Fig 6.16. It is evident from figures that using copper doped titania anode in DSSC affected V_{oc} and J_{sc} of the cell. An increase in V_{oc} and a decrease in J_{sc} is observed in IV characteristics of 3wt% Cu doped titania based DSSC when compared to undoped titania based DSSC.

An 11% increase in V_{oc} and a 4.8% decrease in J_{sc} was calculated from IV curves. Increase in V_{oc} attributes to the reduction in band gap energy of titania. Also co-presence of anatase and rutile phase in 3wt% Cu doped titania film leads to enhanced charge separation [18]. However, smaller particle size and visible light activity mechanisms should have increased J_{sc}. But decrease is J_{sc} occurred due to some other factor inhibiting the cell performance strongly. It was confirmed by XRD, FTIR and UV-Vis analysis of doped titania nanoparticles that copper existed as CuO form in titania lattice. The presence of this amorphous CuO layer causes hindrance in diffusion and injection of electrons leading to a decrease in J_{sc}. Also, due to presence of copper, redox reactions with electrolyte ions can occur causing a decrease in J_{sc}.

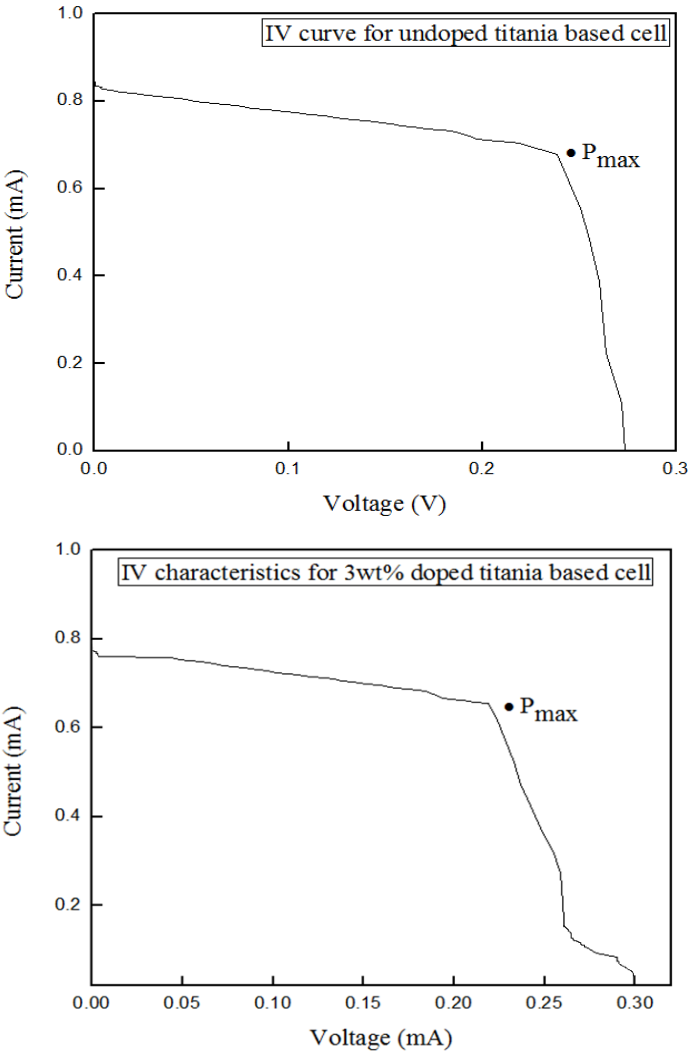

Fig. 9 IV characteristics of undoped and 3wt% Cu doped titania based solar cells.

Table 4 Summary of the IV characteristics of the doped and undoped titania based DSSCs.

Sr No	Cell	Annealing Temperature	V_{oc} (volts)	J_{sc} (mA)	η (%)
1	Undoped titania based DSSC	450 °C	0.27	0.83	0.14
2	3wt% Cu-doped titania based DSSC	450 °C	0.30	0.79	0.15

Conclusions

Titania and doped titania nanoparticles were successfully synthesized using sol-gel method as indicated by XRD, SEM/EDX, UV-Vis spectroscopy and FTIR results. Copper existed as amorphous CuO form in titania. Doping copper introduced structural defects in titania and initiated rutile phase formation. Copper doping into titania also shifted its absorption to visible region and reduced the crystallization temperature of titania. Carbon microspheres were synthesized using hydrothermal method to include them into titania electrode as pore former. The pore formation enhanced the porosity of semiconductor and increased its surface area for greater adsorption of the dye molecules. 3wt% Cu doping rendered good properties to titania and it was observed that the cells fabricated by using 3 wt% Cu doped titania based photoanode showed better V_{oc} than that fabricated using undoped titania based electrodes. A 11% increase in V_{oc} and a 4.8% decrease in J_{sc} were observed.

References

[1] Sahu, M. and P. Biswas, "Single-step processing of copper-doped titania nanomaterials in a flame aerosol reactor", Nanoscale research letters, 2011. 6(1): p. 1-14.

[2] Ni, Y., Y. Zhu, and X. Ma, "A simple solution combustion route for the preparation of metal-doped TiO_2 nanoparticles and their photocatalytic degradation properties", Dalton Transactions, 2011. 40(14): p. 3689-3694.

[3] Feng, X., et al., "Tantalum-Doped Titanium Dioxide Nanowire Arrays for Dye-Sensitized Solar Cells with High Open-Circuit Voltage", Angewandte Chemie, 2009. 121(43): p. 8239-8242.

[4] Geetha, M., K. Suguna, and P. Anbarasan, "Photoanode Modification in DSSC Using Chromium Doped TiO_2 nanoparticles by sol-gel method", Archives of Physics Research, 2012. 3(4): p. 303-308.

[5] Zalas, M. and M. Klein, "The Influence of Titania Electrode Modification with Lanthanide Ions Containing Thin Layer on the Performance of Dye-Sensitized Solar Cells", International Journal of Photoenergy, 2012. 2012.

[6] Lü, X., et al., "Improved-Performance Dye-Sensitized Solar Cells Using Nb-Doped TiO_2 Electrodes: Efficient Electron Injection and Transfer", Advanced Functional Materials, 2010. 20(3): p. 509-515.

[7] Lee, S., et al., "Nb-doped TiO_2: a new compact layer material for TiO_2 dye-sensitized solar cells," The Journal of Physical Chemistry C, 2009. 113(16): p. 6878-6882.

[8] Cao, F.-F., et al., "Wet chemical synthesis of Cu/TiO_2 nanocomposites with integrated nano-current-collectors as high-rate anode materials in lithium-ion batteries", Physical Chemistry Chemical Physics, 2011. 13(6): p. 2014-2020.

[9] B. Choudhury, M. Dey, and A. Choudhury, "Defect generation, dd transition, and band gap reduction in Cu-doped TiO_2 nanoparticles," International Nano Letters, vol. 3, pp. 1-8, 2013.

[10] J. Nair, P. Nair, F. Mizukami, Y. Oosawa, and T. Okubo, "Microstructure and phase transformation behavior of doped nanostructured titania," Materials research bulletin, vol. 34, pp. 1275-1290, 1999.

[11] C. Chia, S. Zakaria, M. Yusoff, S. Goh, C. Haw, S. Ahmadi, N. Huang, and H. Lim, "Size and crystallinity-dependent magnetic properties of CoFe nanocrystals," Ceramics International, vol. 36, pp. 605-609, 2010.

[12] D. C. Hurum, A. G. Agrios, K. A. Gray, T. Rajh, and M. C. Thurnauer, "Explaining the enhanced photocatalytic activity of Degussa P25 mixed-phase TiO2 using EPR," The Journal of Physical Chemistry B, vol. 107, pp. 4545-4549, 2003.

[13] L. Du, A. Furube, K. Hara, R. Katoh, and M. Tachiya, "Mechanism of particle size effect on electron injection efficiency in ruthenium dye-sensitized TiO_2 nanoparticle films," The Journal of Physical Chemistry C, vol. 114, pp. 8135-8143, 2010.

[14] M. Jeng, Y.Wung,, "Particle size effects of TiO_2 layers on the solar efficiency of dye-sensitized solar cells," International Journal of Photoenergy, vol. 2013.

[15] Z.-M. Wang, G. Yang, P. Biswas, "Processing of iron-doped titania powders in flame aerosol reactors," Powder technology, vol. 114, pp. 197-204, 2001.

[16] L. Li, J. Liu, Y. Su, G. Li, X. Chen, X. Qiu, and T. Yan, "Surface doping for photocatalytic purposes: relations between particle size, surface modifications, and photoactivity of SnO2: Zn2+ nanocrystals," Nanotechnology, vol. 20, p. 155706, 2009.

[17] G. Li, N. M. Dimitrijevic, L. Chen, T. Rajh, and K. A. Gray, "Role of Surface/Interfacial Cu2+ Sites in the Photocatalytic Activity of Coupled $CuO{-}TiO_2$ Nanocomposites," The Journal of Physical Chemistry C, vol. 112, pp. 19040-19044, 2008.

[18] X. Qiu, M. Miyauchi, K. Sunada, M. Minoshima, M. Liu, Y. Lu, D. Li, Y. Shimodaira, Y. Hosogi, and Y. Kuroda, "Hybrid Cu x O/TiO_2 Nanocomposites As Risk-Reduction Materials in Indoor Environments," ACS nano, vol. 6, pp. 1609-1618, 2012.

[19] G. Liu, C. Sun, X. Yan, L. Cheng, Z. Chen, X. Wang, L. Wang, S. C. Smith, G. Q. M. Lu, and H.-M. Cheng, "Iodine doped anatase TiO_2 photocatalyst with ultra-long visible light response: correlation between geometric/electronic structures and mechanisms," Journal of Materials Chemistry, vol. 19, pp. 2822-2829, 2009.

[20] H. Jensen, A. Soloviev, Z. Li, and E. G. Søgaard, "XPS and FTIR investigation of the surface properties of different prepared titania nano-powders," Applied Surface Science, vol. 246, pp. 239-249, 2005.

[21] A. Y. A. M.HEMA, P.TAMILSELVI and R.ANBARASAN, "Titania Nanoparticles Synthesized by Sol-Gel Technique," Chem Sci Trans., vol. 1, 2013.

[22] A. Murashkevich, A. Lavitskaya, T. Barannikova, and I. Zharskii, "Infrared absorption spectra and structure of TiO 2-SiO 2 composites," Journal of Applied Spectroscopy, vol. 75, pp. 730-734, 2008.

[23] H. W. N. Slamet, E. Purnama, K. Riyani, and J. Gunlazuardi, "Effect of copper species in a photocatalytic synthesis of methanol from carbon dioxide over copper-doped titania catalysts," World Applied Sciences Journal, vol. 6, pp. 112-122, 2009.

[24] N. WON and N. Vit, "Cu-Doped TiO_2 Nanopowders Synthesized by Sonochemical-assisted Process," Sains Malaysiana, vol. 42, pp. 175-181, 2013.

[25] S. Ratchahat, N. Viriya-empikul, K. Faungnawakij, T. Charinpanitkul, and A. Soottitantawat, "Synthesis of carbon microspheres from starch by hydrothermal process," 2010.

[26] J. Qian, P. Liu, Y. Xiao, Y. Jiang, Y. Cao, X. Ai, and H. Yang, "TiO2-Coated Multilayered SnO2 Hollow Microspheres for Dye-Sensitized Solar Cells," Advanced Materials, vol. 21, pp. 3663-3667, 2009.

[27] S. J. Gregg, K. S. W. Sing, and H. Salzberg, "Adsorption surface area and porosity," Journal of The Electrochemical Society, vol. 114, pp. 279C-279C, 1967.

[28] E. Bayatloo, E. Saievar-Iranizad, and S. S. Polkoo, "Performance enhancement of TiO_2-based dye-sensitized solar cells by carbon nanospheres in photoanode," arXiv preprint arXiv:1311.0415, 2013.

[29] Dipal B. patel, "Effect of Electrode's Geometric shape, Thickness and Porosity on the Performance of Dye Sensitized Solar Cell".